Master's thesis

NTNU
Norwegian University of Science and Technology
Faculty of Engineering
Department of Geoscience and Petroleum

Mohammadsajjad Zeynolabedini

MRST Vertical Equilibrium Model analysis for CO2 Storage

Master's thesis in TPG4920
Supervisor: Ashkan Jahanbani Ghahfarokhi
Co-supervisor: Per Eirik Bergmo
June 2023

NTNU
Norwegian University of
Science and Technology

Mohammadsajjad Zeynolabedini

MRST Vertical Equilibrium Model analysis for CO2 Storage

Master's thesis in TPG4920
Supervisor: Ashkan Jahanbani Ghahfarokhi
Co-supervisor: Per Eirik Bergmo
June 2023

Norwegian University of Science and Technology
Faculty of Engineering
Department of Geoscience and Petroleum

NTNU
Norwegian University of
Science and Technology

NTNU
Kunnskap for en bedre verden

Department of Geo-science and Petroleum

TPG4920 - Master's thesis

MRST Vertical Equilibrium Model analysis for CO2 Storage

Author:
Mohammadsajjad Zeynolabedini

Supervisor:
Ashkan Jahanbani Ghahfarokhi

Co-Supervisor:
Per Eirik Bergmo

June 2023

Abstract

The primary purpose of this study is to import the Aurora model, which is developed at the University of Oslo in cooperation with Gassnova and Ross Offshore, into MATLAB Reservoir Simulation Toolbox (MRST) to apply the Vertical Equilibrium (VE) feature of this simulator. The main reason for the VE application in MRST is to decrease the very long simulation time since the VE feature converts the 3D reservoir model into a 2D model, which takes significantly less time to simulate the reservoir model. Grid and PVT models of MRST and ECLIPSE have been compared together to ensure that the whole reservoir model, including PVT and Grid model, are imported from ECLIPSE into MRST correctly. Gas and water relative permeability comparison confirm that the relative permeability model is defined correctly based on the ECLIPSE relative permeability model. There was an issue regarding pressure initialization in MRST compared with ECLIPSE, which has been resolved by water density adjustment. By considering the water and gas compressibility equations, Water and Gas density models are defined in MRST based on the ECLIPSE PVT model. Gas and Water viscosity comparison between ECLIPSE and MRST shows that a similar trend exists in both MRST and ECLIPSE viscosity models. Although MRST PVT and Grid Model are verified in comparison with the ECLIPSE model, there are differences between CO_2 plume shapes in MRST and ECLIPSE. The main reason for this difference is "Reservoir Heterogeneity". Since the porosity in the upper layers of the Aurora reservoir model is much lower than the lower layers, the one-layer averaged MRST model has more porosity than the upper layers in the ECLIPSE reservoir model, which has the highest contribution in CO_2 flow. Therefore, the MRST plume shape is much wider than the ECLIPSE plume. In the first 50 years of injection, the free plume with approximately 17 [MT] of CO_2 is the most significant storage mechanism. While approximately 17 [MT] (1 [MT] = 1E+09 [kg]) CO_2 can be stored in the reservoir after 530 years by Residual and Dissolution mechanisms, 28 [MT] CO_2 exited from the reservoir boundary. A sensitivity analysis have been carried out on five uncertain parameters of the reservoir model including permeability, porosity, Residual gas saturation, rock compressibility, and relative permeability curve. While injection well bottom-hole pressure is strongly sensitive with permeability and rock compressibility variation, no sensitivity is shown in porosity, residual gas saturation, and relative permeability curve for this parameter. Although plume migration is highly sensitive to permeability, porosity, and rock compressibility variation, it shows a slight change with residual gas saturation and relative permeability curve. Regarding storage mechanisms' contribution, while all five parameters have an impact on the level of storage for each mechanism, Residual gas saturation and Rock compressibility show a more strong effect on the storage mechanisms' breakdown.

Table of Contents

Abstract i

List of Figures v

List of Tables viii

1 Introduction 1

1.1 Background . . . 1

1.2 Aurora . . . 5

1.3 Geology in the Aurora Area . . . 12

1.4 Heterogeneity in the Aurora Area . . . 13

1.5 MATLAB Reservoir Simulation Toolbox (MRST) . . . 14

1.6 Research Objectives . . . 15

1.7 Project Outline . . . 15

2 Theory 16

2.1 CO_2 Storage . . . 16

2.2 Basic Concepts for Geological Storage of CO_2 . . . 16

2.3 Injection Mechanism . . . 20

2.4 Migration mechanism . . . 21

2.5 Trapping Mechanism . . . 22

2.5.1 Capillary Trapping . . . 24

2.5.2 Geological trapping . . . 27

2.5.3 Geochemical trapping . . . 27

2.5.4 CO_2 Dissolution . . . 29

2.6 CO_2 Properties . . . 30

2.7 Reservoir simulations and modeling for CO2 injection . . . 33

2.7.1 Fluid modeling . . . 33

2.7.2 Reservoir modeling 34

3 Methodology, Problem and Model Description 38

3.1 Software 38

3.1.1 MRST 38

3.1.2 ECLIPSE 41

3.2 Vertical Equilibrium 43

3.3 Reservoir Model 45

3.3.1 Fluid Model 46

3.3.2 Static Model 48

3.4 MRST and ECLIPSE model comparison 52

3.4.1 MRST Grid Model Discrepancy 52

3.4.2 MRST and ECLIPSE Fluid Model Comparison 52

3.5 Sensitivity Analysis 55

4 Results and Discussion 56

4.1 Relative Permeability Models comparison 56

4.2 MRST Pressure Initialization 57

4.3 MRST and ECLIPSE PVT model comparison 59

4.4 CO_2 plume comparison 64

4.5 Sensitivity Analysis 68

4.5.1 Permeability Sensitivity Analysis 68

4.5.2 Porosity Sensitivity Analysis 69

4.5.3 Residual Gas Saturation Sensitivity Analysis 71

4.5.4 Rock Compressibility Sensitivity Analysis 73

4.5.5 Relative permeability curve sensitivity analysis 75

5 Conclusion and Recommendation 79

Bibliography **82**

Appendix **90**

A ECLIPSE DATA File 90

B MRST code 101

List of Figures

1.1 Different options for geological storage of CO2 underground 2

1.2 Northern Light project-schematic representation 3

1.3 Utsira and Johansen Formation 4

1.4 Injection Well Location sequences in Johansen Formation 5

1.5 Location of the potential of storage sites in the Horda CO_2 storage hub 6

1.6 Horda CO_2 storage deployment 6

1.7 Horda Platform Area 7

1.8 Horda Platform faults 8

1.9 Johansen Formation Seismic Data 9

1.10 Geological context of the Northern Lights CO_2 storage site 11

1.11 Depth map of Johansen Formation 13

1.12 MRST's beneficial features 15

2.1 CO_2 Density Versus Depth 17

2.2 North Sea Basin stratigraphic sequence 18

2.3 The three key storage issues 19

2.4 Main Phases of a CO_2 storage project 19

2.5 Different Migration Process 22

2.6 Sketches of various trapping techniques before and after injection 23

2.7 CO_2 Storage Trapping Mechanisms 24

2.8 Capillary Trapping of a CO_2 phase in a water-wet porous medium 24

2.9 Analytical capillary trapping models 25

2.10 CO_2 Storage flow processes illustration 26

2.11 Example CO_2-Brine relative permeability curve 27

2.12 Effect of CO_2 reaction with shale 29

2.13 Density-driven flow in CO_2 storage in saline aquifer 30

2.14 CO_2 Thermodynamic Diagram 31

2.15 CO_2 Density and Viscosity 32

2.16 CO_2 temperature Diagram as a function of pressure and specific volume 32

2.17 Reservoir Simulation Model 34

3.1 MRST core 39

3.2 MRST data sets examples 40

3.3 Vertical Equilibrium model in MRST 44

3.4 Vertical Equilibrium of Sleipner CO2 injection 45

3.5 The study area 46

3.6 Histogram of initial pressure distribution 47

3.7 Initial pressure distribution of the Aurora Model 47

3.8 Gas and water relative permeabilities 48

3.9 Intra-block faults within the aurora model 49

3.10 Initial pressure distribution and Injection well location 49

3.11 Initial Average Pore Volume distribution in MRST (Left); Modified Pore Volume Distribution (Right) 53

4.1 Gas Relative Permeability 56

4.2 Water Relative Permeability 57

4.3 Previous case of ECLIPSE and MRST Pressure initialization comparison 57

4.4 Updated case of ECLIPSE and MRST Pressure initialization comparison 58

4.5 ECLIPSE and MRST Gas Injection rate comparison 59

4.6 Field Pressure [Pa] development during and after injection 60

4.7 ECLIPSE CO_2 Compressibility 60

4.8 ECLIPSE and MRST CO_2 Density comparison 61

4.9 ECLIPSE Water Compressibility 62

4.10 MRST and ECLIPSE Water Density comparison 63

4.11 MRST and ECLIPSE CO_2 Viscosity Comparison 63

4.12 MRST and ECLIPSE Water Viscosity 64

4.13 ECLIPSE Gas Saturation during and after injection 65

4.14 MRST Gas Saturation during and after injection 66

4.15 CO_2 mass stored breakdown 67

4.16 3D CO_2 saturation in MRST 67

4.17 Well Bottomhole Pressure in Permeability Sensitivity Analysis 68

4.18 Plume shape in Permeability Sensitivity Analysis after 50 years (20 years after injection stops) 69

4.19 Storage Mechanisms in Permeability Sensitivity Analysis after 50 years (20 years after injection stops) 70

4.20 Well Bottomhole Pressure in Porosity Sensitivity Analysis 70

4.21 Plume shape in Porosity Sensitivity Analysis after 50 years (20 years after injection stops) 71

4.22 Storage Mechanisms in Porosity Sensitivity Analysis after 50 years (20 years after injection stops) 72

4.23 Well Bottomhole Pressure in Residual Gas Saturation Sensitivity Analysis 72

4.24 Plume shape in Residual Gas Saturation Sensitivity Analysis after 50 years (20 years after injection stops) 73

4.25 Storage Mechanisms in Residual Gas Saturation Sensitivity Analysis after 50 years (20 years after injection stops) 74

4.26 Well Bottomhole Pressure in Rock Compressibility Sensitivity Analysis 74

4.27 Plume shape in Rock Compressibility Sensitivity Analysis after 50 years (20 years after injection stops) 75

4.28 Storage Mechanisms in Rock Compressibility Sensitivity Analysis after 50 years (20 years after injection stops) 76

4.29 Well Bottomhole Pressure in Relative Permeability Curve Sensitivity Analysis . . . 76

4.30 Plume shape in Relative Permeability Curve Sensitivity Analysis after 50 years (20 years after injection stops) 78

4.31 Storage Mechanisms in Relative Permeability Curve Sensitivity Analysis after 50 years (20 years after injection stops) 78

List of Tables

3.1 ECLIPSE DATA file section 42

3.2 Aurora Model Overview 51

4.1 Saturation End-point values used in Relative permeability curve sensitivity analysis (Marashi, 2021). 77

1 Introduction

This thesis is written based on the continuation of my specialization project at NTNU/SINTEF. The specialization project concerns CO_2 injection, storage, and monitoring in the Aurora model, part of the Johansen formation. The primary purpose of this study is to import the Aurora model, which is developed at the University of Oslo in cooperation with Gassnova and Ross Offshore (Sundal et al. (2016)), into MATLAB Reservoir Simulation Toolbox (MRST) to apply the Vertical Equilibrium (VE) feature of this simulator. The main reason for the VE application in MRST, which will be discussed in detail, is to decrease the very long simulation time since the VE feature converts the 3D reservoir model into a 2D model, which takes significantly less time to simulate the reservoir model (Zeynolabedini, 2022). This section includes the background, reservoir model introduction, MRST introduction, and research objectives.

1.1 Background

Global warming is one of the most critical environmental issues nowadays. It can threaten human life if it is not resolved globally. It is accepted that CO_2 emission is mostly due to fossil fuel consumption. Unfortunately, fuel consumption has become an inseparable part of human life. Therefore, one method should be adopted to prevent or decrease this environmental catastrophe. In this regard, Carbon Capture and Storage (CCS) is introduced to alleviate the global warming issue (Beck et al., 2018).

The concept of capturing and storing CO_2 in underground reservoirs to limit greenhouse gas emissions to the atmosphere was first proposed in the late 1970s in response to global warming and its associated detrimental environmental effects (Marchetti, 1977). The first commercial CO_2 injection operation was carried out as an Enhanced Oil Recovery (EOR) technique in Texas, USA, in the early 1970s. Since then, there have been a number of CO2-EOR projects around the world (Metz, Davidson, De Coninck et al., 2005). In 1996, Equinor and its partners completed the first CCS plant in Sleipner, successfully storing one million tons of CO_2 annually in this North Sea gas field until this day. Numerous water or hydrocarbon reservoirs can effectively store CO2 underground, as seen in Figure 1.1.

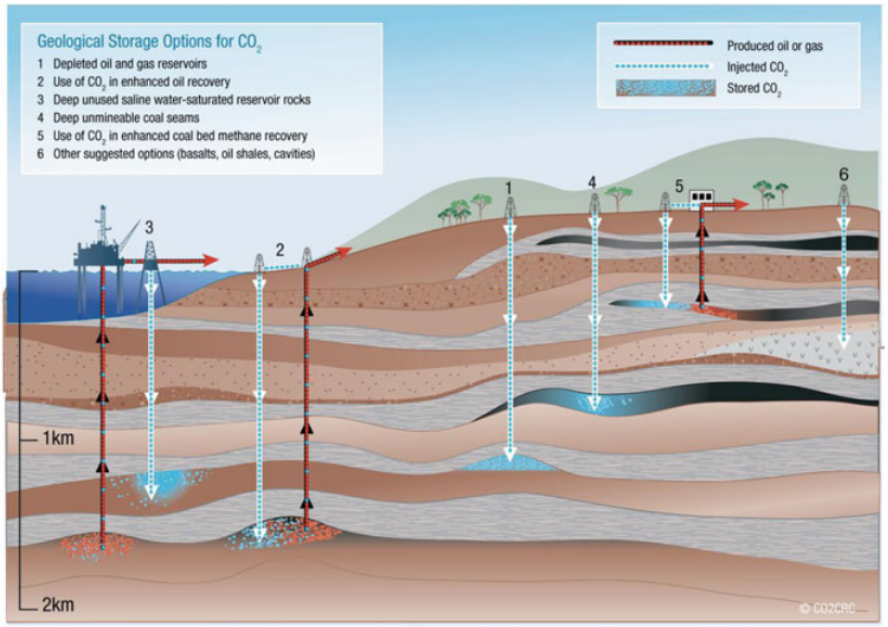

Figure 1.1: Different options for geological storage of CO2 underground(Metz, Davidson, De Coninck et al., 2005)

For the purpose of achieving the goals set forth in the Paris Climate Agreement, geological storage of CO_2 has the potential to dramatically reduce global carbon emissions (Anderson et al., 2005). Such storage will necessitate the massive injection of CO_2 into depleted hydrocarbon sources and underground saline aquifers(P. S. Ringrose et al., 2019; P. S. Ringrose et al., 2021).

To keep global warming below 1.5 to 2°C, geological CO_2 storage (CCS) must be used to reduce atmospheric greenhouse gas emissions (Rogelj et al., 2018). According to Peters et al. (2019) and Longship-Report (2020), CCS is the fastest and safest way to reduce CO_2 emissions. A full-scale (capture, transport, and storage) CO_2 storage project called "Longship" has just been started in the Horda Platform area, offshore Norway, by the Norwegian government and Northern Lights, a joint venture company owned by Equinor, Shell, and TotalEnergies, in recognition of its significance. The transport and storage element of the Longship project is included in Northern Light, which entails the capture of CO_2 from industrial point sources (a cement plant and a waste-to-energy plant) and the subsequent transportation of the captured CO_2 (liquefied) by ships to an onshore terminal (the municipality of Øygarden on the Norwegian west coast). The CO_2 will then be transported through a pipeline that is about 100 km long to the Aurora storage site (31/5-7, Eos well), which is located approximately 2.6 km below the surface of the ocean (Figure 1.2a).

Up to 1.5 Mt of CO_2 can be transported, injected, and stored during Phase 1 (Northern-Lights, 2022). However, the market demand from significant CO_2 emitters throughout Europe will drive investments in the following phases (up to 5 Mt of CO_2 annually) (Northern Lights, 2021).

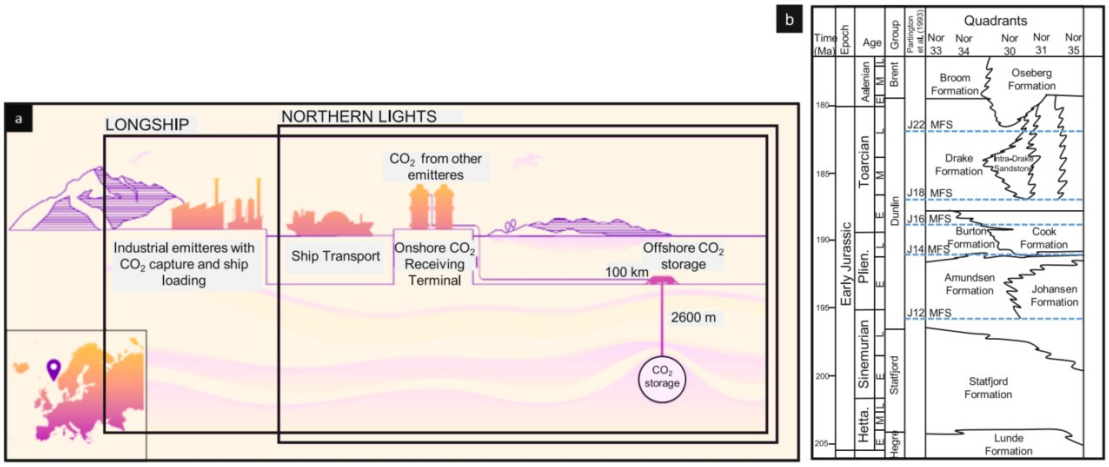

Figure 1.2: (a) A schematic representation of the Longship project (courtesy of Northern Lights). The full-scale CCS project involves capturing CO_2 from the Norcem cement production in Brevik, Norway, and the Fortum Oslo Varme waste landfill in Oslo, Norway. The captured CO_2 is then transported in liquid form to the Øygarden onshore terminal (the municipality of Øygarden on the Norwegian west coast). The liquid CO_2 will be piped to the Aurora location for long-term storage.(b) The lithological variance across the several quadrants represents the Early Jurassic stratigraphic sequence of the studied area (Husmo et al., 2003; Partington et al., 1993).

Other projects have also been initiated by the need for finding ways to alleviate CO_2 emissions. The ultimate goal of all these projects is to store large quantities of CO_2 in deep saline aquifers.

The matched storage capacity that must be demonstrated for potential storage sites is around 4 Mt CO_2/year (Bachu et al., 2007; Bradshaw et al., 2007). The investigation of two geological formations offshore of Norway is currently underway. The Utsira formation is well-documented, and since 1996, 1 Mt CO_2/year has been injected into the Sleipner gas field (Torp et al., 2004). As a result, significant experience has already been gained.
Next, we'll concentrate on the second potential location for storage. Figure 1.3 shows the location of the deep saline aquifer known as the Johansen Formation beneath the Troll field. It is close to Mongstad, has a big volume, suitable pressure regimes at deep depths, close well access from the Troll field, and has potential geological and sealing qualities that have been shown in preliminary modeling. So, it would seem that the Johansen formation would be a great choice for the storage of CO_2. Early case studies have also demonstrated that pipeline solutions perform better in terms of economic sustainability than combined Wessel/pipeline solutions, and a long-term pipeline solution from Mongstad may be conceivable (Gassnova, 2007).

The Sognefjord Formation, in a number of fault blocks west of the Vette Fault, serves as the reservoir for the enormous Troll Field. The Sognefjord Formation's regional pore pressure is thought to be affected by the field's gas production. Although the impact at the east of the Vette Fault is currently unknown, the pressure depletion effect is likely to be significant in the Smeaheia Alpha prospect over the long run (Lauritsen et al., 2018; A. E. Lothe et al., 2019b; Nazarian et al., 2019;

Riis, 2018).

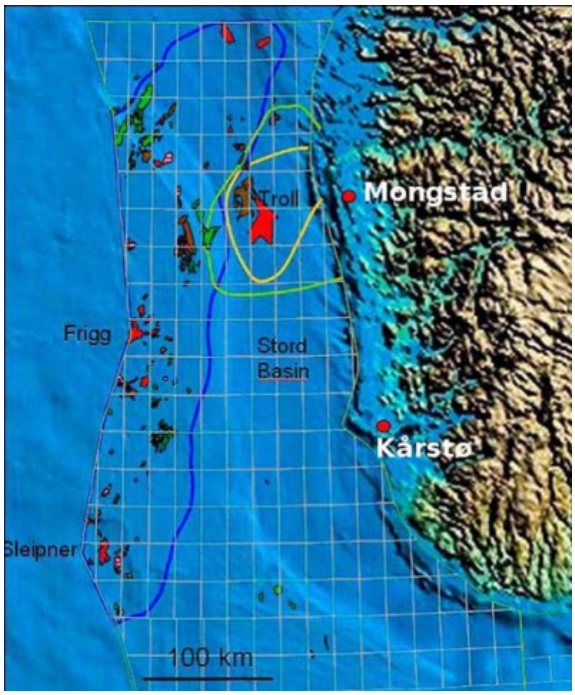

Figure 1.3: Locations of the Utsira and Johansen formations are shown in a figure. The green curve encompasses the Johansen formation, and the yellow curve denotes regions where seismic data is available. The blue line delineates the Norwegian part of the Utsira formation (Gassnova, 2007).

Since numerous trapping mechanisms are involved and operate on multiple time scales, estimating the storage capacity of deep saline aquifers is exceedingly difficult (Bachu, 2008; Bachu et al., 2007; Bradshaw et al., 2007; Lindeberg et al., 2003; Pruess et al., 2003). Its complexity is further increased by geological uncertainty and/or a lack of geological classification. In the end, cautious estimations of the amount of CO_2 that leaks from an aquifer's borders over a specific period of time and the effects of that leaking must be presented.

To carry out this kind of study, new modeling tools must be created due to computational constraints and a lack of knowledge, which demands a stochastic framework. In the context of established sedimentary basins in North America, such modeling methods have been proposed and are being developed by Celia and Nordbotten with partners (Nordbotten, Celia, Bachu and Dahle, 2005; Nordbotten et al., 2006a; Nordbotten et al., 2006b; Nordbotten et al., 2004, 2005). Their main focus has been on managing numerous abandoned and maybe leaking wells within a straightforward layered geometry that enables semi-analytic solutions. On the other hand, North Sea aquifers can provide different difficulties, including complicated geometries and fault/fracture zones that might provide leakage channels. In order to comprehend the primary consequences that need to be taken into consideration in capacity/risk analysis, thorough simulations using validated simulation tools must be carried out as a first step (Eigestad et al., 2009).

In this regard, A. Lothe et al. (2019) have conducted research, which is a component of the

ALIGN-CCUS project, about the description of how to increase the annual storage capacity of a CO_2 storage hub offshore on the west coast of Norway. They create a timetable outlining potential locations for the industrial-scale Horda CO_2 Storage Hub throughout the ensuing thirty years. The predicted CO_2 supply rates (million tonnes per year) from sources in Norway, Sweden, and Northern Europe are matched to the yearly storage capacity. These projections show that the total amount of CO_2 stored throughout time will be between 810 Mt and 1.85 Gt by 2065.

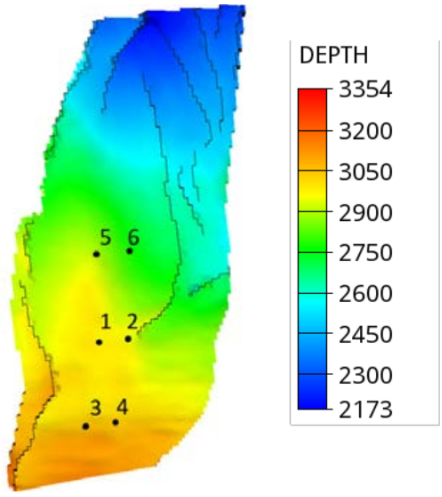

Figure 1.4: Depth map in meters of the Johansen Formation used for the Aurora model simulation. Injection well drilling sequences are shown as a research result of A. Lothe et al. (2019)

1.2 Aurora

As per Figure 1.5, the Horda Platform research region offers at least four potential storage sites, with capacities in million tonnes (Mt) or thousand million tonnes (Gt) CO_2, as shown by simulation of CO_2 storage and capacity estimates: (1) Aurora Structure, Johansen Formation, southeast of the Troll Gas Field (120-293 Mt); (2) Alpha Structure, Sognefjord Formation, northern Smeaheia area (40-50 Mt); (3) Gamma Structure, Sognefjord Formation, southern Smeaheia area (0.15-3 Gt); and (4) Troll Field, Sognefjord Formation, after cessation of gas production (3-5 Gt) (A. Lothe et al., 2019).

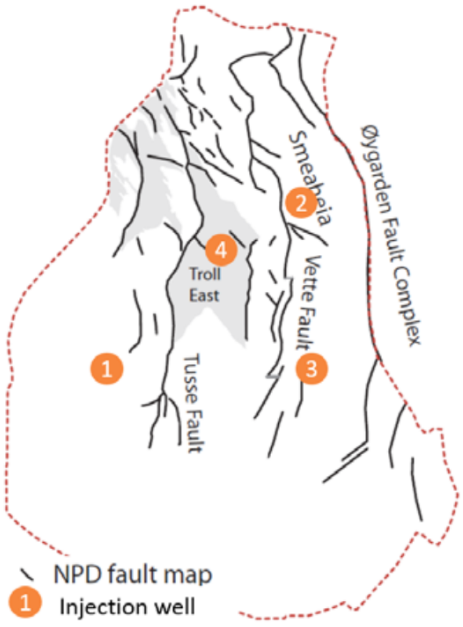

Figure 1.5: Potential storage site locations in the Horda CO_2 storage Hub. (1) Aurora structure, (2) Alpha structure, (3) Gamma structure, and (4) Troll Field (A. Lothe et al., 2019).

The possible deployment of the Horda platform as a CO_2 storage hub for CO_2 supply from Norway, Sweden, and Northern Europe is planned and sketched in Figure 1.6 based on the prospective storage sites linked to a Horda CO_2 Storage Hub.

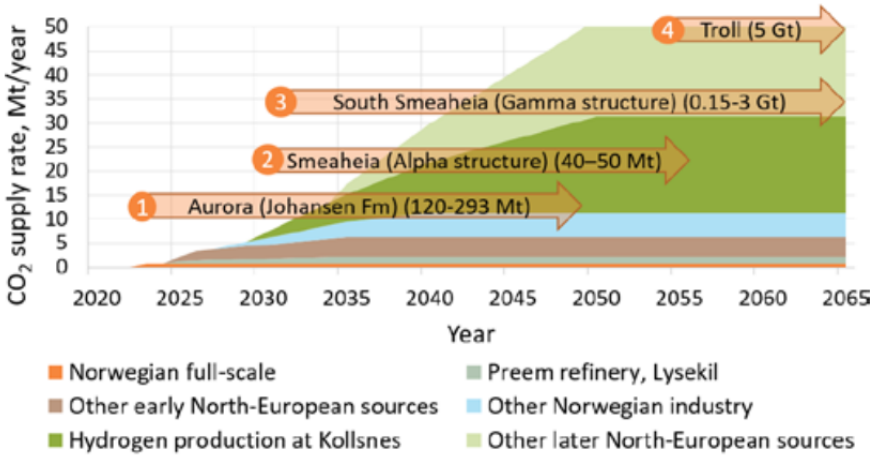

Figure 1.6: Deployment of the Horda CO_2 Storage Hub for CO_2 supply (million tonnes annually) from sources in Norway, Sweden, and Northern Europe. Arrows indicate a potential timetable for tying in the potential storage locations connected to a Horda CO_2 Storage Hub, as outlined in A. Lothe et al. (2019). Possible commencement dates and the estimated potential storage capacity are indicated by the arrows.

A. E. Lothe et al. (2019b) examined the impact of several assumptions for the transmissibility of the faults in the area, in particular, the Vette Fault with two fault ramps close to the Smeaheia area (see Figure 1.7 and Figure 1.8). Actually, Smeaheia is connected to the Troll field hydrodynamically,

therefore when low fault transmissibility is considered for the Vette fault, the local pressure will be higher compared to the high transmissibility values. Since the higher local pressure will result in a smaller occupied pore volume, simulation findings demonstrate that the final extent of the CO_2 plume at Smeaheia Alpha is significantly smaller if poor transmissibility of the fault is considered.

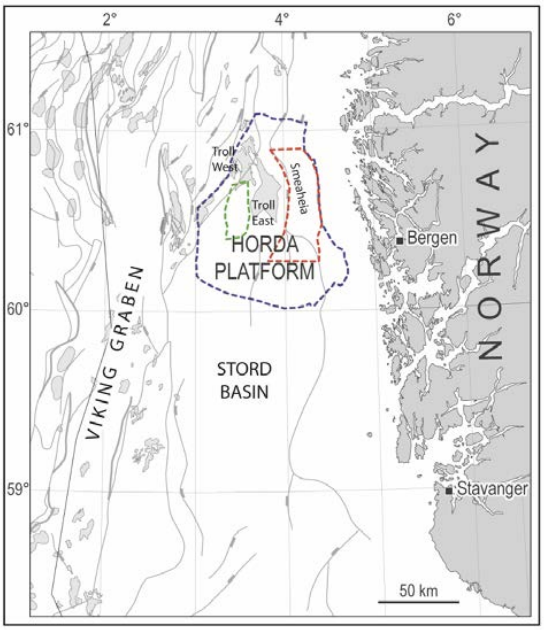

Figure 1.7: The area off the coast of Norway where the Horda Platform is located. The outline for the pressure simulations in A. E. Lothe et al. (2019b) is shown in blue, the outline for the Aurora simulation model is shown in green, and the Smeaheia reservoir model is shown in red. Altered from A. E. Lothe et al. (2019a)

The Cook and Johansen Formation Sandstones are potential reservoir rocks in the Aurora area, and the Drake and Burton Formation Shales are cap rocks from the Early Jurassic Dunlin Group (Figure 1.2b). Although several CCS projects around the world (such as Sleipner and Snøhvit in Norway, In Salah in Algeria, Century Plant in the USA, Quest and Aquistore in Canada, etc.) showed safe and reliable CO_2 storage, the large-scale Longship project—the first of its kind—needs additional analysis to determine the potential risks including the geo-mechanical ones.

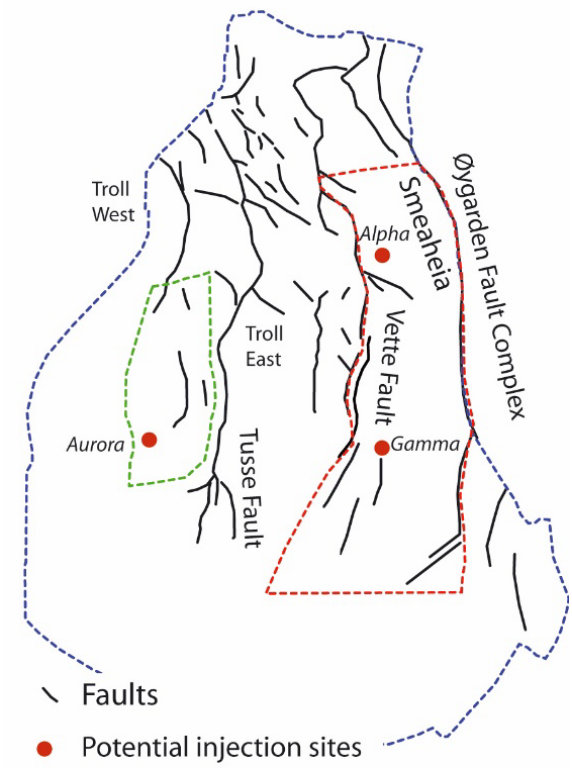

Figure 1.8: Storage opportunities and significant fault systems in the Horda Platform region. The Smeaheia reservoir simulation model and the Aurora simulation model are each marked in red and green, respectively. Altered from A. E. Lothe et al. (2019a) .

Using sparse subsurface data to construct a reliable reservoir model is a significant difficulty with regard to the prediction of injectivity and storage capacity for CO_2 in subsurface saline aquifers. Since the late 1960s, more than 5051 wells (of which 1366 are development wells) have been drilled into the Norwegian continental shelf to explore the hydrocarbons or to develop production. However, there are no known hydrocarbon resources in the Johansen Formation, which explains the shortage of direct lithological evidence (Sundal et al., 2013).

Sundal et al. (2016) defined the stratigraphic framework for the Northern Lights storage site and neighboring areas. This framework has been mapped over seven 3D seismic cubes and contiguous 2D seismic lines which comprise base- and top-Johansen Formation and top-Cook Formation surfaces (Figure 1.9A).

As shown in Figure 1.9B and C, the depositional model of the Johansen and Cook formations and analogous Krossfjord, Fensfjord, and Sognefjord formations include two contrasting components. The first one is the westward progradation of a linear-to-arcuate deltaic shoreline that is more wave-dominated and less influenced through time. The second one is the shoreline-parallel sand transport in the wave-dominated delta.

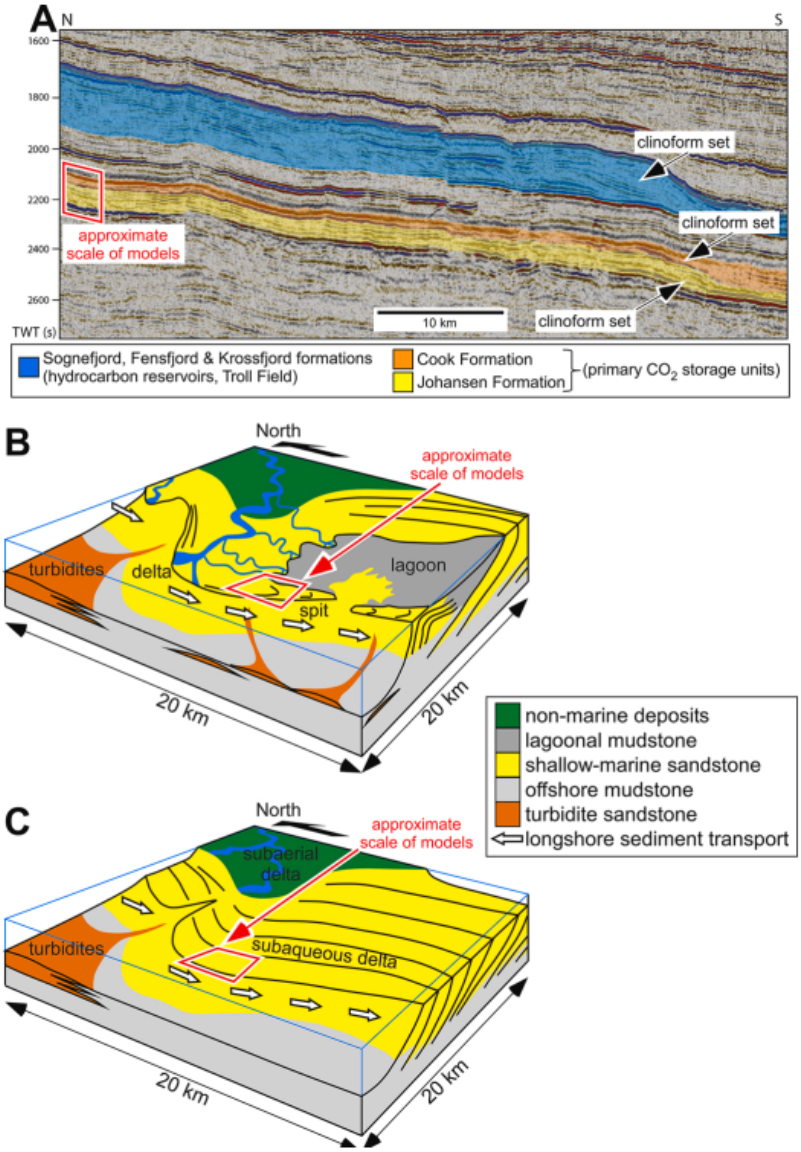

Figure 1.9: (A) Regional 2D seismic line HRTRE-00212 in Figure 1.10C, which has been interpreted, displays the southern (down-dip) pinch-out of the Johansen-Cook CO_2 storage unit and the formations Sognefjord and Krossfjord above it (Sundal et al., 2016). (B, C) For the Johansen Formation, two different depositional scenarios are possible: (B) the progression westward of a delta dominated by southward-deflected waves and fronted by a spit that is located seaward of a sheltered lagoon (Sundal et al., 2015; Sundal et al., 2016); and (C) by analogy with the Sognefjord Formation in the Troll Field, westward progradation of an arcuate wave-dominated delta with subaqueous clinoforms fed by north-to-south sand transport Patruno et al., 2015.

The Northern Lights project, which is the part of "Long ship" project, involves the full-scale storage of CO_2 in the Johansen and Cook formations' saline aquifer sandstones, off the coast of western Norway (Bergmo et al., 2009; A.-K. Furre et al., 2019; Riis, 2018) (Figure 1.10).

These formations were laid down in the early Jurassic, following the Permo-Triassic rifting, near the eastern boundary of the northern North Sea Basin (Figure 1.10A, B) (Husmo et al., 2003). The

formation of north-south trending, westward dipping extensional faults that bound eastward tilted fault blocks as a result of subsequent late Jurassic to early Cretaceous rifting defined the structural trap of the Troll Field and the structural configuration of the Johansen and Cook formations in the Northern Lights storage site (Figure 1.10C, D). Here, the Johansen and Cook formations are located at a depth of 2000–3000 m. (Figure 1.10D).

In order to evaluate the primary storage unit and its primary seal, confirmation well 31/5-7 (Eos) was drilled and tested between December 2019 and March 2020 following the seismic mapping of the Johansen and Cook formations over the Northern Lights storage site (Equinor, 2021; Meneguolo et al., 2022). From 2024, 1.5 Mt of CO_2 will be injected into the primary storage unit of the Johansen and Cook formations annually for 25 years (Riis, 2018).

Based on 2D and 3D seismic data, regional well correlations, limited core data from the area (Meneguolo et al., 2022; Sundal et al., 2013; Sundal et al., 2016), and older regional work (Chamock et al., 2001; Marjanac, 1995; Marjanac et al., 1997), the Johansen and Cook formations at the Northern Lights storage site have previously been classified as shallow-marine sandstones. There is still confusion surrounding specifics of the depositional model of the Johansen and Cook formations as well as the effects of sedimentological heterogeneity on CO_2 migration and storage due to the storage site's limited data coverage (Jackson et al., 2022). The majority of published reservoir modeling and flow simulation studies have concentrated on CO_2 storage capacity and plume migration at the whole storage site, taking into account the simple porosity-depth trends, fault transmissibilities, and CO_2 relative permeability-saturation relationships (Jackson et al., 2022).

Several published reservoir modeling studies have taken into account aspects of sedimentological heterogeneity, such as: (1) subdivision of the Johansen Formation aquifer by laterally widespread mudstone layers above marine flooding surfaces (Sundal et al., 2015), (2) Distributions of porosity and permeability determined via seismic inversion and attribute analysis (Sundal et al., 2015), (3) Permeability anisotropy values (k_v/k_h ratio) that reflect the impact of pervasive micaceous laminae and laterally extensive carbonate-cemented concretions (Sundal et al., 2015), (4) Permeability anisotropy values (k_v/k_h ratio), which represent the effects of heterogeneities within sandstones, and variogram-based permeability distributions conditioned to inferred depositional trends, which represent changes in sandstone extent and connectivity (Meneguolo et al., 2022). Although significant amount of studies have been conducted about sedimentological heterogeneities and their depositional analogues, We still need to conduct a thorough evaluation of how these heterogeneities affect CO_2 migration and retention (Jackson et al., 2022).

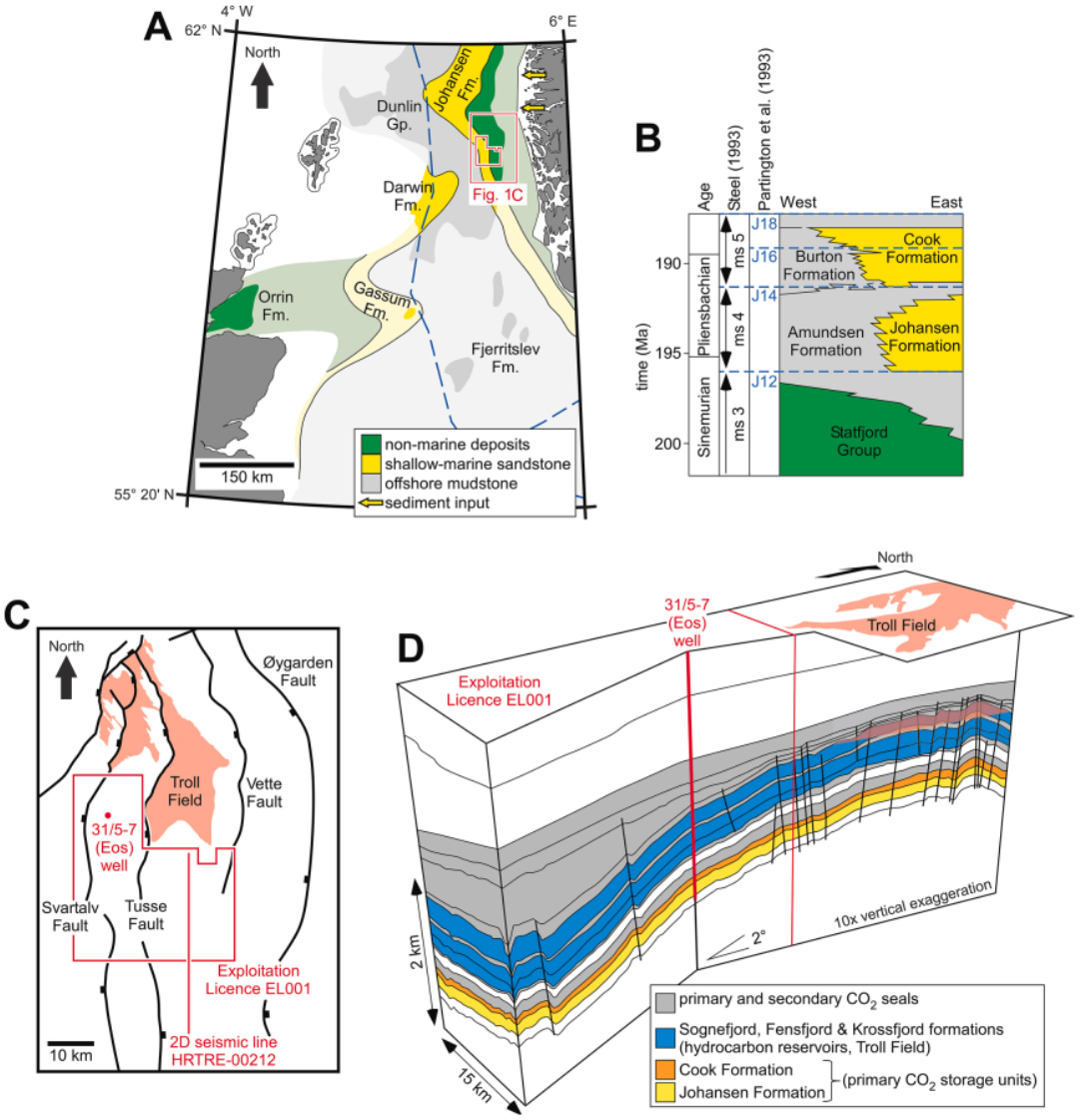

Figure 1.10: (A) Reconstruction of the Pliensbachian's central and northern North Sea's major depositional environments by palaeogeography (Husmo et al., 2003). (B) The upper Statfjord Group and lower-to-middle Dunlin Group sequence stratigraphy and lithostratigraphy offshore Norway are based on the regional maximum flooding surfaces of Partington et al. (1993) and megasequences of Steel (1993). (after Husmo et al. (2003)). (C) Exploitation Licence EL001 and Troll Field are depicted in a condensed manner, with important faults and fault blocks that occurred after the Johansen and Cook formations were deposited. The sites of the 2D seismic line HRTRE-00212 and the 31/5-7 (Eos) well are indicated in Figure 1.9A. (D) The Johansen-Cook CO_2 storage unit's subsurface configuration, as well as the overburden strata in the Troll Field and the western portion of Exploitation Licence EL001 (Figure 1.10C) (Equinor, 2021).

Eigestad et al. (2009) have analyzed the impact of various boundary conditions, sensitivity to vertical grid refinement, and permeability/transmissibility data, as well as the impact of residual gas saturations, as these items have a significant impact on the distribution of CO_2-plumes. Moreover, based on the seismic and borehole data that are now accessible, the geological investigation of

the Johansen Formation is carried out. Additionally, the effect of the selected lateral boundary conditions on the simulation's outcomes has been investigated. Moreover, they demonstrate the necessity of vertical grid refinement for accurate CO_2 plume resolution. The calculations used in the numerical examples in this study, highlight crucial trapping mechanisms. Particularly, stratigraphic traps and residual gas saturation are taken into account. In addition, another outcome of this study is that the relative permeability models that are applied, have a significant impact on how CO_2 spreads. They have also shown that if the integrity of the cap rocks and faults can be confirmed, local domes in combination with sealed faults and cap rocks may offer considerable practical storage volumes. It has also been demonstrated that the permeability description has a considerable impact on the simulated saturation distributions.

1.3 Geology in the Aurora Area

The estimated reservoir temperature is set to 90 °C in the planned injection location at approximately 3 km of burial depth Figure 1.11, along with a typical local geothermal gradient of 30 °C/km. Given the chlorite coating on quartz grains and the high feldspar content (Walderhaug, 1996), the porosity reduction brought on by chemical compaction and quartz overgrowths was estimated to be mild and set at 5% compared to measurements from a distance of around 2 km. From core measurements, horizontal permeability as a function of porosity was deduced (by Shell). The vertical permeability has not been measured. On a micro-scale (mm), it is believed that the presence of oriented mica and long coal pieces in drape layers connected to lower energy settings affects the effective vertical permeability. For comparison, data from the Sognefjord Formation well 31/2-3, which included measurements of both horizontal and vertical permeability, was used. Calcite cemented layers and flooding surfaces are thought to be the key regulating elements on a meso size (m). Silt/clay draping layers are thought to be lateral continuous and have poor permeability. However, in a situation where waves predominate, these might not exist because of erosion (Sundal et al., 2013).

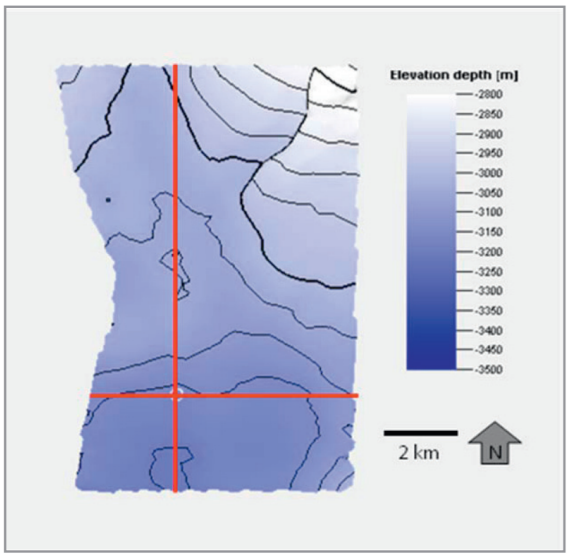

Figure 1.11: Johansen Formation depth map inside the Modeled Area. The injection well is located at the intersection (Sundal et al., 2013).

1.4 Heterogeneity in the Aurora Area

As it is discussed above, the heterogeneity in Aurora model plays a very significant role in fluid flow and CO_2 storage inside the reservoir. While there are a significant amount of studies in this regard, analyzing this effect is very worthwhile, since it determines the CO_2 plume expansion path inside the reservoir.

Jackson et al. (2022) aims to evaluate the depositional model of the Johansen and Cook formations CO_2 storage unit using high-resolution core photographs from the 31/5-7 (Eos) well, develop and assess scenarios for sedimentological heterogeneity in the formations, and identify the key sedimentological heterogeneities that control single-phase flow in the formations. It uses three-dimensional (3D) reservoir models to quantify the impact of heterogeneity on flow. Single-phase flow diagnostics are used to assess the influence of heterogeneity on CO_2 migration and retention. The methodology is fast, efficient and allows a large number of geological scenarios to be explored prior to more detailed flow simulation.

Sundal et al. (2015) conducted a study about the effects of directional anisotropy and site-specific geological heterogeneities on the CO_2 storage potential in the Johansen formation by using scenario modeling. The foundation of this modeling work is a recent data contribution, new 3D seismic data, attribute evaluations, and a change of the depositional model. Differentiated relative permeability curves were assigned in accordance with the diverse reservoir qualities seen in different sedimentary facies. The results showed that depending on the migratory patterns, different amounts of injected CO_2 may dissolve and be retained for up to 80 % after 150 years. Increased sweep through reservoir zones with high irreducible gas percentages and situations where plume separation took place led

to more effective immobilization. The well site and injection strategy, however, play a major role in determining how to increase trapping efficiency.

Sundal et al. (2013) have investigated the effect of site-typical geological heterogeneities of Johansen formation depositional origin through scenario modeling. The aim of this study is to investigate the reservoir properties and the effect of site-typical depositional geological heterogeneities with respect to CO_2 storage in the Johansen Formation (Northern North Sea, Norway). In this study, 5 different geological scenario modeling have been generated in order to assess the effect of geological heterogeneity in the Johansen formation.

1.5 MATLAB Reservoir Simulation Toolbox (MRST)

The Computational Geosciences group at the Department of Mathematics and Cybernetics at SINTEF Digital developed the MATLAB Reservoir Simulation Toolbox (MRST), a free and open-source program for reservoir modeling and simulation. Researchers from Heriot-Watt University, NTNU, University of Bergen, TNO, and TU Delft developed third-party modules for the program, which has a sizable international user base (SINTEF, 2023).

The MRST research tool offers a wide range of data structures and computational methods that can be used as custom modeling and simulation tools. Moreover, it is designed as a research tool for rapid prototyping and demonstration of new simulation methods and modeling concepts. MRST provides thorough black oil and compositional reservoir simulators that can simulate commercial models. Additionally, MRST has user interfaces for post-processing simulation results (SINTEF, 2023).

The software consists of two fundamental modules that provide the basic necessities of functionality and data structures, as well as a huge number of add-on modules that include discretization, solvers, physical models, a variety of simulators, and workflow tools (SINTEF, 2023).

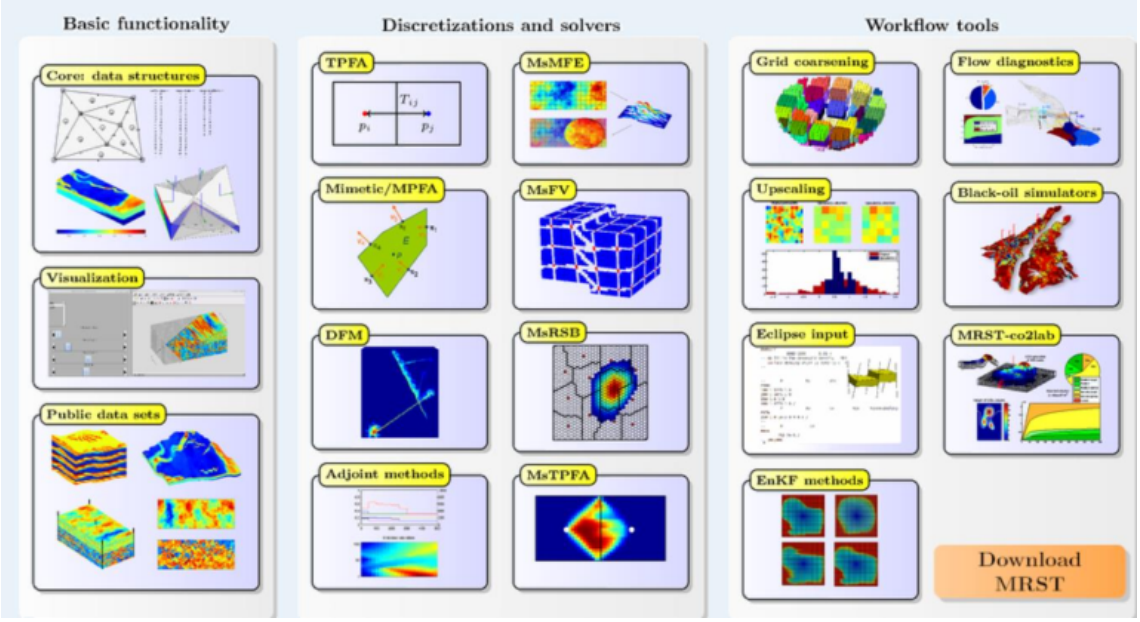

Figure 1.12: MRST's beneficial features (SINTEF, 2023).

1.6 Research Objectives

Following importing the Aurora reservoir model into MATLAB Reservoir Simulation Toolbox, using the Vertical Equilibrium (VE) feature of this simulator, and comparing the simulation results of MRST to the ECLIPSE simulator by Zeynolabedini (2022) as model verification, the purpose of this study is to correct the fluid model in MRST, analyze the model heterogeneity, perform sensitivity analysis on reservoir and fluid model parameters, and investigate the related effects on the CO_2 plume shape in MRST compared to ECLIPSE.

1.7 Project Outline

This thesis contains five chapters. Chapter one is the introduction, background, the Aurora site description, and the research objectives. Chapter two describes the different aspects of CO_2 injection into aquifers and some theories behind this operation. Chapter three summarizes the methodology, problem, model description, and software which are used in this study. Chapter four describes the final results, and discusses the model heterogeneity effects on the CO_2 plume shape, and plume shape comparison between MRST and ECLIPSE. Finally, chapter six mentions some conclusions and recommendations.

2 Theory

In this section, all theories behind CO_2 injection and storage, frameworks, and basic concepts are discussed.

2.1 CO_2 Storage

After injection, CO_2 operates as a low-buoyancy, non-wetting phase that produces a plume in saline aquifer sandstones (Anderson et al., 2005). Initially, structural and stratigraphic traps are the primary locations for short-term (100 years) CO_2 storage. The porosity and permeability properties of the aquifer, the spill points of the trap, and the capillary entry pressure of the seal all affect the possibility for structural and stratigraphic trapping as well as the volume of CO_2 storage. While maintaining a high CO_2 injection rate, high permeability, and effective pore volume allow pressure to be dissipated away from the injection well(s) (Ajayi et al., 2019; Anderson et al., 2005). In saline aquifer sandstones, high effective porosity also tends to increase the capacity for capillary, dissolution, and mineral entrapment over medium- and long-term (100–10,000 years) duration (Ajayi et al., 2019; Gibson-Poole et al., 2010). However, geological heterogeneities that lessen permeability in the storage unit can be significant in two different ways. First, they distribute CO_2, which slows down the rate at which the CO_2 plume reaches the storage site's boundaries, and second, they build stratigraphic traps and baffles at a smaller scale, which improves storage effectiveness (Flett et al., 2007; Gibson-Poole et al., 2010).

2.2 Basic Concepts for Geological Storage of CO_2

The primary idea is to isolate CO_2 from the atmosphere by storing CO_2 that has been obtained from places where anthropogenic emissions of CO_2 occur underground in rock formations. The porous reservoirs of rock formations employed for long-term CO_2 storage are ones that ordinarily contain water, oil, or gas. These permeable reservoirs can be divided into two major categories:

- Saline Aquifer Formations
- Depleted reserves of oil and gas (P. Ringrose, 2020).

By volume, the kinds of porous rock formations known as coal beds, shale units, volcanic rocks, and underground caverns are less significant. We shall concentrate on saline aquifer formations and depleted oil and gas reservoirs in terms of the key processes involved. However, many of the techniques involved are equally applicable to storage in CO_2 EOR projects as well as other storage domains (P. Ringrose, 2020).

Another fundamental idea is that in order to keep CO_2 in a dense state, such as a liquid or a super-critical phase, we must store it relatively deep (more than 800 m) (Figure 2.1). This is crucial for storage effectiveness (greater density equals more efficient storage), which leads to the

widely acknowledged rule that CO_2 storage sites must be deeper than around 800 m. (although the actual transition to the liquid phase also depends on temperature and the local geothermal gradient) (P. Ringrose, 2020).

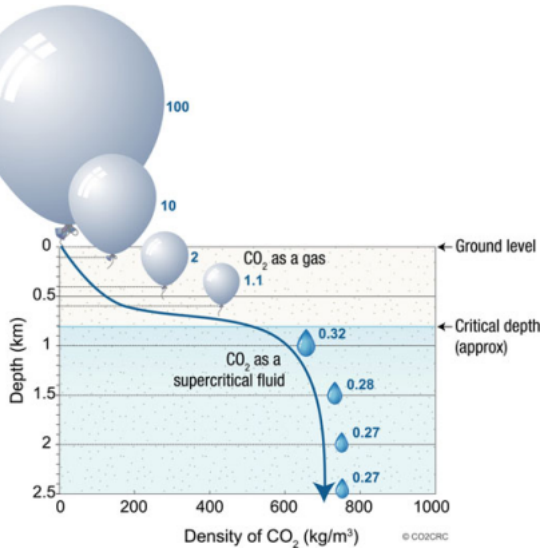

Figure 2.1: CO_2 Density versus depth diagram (CO2CRC, 2021)

For storage security, depth is also crucial, which brings us to the third key idea—the requirement for a storage seal. We enter the realm of compacted and cemented rocks, which may have low-permeable sealing units, as we descend to depths of about 1 km or more (e.g. shales, faults, and salt units). Since natural gas has been confined at these depths for millions of years by geological seals, it seems obvious that CO_2 may likewise be trapped there for an extended period of time.

A deeper CO_2 storage target formation overlain by a mudstone sequence might make up a CO_2 storage system, as shown in Figure 2.2, which depicts a proposed shallow stratigraphic sequence indicative of the North Sea basin. Site investigation and assessment studies should be used to ascertain the actual qualities of sealing units.

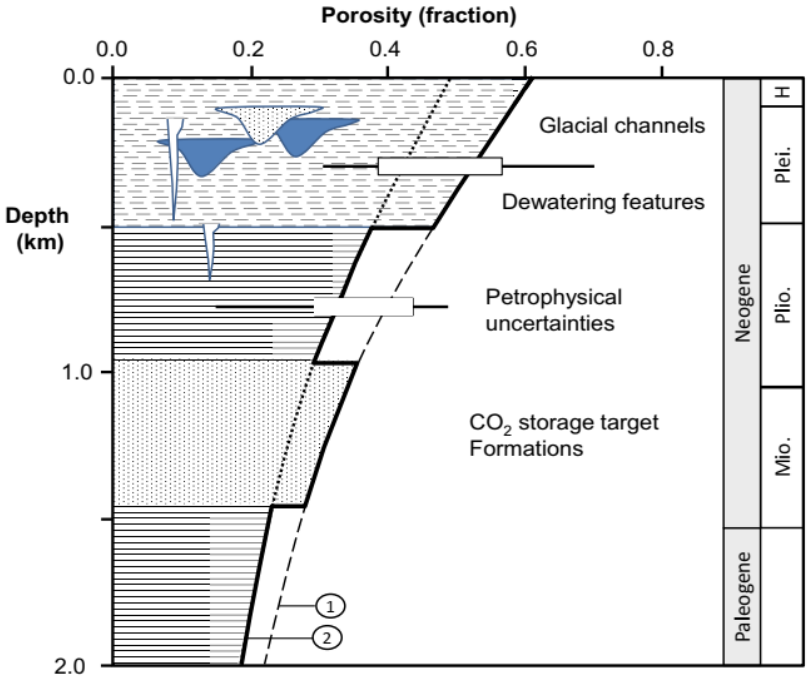

Figure 2.2: An abstract drawing depicting a shallow stratigraphic series from the North Sea basin. Typically, a Pliocene mudstone sequence serving as the primary containment system would cap a Miocene CO_2 storage target formation. A crucial concern for guaranteeing storage confinement may be the function of shallow glacial channels and dewatering features in the underlying Pleistocene sequence. Based on (1) Sclater et al. (1980) and (2) Marcussen et al. (2009), reference porosity curves are displayed. Site research investigations would be required to ascertain the shallow basin sequence's true porosity and permeability (1000 m), which is variable and unknown.

The crucial concerns for every CO_2 storage project are:

• Where can we store the CO_2?

• Which amount of CO_2 can we inject?

• Can we safely store it?

• Is it cost-effective to store?

The three primary storage challenges (Fig. 2.3) are supported by some generic inquiries, as well as some more project-specific inquiries:

• Capacity: Will there be enough room to store the required amount of CO_2 during the course of the project?

• Injectivity: Will the available injection wells allow us to inject CO_2 at a rate that is sufficient?

• Containment: Will the CO_2 stay in the underground storage facility, or may it migrate to another geological formation or perhaps leak out?

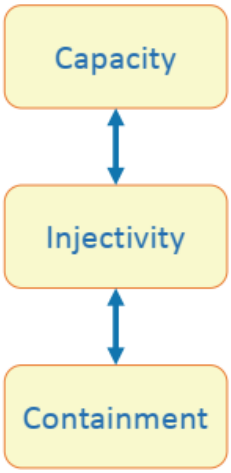

Figure 2.3: The three key storage issues P. Ringrose (2020).

It is helpful at this time to relate these important queries and concerns to the primary stages of a CO_2 storage project (Figure 2.4).

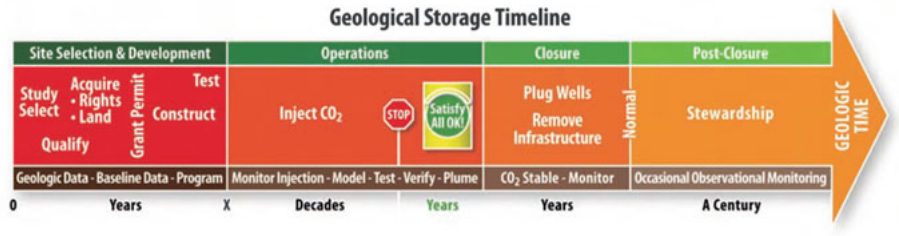

Figure 2.4: Main phases of a CO_2 storage project (from Cooper et al. (2009); Reproduced with permission, CO_2 capture project, www.CO_2captureproject.org/

The three main storage issues are crucial for each phase, but in terms of emphasis, the capacity issue usually takes center stage during the site selection phase, the injectivity issue rules during the site operation phase, and containment is the key concern during the site closure and post-closure phases (P. Ringrose, 2020).

The site selection and development phase also adhere to the principles of maturity and refinement. When decisions are made to move forward with project milestones and eventual site operation, the uncertainties surrounding estimates of capacity, injectivity, and containment should gradually decrease towards an acceptable level as more data is gathered (from regional mapping studies, site surveys, and drilling of exploration and appraisal wells). The right course of action is to reject the site if, during site planning and mapping, any of these difficulties (such as capacity or injectivity proving to be lower than required or containment barriers seeming extremely flimsy) fall below a specified cut-off threshold (P. Ringrose, 2020).

2.3 Injection Mechanism

The three primary CO_2 injection zones—near the wellbore, relatively far from the well, and very far from the well—can be separated in the process of injecting CO_2 from an injector well. The predominant driving force in the area close to the wellbore is the viscous force brought on by the pressure gradient caused by the injection pressure, which pushes the in situ brine during the drainage process. Since the two separate phases are occupying small sizes of pores at this point, there is very little brine evaporation into the gas phase and very little CO_2 dissolution into the brine phase. The extremely low viscosity of the supercritical CO_2 phase causes the CO_2 flow to become unstable, which in some areas results in the fingering phenomenon (Zeynolabedini, 2022).

Heterogeneity is another factor that contributes to fingering since it causes the injected CO_2 to be channeled to permeable routes because the magnitude of permeability varies in different directions. Fluid flow in this area is greatly influenced by the injection flow rate (Zeynolabedini, 2022).

Gravitational forces are in charge of the flow at quite a distance from the well, which means that because CO_2 and brine have different specific gravities, CO_2 migrates upward until it reaches the sealing caprock, which obstructs the upward flow. In this zone, the density difference is crucial because it affects the degree of phase separation, lateral distribution, and vertical migration of the lighter phase. CO_2 must overcome the capillary pressure of the sealing unit when it reaches the sealing caprock to enter the caprock.

Fluid flows primarily as a result of the capillary pressure differential between two phases in the region that is extremely remote from the wellbore where capillary pressure predominates.

The reservoir's heterogeneity, the flow rate, and the disparity in densities between the CO_2 and brine all have a significant role in the plume's geometry and structure. When CO_2 is added to a formation, the brine is displaced until it reaches the irreducible water saturation, from which no extraction is feasible. Injectivity issues may arise when trapped brine turns to solid salt in the pores of the aquifer after evaporating into dry CO_2 that has been injected there (Miri et al., 2016).

Expanding CO_2 storage capability in the formation is primarily mediated by two mechanisms: compressibility and progressive migration of brine. Additional storage areas for CO_2 can be created by the gradual migration of brine either through the caprock or across lateral borders. Due to the capillary pressure barrier, CO_2 can scarcely penetrate caprock; however, brine has a larger likelihood of flowing through the low-permeable caprock, albeit slowly. The third mechanism is compressibility, whereby when pressure rises, brine and CO_2 densities also rise, resulting in a greater volume of fluid being held in the reservoir. Additionally, because of the compressibility of the rock, pore space expands more under increased pressure, creating more area for CO_2 storage.

However, the increased pressure can also have unfavorable effects, such as rock fracture and fault reactivation, which cause CO_2 leakage. Additionally, considering that the differential temperature

between the injected fluid and the rock formation might cause thermal fracture and CO_2 leakage, it is important to include the thermal effect when conducting injection analysis (Thompson et al., 2021).

2.4 Migration mechanism

When the injection operation is terminated, the pressure in the formation begins to decrease, and a short distance from the well, the advection mechanism takes over and dominates the viscous force. Due to gravitational and capillary forces, the fluid phases in the porous medium begin to equilibrate at this point. Meanwhile, beneath the caprock, the CO_2 plume is spreading outward. The trail of CO_2 is displaced by brine as it flows upward due to gravity, but because of capillary pressure, it is impossible to transport all the CO_2; as a result, the remaining CO_2, known as residual saturation, remains trapped in the reservoir. "Residual Trapping" is the name of this trapping technique (Zeynolabedini, 2022).

When CO_2 reaches the top of the formation, sealing the caprock prevents further vertical migration, although CO_2 can still migrate slowly upslope beneath the caprock. "Hydrodynamic Trapping" is the name given to this phenomenon.

It is known as "structural trapping" when CO_2 is permanently trapped in nearby pockets, sealed fault blocks, or salt domes during its upward migration.

The same kind of trapping is known as "Stratigraphic Trapping," but it occurs because of rock type changes, pinch-outs, or unconformities within the storage (Zeynolabedini, 2022).

The CO_2 begins to dissolve into the brine due to the "Dissolution Trapping" mechanism, which creates CO_2-rich brine, as the plume grows under the caprock and widens the area where the two media come into contact. This sort of brine descends to the bottom of the formation known as "Convection Enhanced Dissolution" because it is denser than undersaturated brine.

After some time, in the "Mineral Trapping" mechanism, CO_2-rich brine can slowly precipitate as carbonate minerals, a process that is highly reliant on the chemical makeup of the brine and rock, pressure, and temperature. Figure 2.5 depicts several CO_2 injection and storage movement and trapping mechanisms.

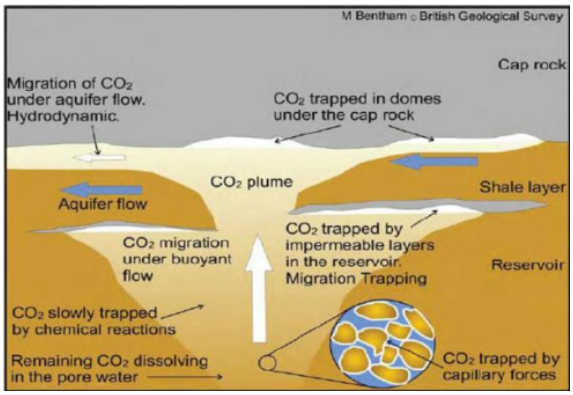

Figure 2.5: various migration methods (Gough et al., 2005)

2.5 Trapping Mechanism

First, the containment theme must be addressed, which is made up of various subsurface CO_2 retaining or trapping systems. These trapping and containment mechanisms can be categorized in a variety of ways, but most essentially, they can be divided into physical and chemical factors:

1. Physical mechanisms of basin-scale processes that help to CO_2 trapping include (P. Ringrose, 2020):
    - Regional structure, basin history, fluid flow, and pressure distribution.
2. Physical mechanisms of structural and stratigraphic trapping:
    - Regulated by the storage complex's rocky architecture;
3. Physical trapping mechanisms related to fluid flow processes:
    - Fluids' capillary interfaces;
    - CO_2 retention as a residual phase;
4. Main geochemical CO_2 trapping mechanisms:
    - CO_2 precipitation as mineral phases;
    - CO_2 dissolution in the brine phase;
    - Sorption/absorption of CO_2 (e.g. on clay minerals);

Figure 2.6 is showing the contribution of different trapping mechanisms during and after injection operation.

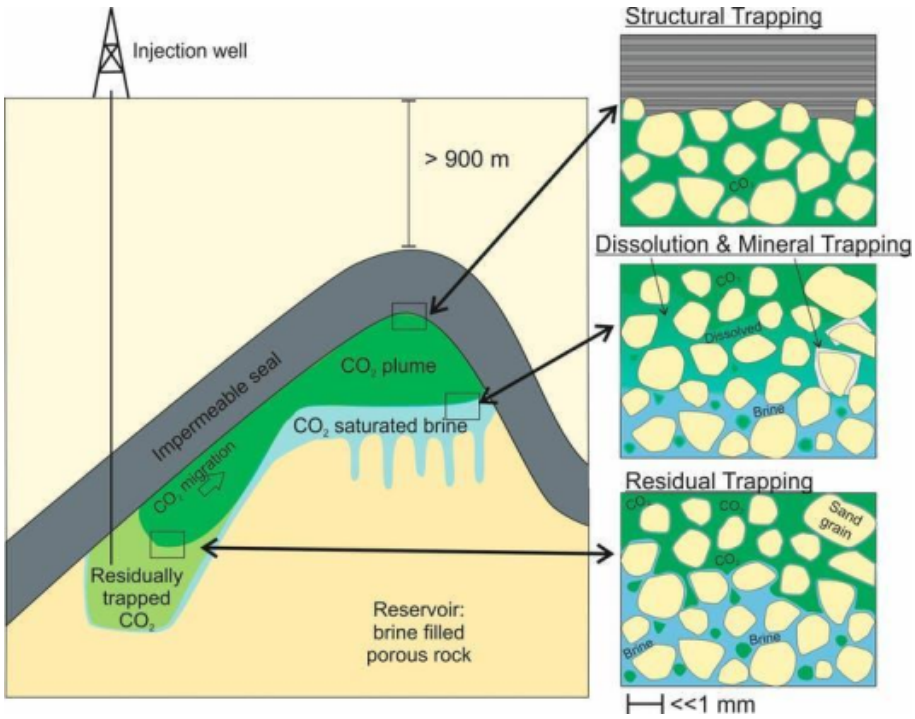

Figure 2.6: Sketches of various trapping techniques before and after injection (Flude et al., 2020)

The IPCC special report (Metz, Davidson, Coninck et al., 2005) conceptually merged these mechanisms into a trapping versus time diagram (Figure 2.7) to illustrate the idea that the different trapping mechanisms ought to cooperate to increase storage security as a function of time. There is broad consensus that this concept is qualitatively accurate, even though there is considerable disagreement over the rates and sizes of the various trapping mechanisms. (From Benson et al. (2005); reprinted with permission from Cambridge University Press).

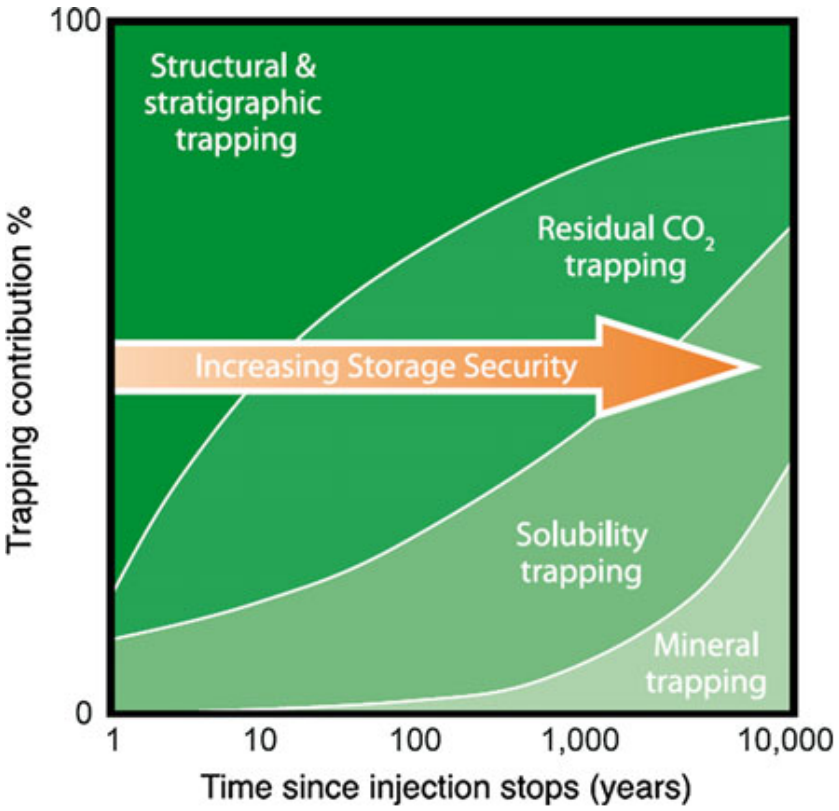

Figure 2.7: CO_2 Storage Trapping Mechanisms (Benson et al., 2005)

2.5.1 Capillary Trapping

The first two mechanisms in this figure are dependent on the capillary trapping phenomenon, which is a physical phenomenon brought on by the interfacial tension at the interface between two fluids in a porous media (Figure 2.8).

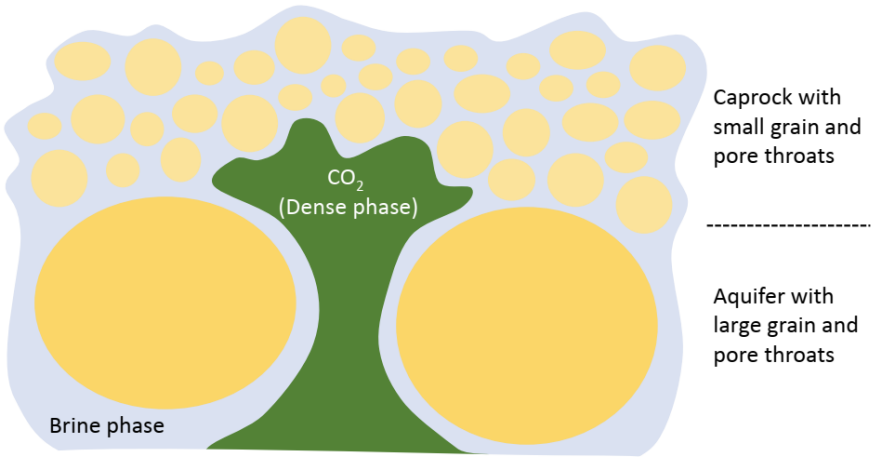

Figure 2.8: A simple schematic of capillary trapping of a CO_2 phase in a water-wet porous media at the intersection of large and tiny pore throats at the aquifer-caprock interface (P. Ringrose, 2020).

It has been well established that interfacial tension plays a crucial role in regulating the amount of subsurface oil and gas accumulations, and the same theory may be used to explain CO_2 accumulations that are either naturally occurring or the result of human activity. The thickness of a gas or oil column, z_g, that can be held against gravity by the capillary entry pressure of the sealing rock was defined by Berg (1975) as follows:

$$z_g = \frac{2\gamma \cos\theta(\frac{1}{r_{cap}} - \frac{1}{r_{res}})}{g(\rho_w - \rho_g)} \tag{2.1}$$

where ρ_w and ρ_g are the densities of water and gas, respectively, r_{cap} and r_{res} are the pore throat radii in the cap rock and reservoir, γ is the interfacial tension, θ is fluid contact angle and g is the gravitational acceleration. The analytical models in (Figure 2.9), which apply to any buoyant non-wetting fluid, serve as an illustration of this idea.

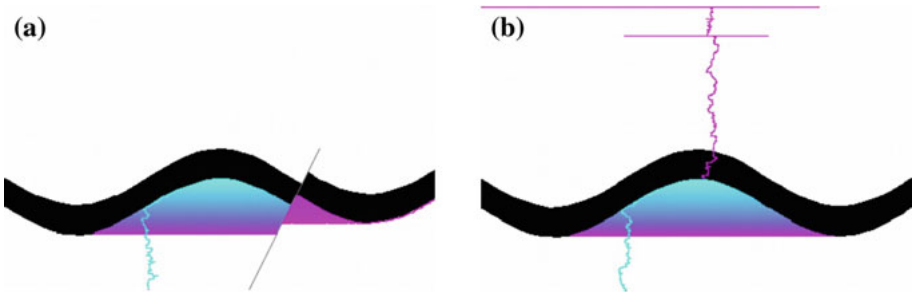

Figure 2.9: Models for analytical capillary trapping that have been modified from those used by P. Ringrose et al. (2000) include: (a) filled trap with a leaky fault and tight caprock (leaking through a lateral spill point); (b) filled trap leaking through caprock (due to a lower capillary threshold pressure in the caprock unit). Black represents the caprock layer; colors indicate migration times for the non-wetting phase (blue early; purple late). The analytical model was simulated using the invasion percolation tool Permedia-Mpath

Consequently, we may calculate the maximum CO_2 column height that can be kept behind a specific caprock unit if we know the pore throat radii, interfacial tension, fluid contact angle, and fluid densities. Keep in mind that temperature, pressure, and composition all have a significant impact on the fluid's properties (especially the brine salinity and the effect of minor gas components). When the fluid clings to the rock surface due to molecular forces, a fluid contact angle of zero indicates perfect wetting, whereas a fluid contact angle of 180° indicates perfect non-wetting (the rock surface repels the fluid).

Residual trapping within the storage unit is the second significant capillary trapping phenomenon. This is a known factor that reduces the amount of oil and gas that can be recovered from hydrocarbon fields, and the same idea holds true for CO_2. Considering the migration of CO_2 plume in a permeable reservoir unit, as the CO_2 rises due to the buoyancy, pore-scale CO_2 trapping causes a trail of leftover gas or liquid to be remained behind (Figure 2.10).

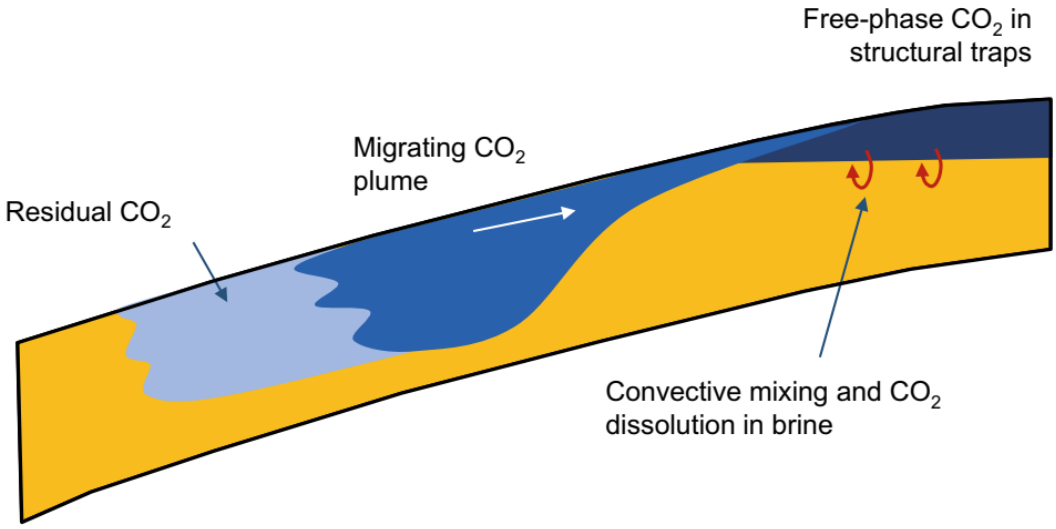

Figure 2.10: illustration of CO_2 Storage flow processes (P. Ringrose, 2020)

The size of the pore throat, the interfacial tension, and the wettability are the three main variables that determine how much trapping occurs. While it is typically true that CO_2 behaves as a non-wetting phase in sandstone reservoirs, certain circumstances could result in partial wetting behavior, particularly for carbonate and clay material surfaces. Along with pressure, temperature, and fluid composition, the contact angle varies as well (P. Ringrose, 2020).

The fluid engineering term for these pore-scale processes, which is governed by molecular phenomena, is "residual CO_2 saturation". As an example, the drainage and imbibition flooding cycles were recorded, resulting in a measured residual CO_2 saturation of 22 % (Sw = 0.78), as shown in Figure 2.11, which is an example of CO_2-brine relative permeability curves. The true degree of residual CO_2 trapping, however, is typically determined using dynamic flow simulations since rock heterogeneity and fluid dynamics play a significant role in controlling the residual saturation as well as pore-scale processes (although analytical approaches can also be used).

A gravity-stable body of CO_2 inside a structural trap that was filling from the top would have virtually no residual trapping volume, which is another reason why the CO_2 plume must migrate in order to generate residual trapping. Recent reviews and insights into the accurate measurement of residual CO_2 trapping have been offered by Krevor et al. (2015) and Reynolds et al. (2015).

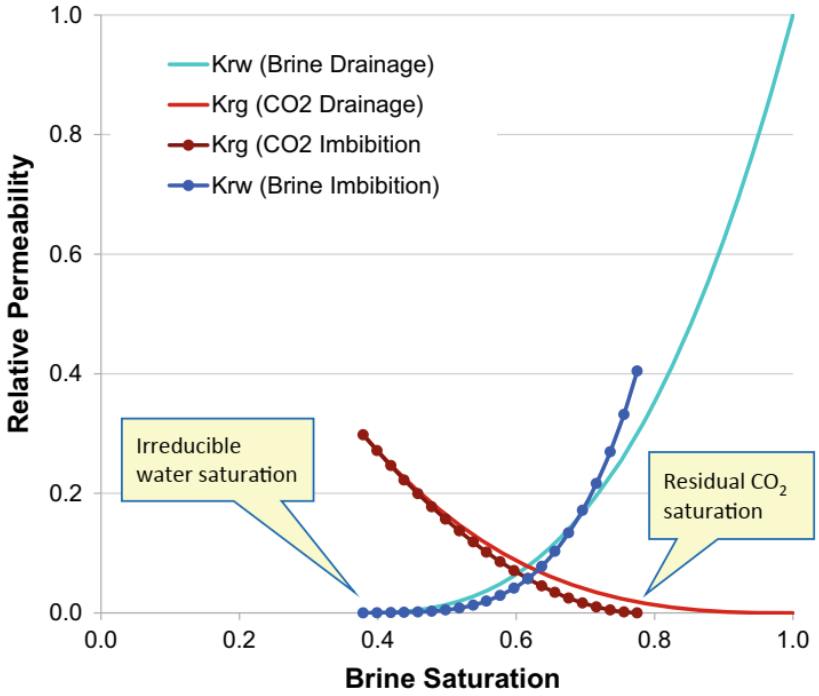

Figure 2.11: Example CO_2-Brine relative permeability curve (Bennion et al., n.d.)

2.5.2 Geological trapping

Given a thorough understanding of the fluid physics governing CO_2 trapping mechanisms, it is crucial to emphasize—perhaps too obvious for some—that the geological system ultimately determines how well CO_2 containment and trapping mechanisms work. As a result, any genuine CO_2 storage project must put in the time and effort necessary for site assessment and reservoir characterization (e.g. Gibson-Poole et al., 2008). It may be less clear how the multi-scale character of geological systems necessitates the assessment of a wide range of geological events and occurrences in order to evaluate the various trapping mechanisms. As a result, basin scale processes, structural geology, sedimentary geology, and small-scale petrophysical investigations must all be included in geological characterization work.

2.5.3 Geochemical trapping

The CO_2 molecule is crucial to the Earth's carbon cycle because it is produced and consumed in a variety of organic and inorganic chemical processes. When, for instance, the shelly material from marine life is dissolved in acid (rainwater is slightly acidic), the result is carbonate dissolution, which is one of the most significant natural reactions and produces CO_2 in the process:

$$CaCO_3(s) + 2HCl(aq) \rightarrow CaCl_2(aq) + CO_2(g) + H_2O(l) \tag{2.2}$$

A key reaction in the weathering of carbonate rock formations, producing limestone caves, and

causing the scale to precipitate in areas with hard water occurs when surface waters are saturated with carbon dioxide and calcium carbonate. The primary carbonate weathering reaction is as follows:

$$CaCO_3 + CO_2 + H_2O \rightarrow Ca(HCO_3)_2 \tag{2.3}$$

Conversely, a reaction between calcium hydroxide (Portlandite) and CO_2 (from air or water) can result in the formation of carbonate minerals, which is significant for wellbore cement types and concrete:

$$Ca(OH)_2 + CO_2 \rightarrow CaCO_3 + H_2O \tag{2.4}$$

These are the most important reactions in CO_2 mineralization trapping in the reservoir.

Early CO_2 storage injection operations like Sleipner, In Salah, and Snøhvit have provided evidence that geochemical reactions are gradual and rather small (Black et al., 2015; Carroll et al., 2011), with almost all the CO_2 remaining as a distinct phase (liquid, gas, or dense phase). Wilkinson et al. (2009) demonstrated that, after tens of millions of years, 70–95 percent of the CO_2 is present as a free phase in an analysis of data from a natural CO_2 reservoir (a CO_2-rich gas field), with only about 2.4 percent of the CO_2 stored in the mineral phase and a comparable amount dissolved in the pore waters.

The main takeaway from this is that although dissolution and precipitation events do happen when new CO_2 is introduced into the subsurface, the CO_2 quickly creates a new chemical equilibrium with the in-situ pore fluids, after which reaction rates are very sluggish. However, considerable CO_2 dissolution into the brine phase can occur.

The potential reactions and consequences that might take place when CO_2 comes into contact with clay minerals are quite complex. However, this fixation of CO_2 in the mineral system is related to a combination of processes including aqueous solubility, geochemical reactions, and physical sorption on clay minerals. Busch et al. (2008) demonstrated that gas sorption could lead to significant CO_2 storage capacity in shale sequences (Figure 2.12). The porosity, permeability, and diffusion characteristics of shales could potentially be affected by geochemical processes such as silicate mineral dissolution and carbonate mineral precipitation.

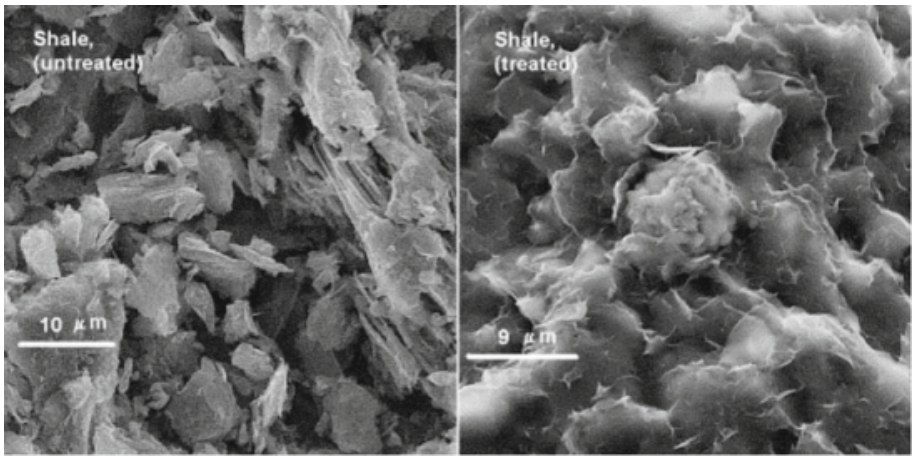

Figure 2.12: Effect of CO_2 reaction with shale (Kaszuba et al., 2003).

Therefore, to sum up the geochemical features of CO_2 storage, it is possible for some CO_2 to be trapped (or bonded) as a mineral phase, but the rates of reaction are very slow. Carbonate minerals may also dissolve to some extent, though once more at extremely slow rates. Therefore, a site-specific assessment of these processes will be necessary to evaluate a suitable geological storage location. Typically, responses in the wellbore environment are the most concerning.

2.5.4 CO_2 Dissolution

Injected CO_2 has a tendency to expand horizontally beneath the caprock, which leads to the development of a contact area between CO_2 and brine and, on a long-term scale, the dissolution of CO_2 into the brine. Dissolution trapping is the name of this procedure. The following chemical reaction provides the basis for the dissolution:

$$CO_2(g) + H_2O \leftrightarrow H_2CO_3 \leftrightarrow HCO_3^- + H^+ \leftrightarrow CO_3^{-2} + 2H^+ \tag{2.5}$$

CO_2 dissolution in the brine phase is the most significant geochemical response for projects including CO_2 storage. The influence of this process on long-term storage has significant potential, but the related estimates can vary enormously. We are aware of how slowly CO_2 molecules diffuse through a saline aqueous phase (Bensabat, 2017). We also know that the rate of CO_2 dissolution is mostly determined by the considerably faster convective mixing mechanism at the CO_2-brine interface (Figure 2.13). Before convection happens, a diffusive boundary layer needs to form and reach a certain thickness in order to start convective mixing.

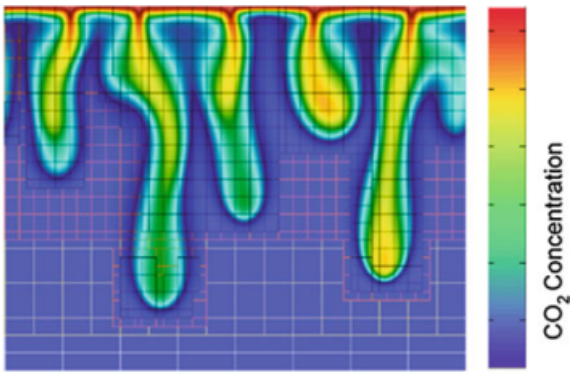

Figure 2.13: Density-driven flow in CO_2 storage in saline aquifer(Pau et al., 2010).

Riaz et al. (2006) showed through numerical analysis based on experimental data that the critical time (t_c) for convection to begin and the characteristic wavelength (λ_c) are predicted to be in the range of:

- 10 days $< t_c <$ 2000 Years
- 0.3 m $< \lambda_c <$ 200 m.

Although this is a rather wide range, it clearly shows the anticipated dimensions and associated uncertainty. The actual rate of this process will depend on the in-situ fluid conditions and the intricate geological architecture. It seems likely that the actual in-situ CO_2 dissolving rate in the Sleipner example, where we have solid monitoring data on the expansion of the plume, is between 0.5 and 1 percent per year, or roughly 10 percent after 20 years (Alnes et al., 2011; Cavanagh et al., 2015; P. S. Ringrose, 2018). Recent laboratory measurements of dissolution rates in porous media (with supercritical CO_2 at in-situ conditions) show a 0.5 m thick CO_2-saturated water layer below the CO_2 layer after 5 years, indicating a 2 m thick layer would be expected at Sleipner after 20 years. This level of CO_2 dissolution is also consistent with field monitoring results (Amarasinghe et al., 2020).

2.6 CO_2 Properties

At atmospheric pressure, CO_2 has a density of 1.87 kg/m^3, making it heavier than air and a thermodynamically stable gas. CO_2 is somewhat compressible and exhibits a variety of thermodynamic behaviors. According to Figure 2.14 , CO_2 forms a liquid phase at high pressure and temperatures. As pressure and temperature rise even higher, CO_2 transitions into a supercritical phase, where its density ranges from 150 to more than 800 kg/m^3 (Bachu, 2002).

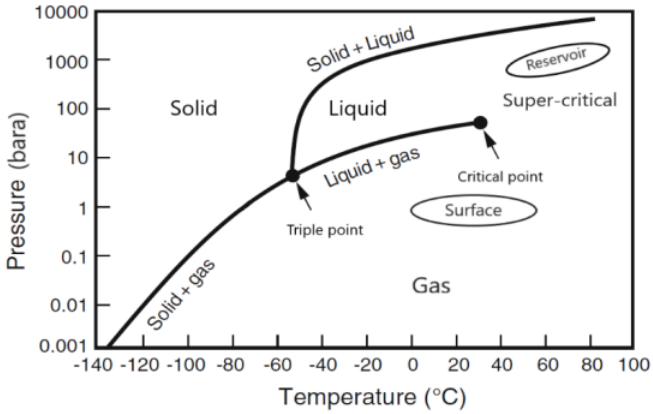

Figure 2.14: CO_2 Thermodynamic Diagram (Bensabat, 2017).

As was previously said, CO_2 is typically injected into the reservoir in the liquid or super-critical phase since it is denser and takes up less space, making the procedure easier. The porous medium is completely saturated with brine at the first step of the injection process, and its salinity ranges from 10 to 100 g/L (Bensabat, 2017). CO_2 can exist in a variety of phases depending on temperature and pressure, including solid, liquid, and gas. It can also coexist in a two-phase system. Additionally, two particular circumstances may occur. The first one is a "triple point," where three phases coexist at once, and the second is a "critical point," when the gaseous and liquid phases change seamlessly. Since pressure and temperature are above the critical threshold in a deep saline aquifer, CO_2 is in a super-critical state.

Equation of State (EOS) is used to explain the relationship between pressure, temperature, volume, and CO_2 characteristics in the set of thermodynamic conditions (pressure and temperature). The Gibbs phase rule equation, which is used to determine a fluid system's degree of freedom, is shown in the equation below:

$$F = C - P + 2 \tag{2.6}$$

F, C and P are the variables in this equation that represent the degrees of freedom, components, and phases, respectively. If we have two state variables, such as pressure, temperature, or composition, two degrees of freedom, for instance, entails the ability to estimate a third state variable, such as density.

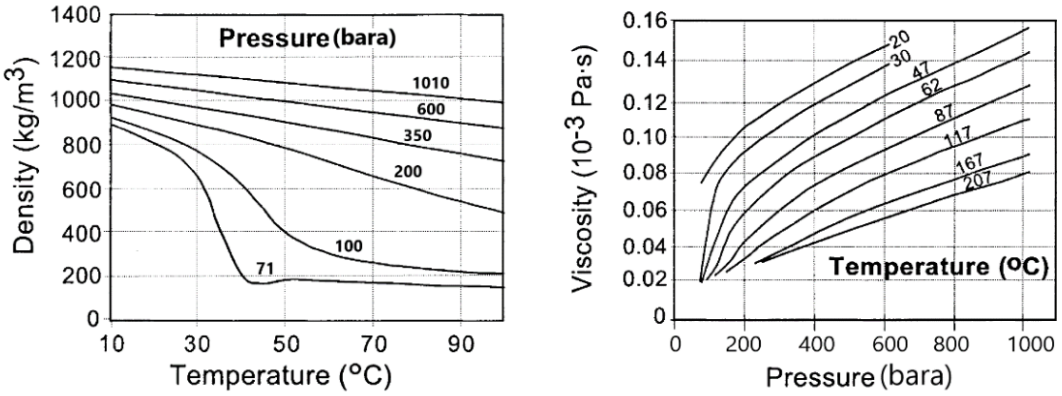

Figure 2.15: Left: Relationship between CO_2 density, pressure, and temperature for liquid and super-critical phase; Right: Relationship between CO_2 viscosity, pressure, and temperature for liquid and super-critical phase (Bachu, 2002).

Figure 2.15 (Left) illustrates how increasing temperature causes the density to decrease while increasing pressure causes the density to rise. As a result, density has an inverse relationship with temperature and a direct relationship with pressure. Furthermore, Figure 2.15 (Right) shows that the viscosity of CO_2 in the liquid and super-critical phases is directly related to pressure, and inversely related to temperature. However, viscosity in the gaseous phase has a direct relationship with temperature.

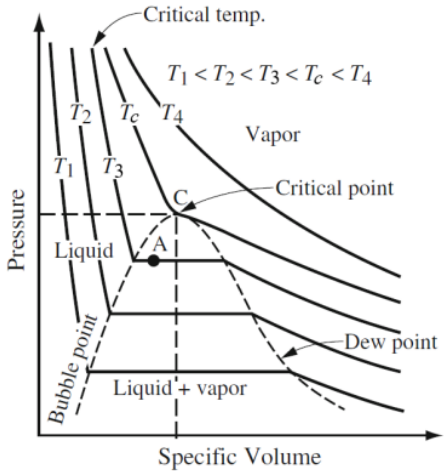

Figure 2.16: Relationship between CO_2 pressure, temperature and specific volume (Bensabat, 2017).

Specific volume is another state variable that is frequently employed in EOS. Volume per mass unit is the definition of this quantity, which has an inverse relationship to density and a value of $1/\rho$. Pressure, temperature, and specific volume are related in Figure 2.16. According to this graph, CO_2 has a lower specific volume at low temperatures, which is very advantageous when injecting CO_2. On the other hand, a large disparity between the temperature of the formation and the CO_2 might have unfavorable effects, such as thermal fracture, which may result in CO_2 leakage.

2.7 Reservoir simulations and modeling for CO2 injection

"Reservoir Simulation" is one method for forecasting reservoir behavior during CO2 injection. Moreover, it is a technique that analyzes and predicts how fluids will flow through the reservoir rock to the stock tank or transport pipeline over time using a numerical model of the geological and petrophysical properties of a subsurface reservoir, the (multiphase) fluid system, and the production equipment (wells and surface facilities) (Lie, 2019). This technique uses computer software to numerically solve fluid flow equations and simulate the performance of a reservoir. Since temperature is regarded as a weak parameter in terms of altering rock and fluid properties, PVT data input for the reservoir simulator is often gathered under isothermal settings. However, temperature effects may result in fractures in the formation and caprock, therefore the thermal effects of CO2 injection near the wellbore are extremely significant (Thompson et al., 2021). Moreover, the temperature can change the fluid properties significantly, which bring some issue in black-oil simulation, in which the constant temperature simulation is carried out.

Generally speaking, it is highly challenging to monitor, comprehend, and quantify all the elements that affect the flow behavior of dynamic fluids inside a reservoir, as well as to define the physical processes involved. Therefore, there is a great deal of uncertainty when predicting how a reservoir will produce over time and in response to various driving and displacement processes (Lie, 2019).

Beginning in the middle of the 1950s as a way to quantify and lessen this uncertainty, the simulation of petroleum reservoirs has since grown into a crucial instrument for both qualitative and quantitative prediction of the flow of fluid phases. Reservoir engineers use reservoir simulation to investigate displacement processes, contrast and compare the characteristics of various production scenarios, or as part of inverse modeling to calibrate reservoir parameters by integrating static and dynamic (production) data. Reservoir simulation is a complement to field observations, pilot and laboratory tests, well-testing, and analytical models (Lie, 2019).

Reservoir modeling is mostly utilized in the broad picture to aid with two different sorts of judgments:

1. to optimize development plans for new fields, and
2. to support operational and investment decisions.

2.7.1 Fluid modeling

Different methods are used by reservoir simulators to process fluid compositions. The fluid for CO2 injection can be modeled in two different ways:

1. **Black-oil model**

   Water, gas, and oil are the three elements that make up this model. Since gas can dissolve in oil in a commercial simulator and be controlled using PVT tables, CO2 injection simulations consist of two components: gas and oil, which represent water and CO2 respectively.

2. **Compositional model**

   The equation of state (EOS), which is used in this model to handle composition variations of a particular fluid phase, demands substantially more calculation time than the black-oil model. This model allows processing of more numerous components in the simulation.

2.7.2 Reservoir modeling

A simulation model has three primary components to mathematically represent the subsurface flow processes. First, a mathematical flow model that depicts fluid movement in a porous media is required. These models are frequently presented as a collection of partial differential equations that represent the mass conservation of fluid phases along with an appropriate collection of constitutive relations that explain the link between various physical parameters. Second, a geological model describing the specified porous rock formation is required (the reservoir). The reservoir simulation model is created by combining the geology model with the flow model, which is realized as a grid populated with petrophysical parameters. The wells and production facilities that transmit pressure and fluid between the reservoir and the surface also need to be modeled as well (Lie, 2019). Figure 2.17 shows the three main constituents of reservoir modeling.

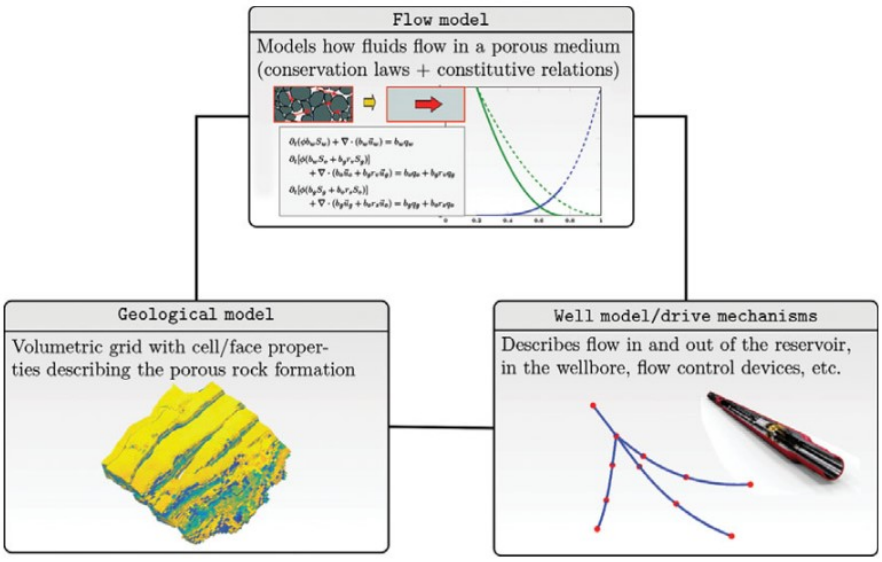

Figure 2.17: The main parts of a reservoir simulation model (Lie, 2019).

It is challenging to anticipate reservoir flow scenarios with accuracy. One problem is that we can never characterize the rock properties that affect the flow pattern completely and accurately.

Even if we could, we wouldn't be able to run simulations that fully utilize the knowledge since this would necessitate computer resources well above what is accessible on contemporary multiprocessor machines. On the other hand, a contemporaneous depiction of the flow scenario on all scales down to the pore scale is neither necessary nor desired. Usually, describing the broad trends in the reservoir flow pattern suffices for reservoir management (Lie, 2019).

Early reservoir simulation models were constructed using two-dimensional slices, with 10^2–10^3 Cartesian grid cells standing in for the entire reservoir. Modern reservoir characterization techniques, on the other hand, can represent porous rock formations using grid-blocks down to the meter scale. As a result, three-dimensional models with millions of cells are produced. Stratigraphic grid models, which are the current norm in the industry, are based on the extrusion of 2D areal grids to create volumetric descriptions. Unstructured grid-based techniques, however, are becoming more and more popular (Lie, 2019).

Commercial reservoir simulators are infrequently utilized to execute simulations directly on geological grid models, despite an astounding rise in computer power and much study on computation approaches. Instead, some form of upscaling of the geophysical characteristics is used to create coarse grid models with grid-blocks that are typically ten to one hundred times larger. The method for carrying out this scaling is not simple. In reality, one of the most active research fields in the oil business has been and likely still is upscaling. This effort reflects the widespread belief that it is unrealistic to expect to conduct simulations directly on geological models in the near future due to the size and complexity of geological reservoir models, which are always growing (Lie, 2019).

The advancement of numerical methods has been equally important to the advancement of better computers, innovative and more reliable upscaling technologies, and more thorough reservoir and fluid characterization. Modern simulators use numerical techniques that can benefit from numerous processors, distributed memory computer systems, adaptive grid refinement methodologies, and linear complexity iterative techniques. There are several distinct numerical schemes for the simulation, each with advantages and disadvantages. With all these tools at our disposal, we observe a shift away from traditional approaches that were created for a broad class of differential equations, toward methods from the cutting edge of research that are geared to a specific set of applications and mathematical models (Lie, 2019).

Together, these advancements have made it possible for reservoir engineers and geologists to create increasingly intricate geological and reservoir models. It is definitely crucial to keep developing these models in order to comprehend the reservoir better and lower uncertainty. However, you shouldn't forget that a simulation study's primary goal is to assist your business in making better decisions. As a result, the study's value typically depends on how much it influences those decisions and results in higher profit, such as by boosting recovery and/or lowering capital expenditures (CAPEX) or operational expenses (OPEX) (Lie, 2019).

It may thus not be essential to develop a very sophisticated model that includes all conceivable physical effects in order to provide a response to a particular query. In fact, a simulation model should be as basic as feasible, but not simpler, to paraphrase the well-known Occam's razor. In the upcoming years, hybrid modeling—which mixes models based on physical principles with data-driven methodologies—will likely become more prevalent (Lie, 2019).

Like other industrial processes, CO2 storage demands a substantial financial commitment, thus it needs to be properly researched. In order to forecast the behavior of CO2 in the reservoir, researchers have developed a number of methodologies, including numerical and analytical analysis of CO2 modeling. For instance, certain analytical models are suggested to estimate the storage capacity of saline aquifers, anticipate the growth of CO2 migration, and predict pressure accumulation during storage operation. Additionally, by taking into account Forchheimer flow of CO2 and brine, a solution is proposed to estimate the pressure elevation in aquifers using the vertical equilibrium approach (Zeynolabedini, 2022).

The assumptions in these models are so simple that even though analytical solutions can work extremely quickly, they are unreliable for risk assessment and final decision-making. Therefore, in CO2 injection and storage operations, numerical modeling performs significantly more accurately. For CO2 storage, there have been three different numerical methodologies used: vertical equilibrium modeling (VE), grid-based numerical modeling, and streamlining simulation (Zeynolabedini, 2022).

The VE technique has been used in this study. The primary presumption in the VE model is that the flow system is in vertical equilibrium, meaning that the vertical distribution of fluid phases can be calculated using an analytical expression. Due to the fact that VE models only have one layer in the vertical plane, all simulations and computations are carried out in the horizontal direction, which takes substantially less computational time than 3D modeling. This layer might be homogeneous or heterogeneous depending on the geological characteristics of the reservoir. This model focuses more on the significant vertical migration of CO2 and brine phase than viscous forces because of the large density difference between phases. This model's primary drawback is that it is unable to account for heterogeneity in the vertical direction (Zeynolabedini, 2022).

The fluid flow equations (Darcy's law) and problems involving mass conservation are solved numerically using a variety of techniques, such as finite difference, finite element, and finite volume with accurate estimation. These models, although are very effective on the results in the end, can be computationally expensive and typically are not precise in the early stages of the simulation due to the uncertainty of the data collected (Zeynolabedini, 2022).

The uncertainties can be greatly decreased by using techniques like seismic surveys, core analysis, well logging, and well testing. Additionally, by taking data history into account—a process known as history matching—and gathering fresh data, these models can be later modified. The ability to take into account all data in both vertical and horizontal directions, as well as to relate significant

physical processes like geochemistry, thermal changes, and geomechanics, is the main benefit of employing numerical simulation (Zeynolabedini, 2022).

3 Methodology, Problem and Model Description

The investigation of this study is the continuation of the specialization project, which has been conducted by Zeynolabedini (2022). In the mentioned project, the Aurora model is imported into MRST in order to use the Vertical Equilibrium module to simulate the 2D model of CO_2 injection. The results from MRST and ECLIPSE, a commercial simulator, are then compared with one another to ensure that the VE simulation performs accurately. While proper **GRID** model import from ECLIPSE model to MRST is focused by Zeynolabedini (2022), in this study the proper **FLUID** model import from ECLIPSE to MRST, and sensitivity analysis of reservoir and fluid model parameters are taken into consideration.

3.1 Software

The software programs employed in this study are MATLAB Reservoir Simulation Toolbox (MRST), which is developed by SINTEF, and ECLIPSE slb, as a commercial simulator. In this section, these programs and the related features, which are used in this study, are described.

3.1.1 MRST

The purpose of the MRST research tool is to assist in studies on the modeling and simulation of flow in porous media. This software expands MATLAB in the direction of reservoir modeling by providing a large range of mathematical models, computational techniques, charting tools, and utility routines. As shown in Figure 3.1, the program is organized very similarly to MATLAB and comprises a collection of core routines and a set of add-on modules to make it as versatile as feasible (Lie, 2019).

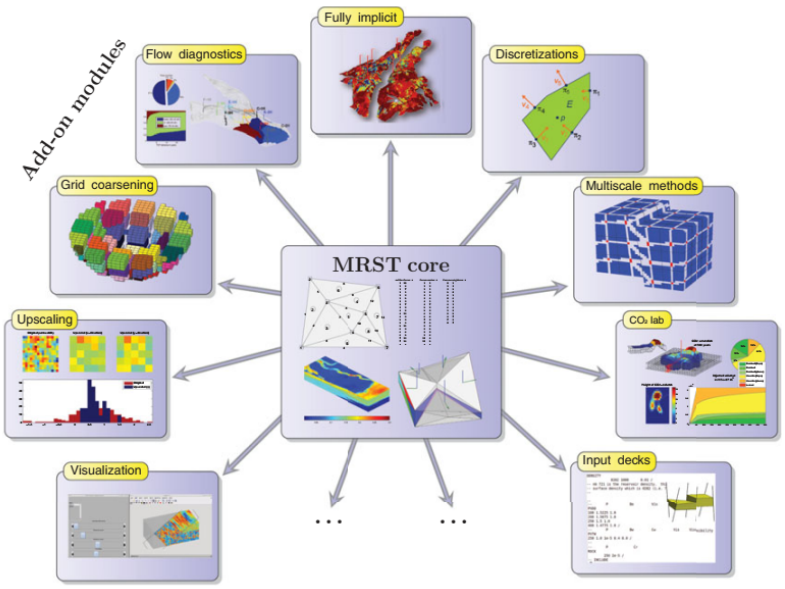

Figure 3.1: A set of add-on modules for MRST provide discretizations and solvers, simulators for compressible and incompressible flow, and a variety of workflow tools, including flow diagnostics, grid coarsening, upscaling, visualization of simulation output, and others. The core functionality of MRST offers fundamental data structures and utility functions (Lie, 2019).

Routines and data structures for constructing and manipulating grids, petrophysical data, and global driving mechanisms like gravity, boundary conditions, source terms, and wells are all part of the general core functionality. The core functionality also includes a few routines for plotting cell and face data defined over a grid, as well as an implementation of automatic differentiation - you write the formulas and specify the independent variables, and the software computes the corresponding derivatives or Jacobians - based on operator overloading. Future versions of the software are not anticipated to dramatically alter the fundamental functionality, which is thought to remain stable (Lie, 2019).

MRST core lacks flow equations, discretization, and solvers in order to save maintenance costs and increase flexibility; these are implemented in several add-on modules. For example, `incompTPFA` solver from the `incomp` module implements fluid behavior and standard solutions for incompressible, immiscible, single-phase, and two-phase flow (Lie, 2019).

MRST Data sets

Adequate data sets are necessary to allow the testing of novel computational techniques in a practical environment. Such data sets are difficult to get, thus MRST developer (SINTEF Digital) made an effort to make it easy to access a variety of open data sets that are available for free download. All examples discussed in the guidance book either use MRST to create their input data or rely on openly available public data sets that can be downloaded for free from the internet,

with some exceptions that are based on data that cannot be publicly disclosed (Lie, 2019).

MRST provides a graphical user interface to streamline data set administration. `mrstDatasetGUI()` can download and unpack the majority of data sets to the appropriate subfolder of the default path in addition to listing all public data sets that the software is aware of and providing a brief description of each. Some of the data sets that are accessible through the graphical user interface are shown in Figure 3.2.

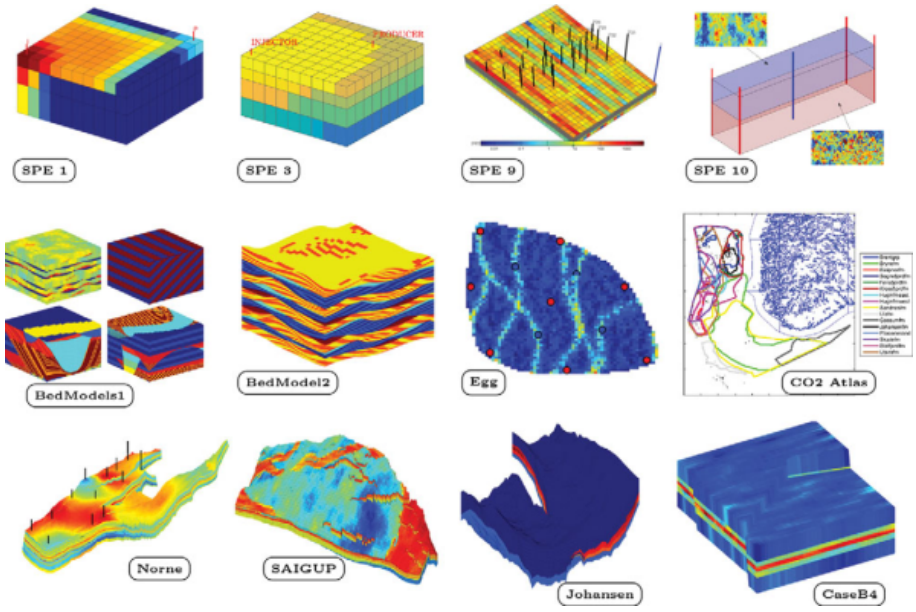

Figure 3.2: Free data sets examples in MRST (Lie, 2019).

MRST Modules

Grids, petrophysics, discretization, and solvers for incompressible flow are all covered in the MRST guidebook. Additionally, it explains how to create fully implicit multiphase simulators in MATLAB by combining automatic differentiation, a flexible grid format, discrete differential operators, and vectorization. Additionally, the guidance book describes grid coarsening, upscaling, and flow diagnostics (Lie, 2019).

A straightforward tool for expanding and changing the feature set is the module system. The module architecture, in particular, allows for the on-demand activation and deactivation of sophisticated features that are not essential to the core functioning (Lie, 2019).

The `mrstPath` function on your computer maintains the mapping between module names and paths. The paths must be complete paths to already-existing folders on your computer. You can use the `mrstPath` function as a command to find out which modules are included in your current installation.

The software will list every module it is aware of and has the ability to activate. You can use the

function `mrstModule` to activate a certain module.

For instance by calling: `mrstModule add ad-blackoil ad-core co2lab deckformat coarsegrid`, five useful modules in this study will be loaded by MRST. These modules are detailed below:

1. **`ad-blackoil`**: In order to implement the black-oil equations for multiphase, miscible, and compressible flow, this module includes additional models. The module offers solvers for one, two, and three phases. In three-phase solutions, oil can evaporate into the gas phase (Rv) and/or gas can dissolve into the oil (Rs). Various boundary conditions, source terms, wells with production limits, and wells with multiple segments are also supported by the solver.

2. **`ad-core`**: This module is not a complete simulator, but it provides the common framework that is used in other modules, such as `ad-blackoil`. This framework consists of abstract classes for reservoir models, for time-stepping, nonlinear solvers, and linear solvers, as well as functionality for variables updating/switching and routines for plotting well responses.

3. **`co2lab`**: The outcomes of more than ten years of academic study and development on CO_2 storage have been compiled in this module. It includes computational techniques and graphical user interfaces to depict migration path, which makes it easier to analyze long-term trapping in massive saline aquifers. Additionally, upper theoretical bounds on the structural, residual, and solubility trapping can be computed using this module. Additionally, it oversees the effective simulators that use a vertical-equilibrium formulation to compute precise trapping potentials and investigate pressure build-up and plume migration.

4. **`deckformat`**: This module enables the entry of full simulation decks from the ECLIPSE format, including input reading, unit conversion to SI, and creation of MRST objects for grids, fluids, rock characteristics, and wells. For the fully implicit simulators created in the ad-backoil and ad-eor modules, this module is absolutely essential.

5. **`coarsegrid`**: The basic grid structure for coarsegrid representation is defined in this module, along with some straightforward techniques for integrating grids with Cartesian topology (Lie, 2019).

3.1.2 ECLIPSE

This program is a hydrocarbon reservoir simulator, which offers techniques for numerically solving reservoir flow equations to forecast fluid flow behavior in the reservoir. This program can also provide planning and management for reservoir development. ECLIPSE can also be used for a variety of purposes, such as heavy oil recovery, water flooding, and chemical-enhanced oil recovery. The black oil, compositional, thermal, vertical equilibrium, and streamline simulations are only a few of the many simulation types that can be controlled by ECLIPSE Schlumberger. In this study,

Table 3.1: ECLIPSE DATA file section

Section	Function
RUNSPEC	Simulation set: title, unit system, present phases, start date, simulation grid dimension.
GRID	Grid dimensions, shape, porosity, permeability, and fault
EDIT (Optional)	Grid structure adjustment
PROPS	Fluid and Rock properties
REGIONS (Optional)	Sub-regions definition
SOLUTION	Model Initialization
SUMMARY (Optional)	Saving parameters definition
SCHEDULE	Well placement, operation schedule, and reports in time steps

the CO_2 injection and storage operation is only studied using the black-oil simulator of ECLIPSE (Zeynolabedini, 2022).

The reservoir and fluid data are read by the ECLIPSE simulator in the initial stage, where they are processed at a starting date. In the actual simulation stage, time is advanced, and the reservoir conditions—including pressure and saturation—are evaluated and calculated based on the timing of the previous timestep. Eight components make up the ECLIPSE data file, of which five are necessary and three are optional (see Table 3.1).

Controlling variables, such as timesteps and well specifications, are defined in the SCHEDULE section, and the model's initial input data is given in other sections. Although the simulator arranges the simulation input data file automatically, the aforementioned sections must be defined in the correct order.

Black-Oil Simulator

The ECLIPSE 100 or E100 black-oil simulator offers one, two, or three-phase systems. Since gas (CO_2) is assumed to be soluble in oil rather than water, a two-phase system of gas-oil is used for CO_2 injection simulation, where gas represents CO_2 and oil represents the brine.

Equations for pressure and saturation are solved using the fully implicit technique in this simulation, which can produce very stable solutions by allowing residuals to be reduced to values close to zero. The PVT relations are used by the E100 simulator to translate changes in physical qualities,

such as density, viscosity, and compressibility into changes in temperature and pressure. By utilizing the formation volume factors and the solution gas/oil ratio, these tables may relate the surface and reservoir conditions. PVT relationships are typically established based on experimental studies or relevant correlations. Additionally, the E100 defines the densities of various phases as an input under standard conditions, and the simulator then transforms this information into reservoir conditions.

3.2 Vertical Equilibrium

CO_2 migration is a multi-scale issue with a great deal of geological uncertainty. The best techniques for effectively describing the combined large-scale and long-term impacts of structural, residual, and solubility trapping are vertical-equilibrium modeling. The MRST-co2lab provides a wide class of vertical-equilibrium models that represent compressibility, the impact of small-scale trapping, and hysteresis effects in the fine-scale capillary and relative permeability functions by using model formulations that are as similar as possible to the standard black-oil framework used in the petroleum industry (SINTEF, 2023).

Because CO_2 is so mobile, it can travel large distances when injected into porous rock formations. It is also possible that vertical migration and two-phase separation are much faster than horizontal migration because a typical saline aquifer chosen to store CO_2 is a thin, slightly inclined sheet that expands thousands of kilometers. Therefore, with a large density difference between CO_2 and brine, it can be assumed that vertical fluid segregation is an instantaneous process in comparison to up-dip migration. Accordingly, it clarifies the reason why Vertical Equilibrium (VE) can be used (SINTEF, 2014).

Overall, the vertical distribution of fluid phases can be calculated from analytical formulas in a vertical equilibrium model because it is believed that the system is in vertical equilibrium. As a result, the flow equations can be integrated with the vertical plane to generate a 2D model rather than a 3D model, which considerably reduces the number of grid cells and computational time (SINTEF, 2014).

Figure 3.3 demonstrates how the vertical equilibrium model may be used to translate the flow of a CO_2 plume into a 2D simulation model in terms of thickness. While applying the vertical equilibrium method reduces the number of dimensions, applying vertical properties averaging preserves significant information about heterogeneities in the underlying 3D medium, depending on the specific assumption used to model the vertical fluid distribution (SINTEF, 2014).

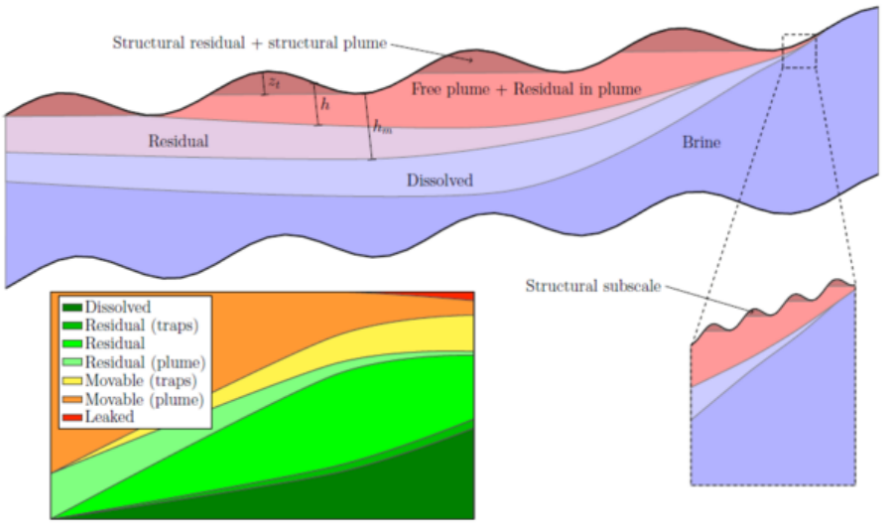

Figure 3.3: Vertical Equilibrium model in MRST (SINTEF, 2014).

In MRST-co2lab, a fully implicit discretization is used in the numerical formulation. This is a sensible decision since it makes it possible to construct hybrid models that mix VE and 3D models in several domains by combining commercial simulators and VE. These techniques are excellent for precisely calculating steady states that represent different types of trapping in the long-term transient migration of CO_2 (SINTEF, 2014).

Meanwhile, MRST-co2lab offers sequential solvers for straightforward incompressible, sharp-interface models. Generally speaking, the errors from the VE assumption may be substantially fewer than the errors introduced by the 3D model when analyzing the long-term migration of a well-formed CO_2 plume. However, when simulating the fluid movement near the injection point during injection or when simulating the system where the migration of CO_2 is not dominated by the topography of the caprock, the conventional 3D simulation will typically be more appropriate than using a VE approximation (SINTEF, 2014).

The management of both simulation options by MRST is one of the advantages of employing this simulator. In this regard, there are certain MRST implementation examples where VE models in the far-field region are connected with 3D flow equations in the near-well region (SINTEF, 2014). The Sleipner CO_2 injection in the VE model is depicted in Figure 3.4.

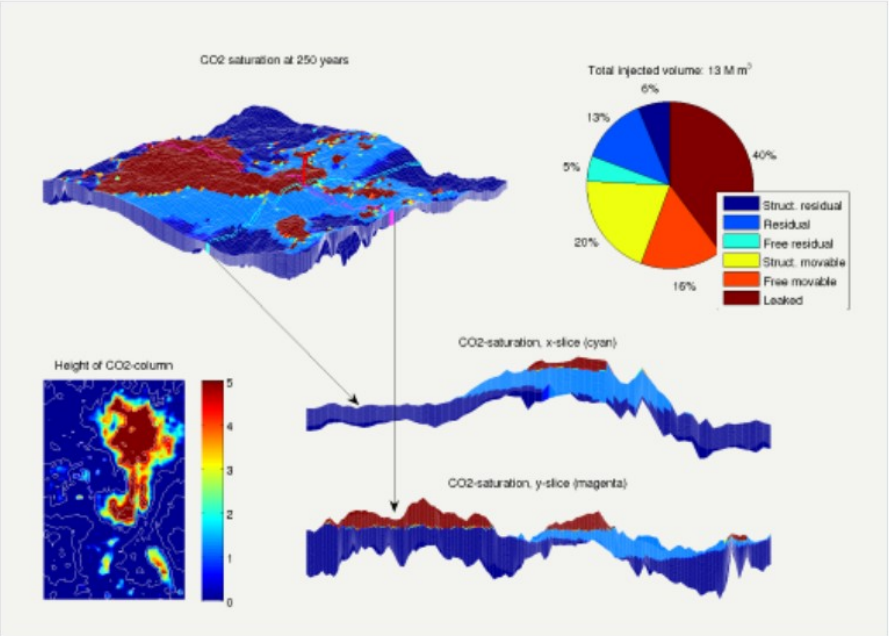

Figure 3.4: Vertical Equilibrium of Sleipner CO_2 injection (SINTEF, 2014).

3.3 Reservoir Model

Eigestad et al. (2009) were pioneers in carrying out benchmark research on CO_2 storage in the Johansen Formation, utilizing 2D seismic data and long-distance well data interpolation to make the model online in order to facilitate the subsequent studies. Gassnova (2012) gathered fresh 3D seismic data, and performed analysis, and property modeling on the dataset in order to validate earlier research on the Johansen Formation as a potential site for CO_2 storage. Sundal et al. (2015) offered a revised model for the Johansen formation based on the research and gathered data, as well as further mineralogical samples and re-interpolation of wells. This model is used in this thesis.

The initiative aim of this study is to store CO_2 in the Cook Formation, which is layered on top of the sandy, saline Johansen Formation. 16 exploration wells have been drilled in the Horda platform, including the Smearheia area, the Trollfield, and Aurora site (research area). In 2019 a well named the Eos confirmation was also drilled to examine further data in the Johansen formation. The intermediate report for Johansen formation by Gassnova (2012) contains the well-log measurement data and core data. Equinor Open Data, which can be accessed at Equinor Open Data, also provides access to the Eos well data. The Horda platform area is shown in Figure 3.5, along with the enormous TrollField, the Smeaheia region, and the Aurora site, where the Cook-Johansen formations serve as the saline aquifer reservoir.

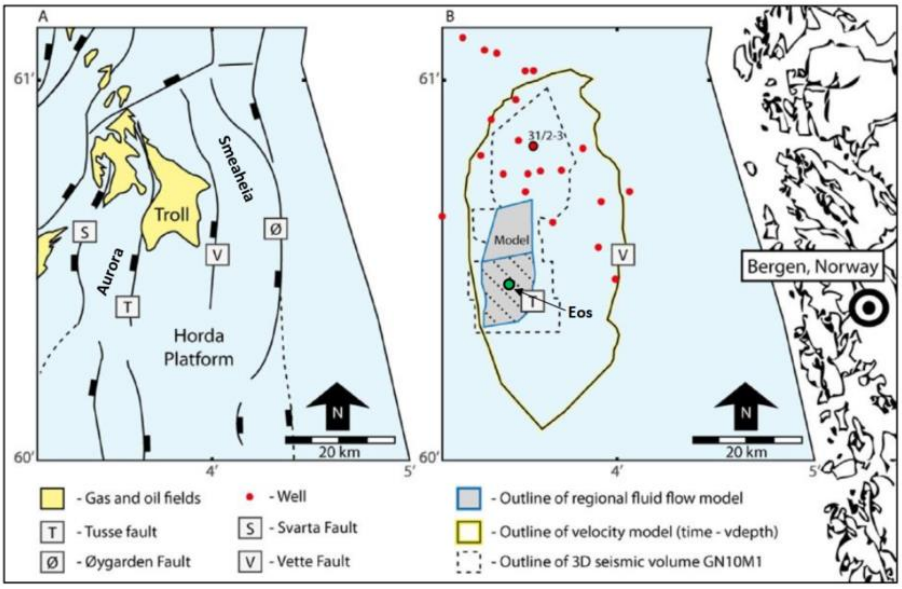

Figure 3.5: The study area, A: Horda Platform; B: Data Coverage (Sundal et al., 2015).

3.3.1 Fluid Model

It is thought that CO_2 is the non-wetting phase and formation water (brine) is the wetting phase. The PVT tables for these two phases are based on CO_2 and brine properties at a constant reservoir temperature of 98 °C, while pressure-dependent changes in densities, viscosities, and formation volume factors are observed. Although the isothermal condition assumption is far from reality, it is assumed; otherwise, multiple PVT tables should be produced for different reservoir temperatures.

The formation volume factor is used to convert the densities of water and CO_2 under surface conditions, which are 1050.48 kg/m3 and 1.87 kg/m3, respectively, to densities at reservoir conditions. Although the capillary pressure has a substantial impact on the migration of the CO_2 plume, this effect is ignored in this work since the cores may not be representative of capillary pressure measurements; hence, it should be considered for future research (Liu et al., 2014).

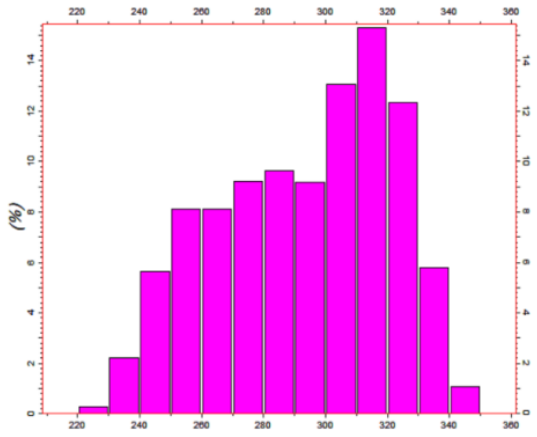

Figure 3.6: Histogram of initial pressure distribution of the Aurora Model (Marashi, 2021).

The black-oil model for CO_2 storage substitutes brine for oil and supercritical CO_2 for gas. As a result, the active phases are included in the ECLIPSE data file using the three terms OIL, GAS, and DISGAS. Assuming that the Johansen-Cook formations are in an equilibrium state, the initial pressure is 260 bar at the datum depth of 2600 m. According to Figure 3.6, the initial pressure varies depending on the depth of the formation from 220 to 350 bar. One of the most crucial aspects of the CO_2 injection study is typically the pressure investigation before, during, and after the injection operation. Figure 3.7 shows the initial pressure distribution in the Aurora model.

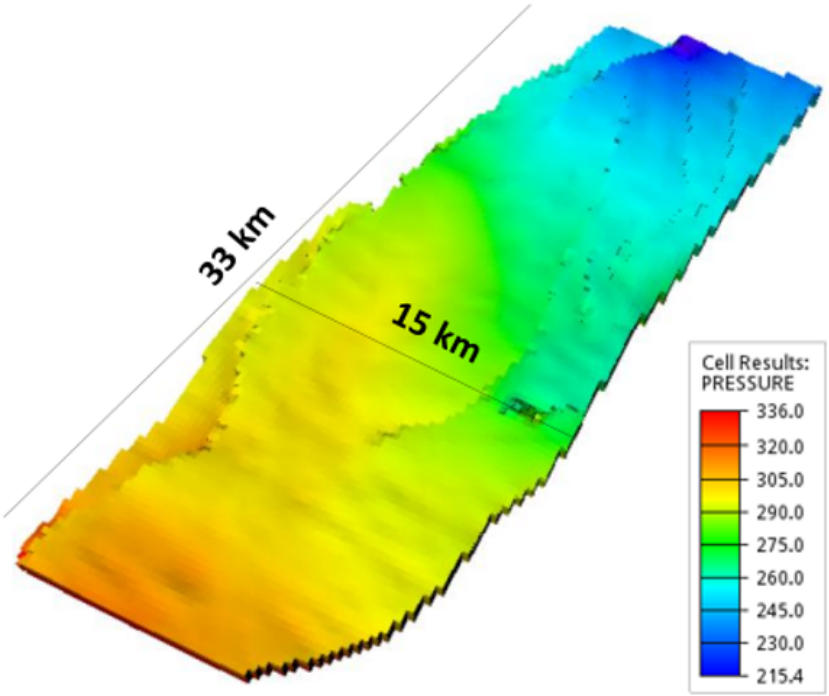

Figure 3.7: Initial pressure distribution of the Aurora Model.

In the fluid model, the irreducible water saturation is 0.07 and the residual gas saturation is 0.2, respectively. The relative permeabilities utilized in this study are shown in Figure 3.8. As previously indicated, this model is a component of the Johansen Formation, which has a permeability range of 0.1 to 500 millidarcy (mD) and a porosity range of 7.3 to 31.4 percent (Sundal et al., 2015; Williams et al., 2021).

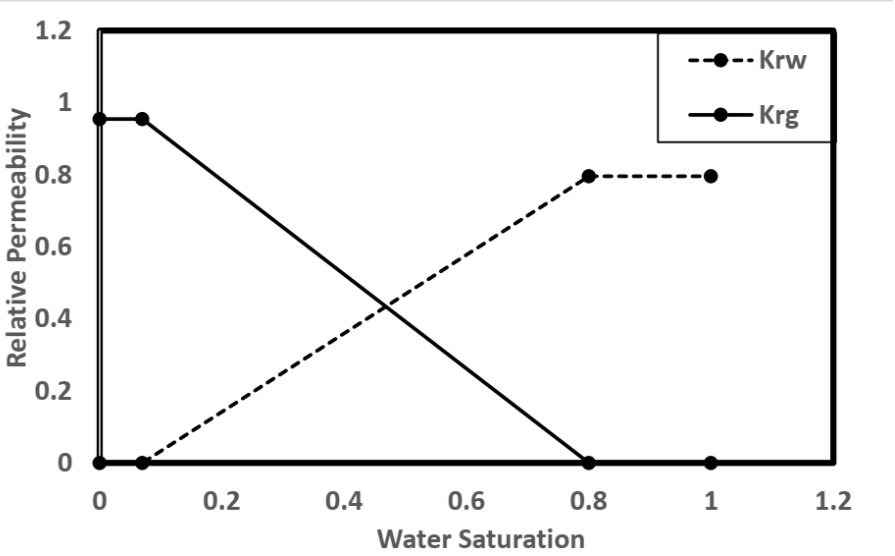

Figure 3.8: Gas and water relative permeabilities in the Aurora Model (Zeynolabedini, 2022).

3.3.2 Static Model

Aurora zone is surrounded by the Tusse fault zone from the east and Svarta fault from the west. Moreover, Aurora is located at Troll West's fault. In addition, the storage complex of the Aurora model is intersected by several intra-block faults (A. K. Furre et al., 2020). Based on the recent investigation of fault assessment in the Aurora site, the eastern, north-eastern dipping intra-block faults are very probable to baffle fluid flow compared to other faults, but more assessment and investigation on the related fault assessment are required (Holden et al., 2022).

Sundal et al. (2015) described 13 Aurora model's faults on a small scale, which is shown in Figure 3.9. Except for F1, F6 with the transmissibility of 0.1, and F7, whose MULTFLT value is 0.5, all fault transmissibility values are set to 1. F6 is the most significant fault in this investigation due to its proximity to the Eos well and its extensive coverage in the model. Due to the fact that the injection has not yet started and there are a lot of unanswered questions regarding the properties of the faults, a sensitivity study on the faults has been carried out by Marashi (2021) in order to demonstrate the effects of faults on the fluid flow during CO_2 injection.

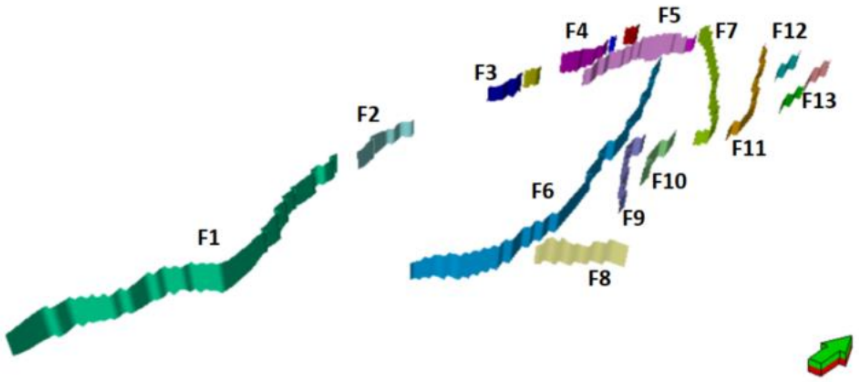

Figure 3.9: Intra-block faults within the aurora model (Marashi, 2021).

The original aurora model had two injection wells in its southernmost regions, however, this was changed to just one injection well (WGI-1) so that it would be simpler to compare to ECLIPSE. Moreover, Eos well is not considered in this analysis, therefore totally there is one injection well in the southern portion of the reservoir, which is completed vertically spanning all the length of the aquifer. Additionally, 1.5 million tons are injected annually.

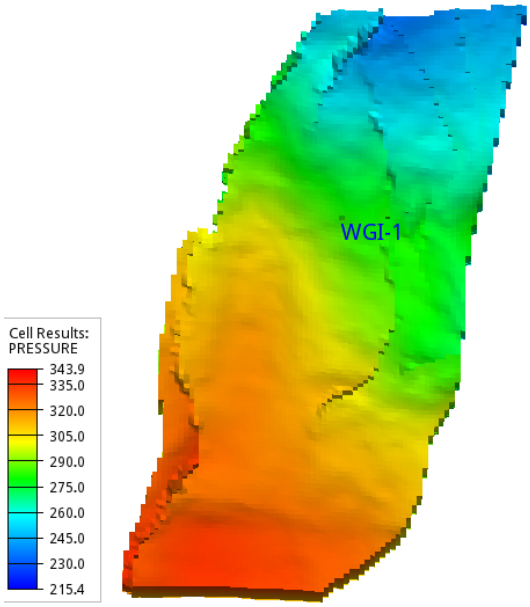

Figure 3.10: Initial pressure distribution and Injection well location.

There are 1,216,800 grid cells in total (78 × 130 × 120), while there are 747,890 active cells. The Petrel SE software platform's cornerpoint structure is used for the grid format. Table 3.2 lists every static and fluid model for the Aurora injection site. The injection lasts for 30 years, after which it is stopped and the migration of the CO_2 plume is studied for about 500 years. Zeynolabedini

(2022) compared the plume migration of CO_2 plume between ECLIPSE and MRST after 10, 30 (the point at which the injection stops), 100, and 500 years. In other words, the injection begins on January 1st, 2023, and lasts until January 1st, 2053. After that, the injection ceases, and the plume growth is simulated and monitored until January 1st, 2553.

Table 3.2: Aurora Model Overview

Parameter	**Value**
Reservoir	Johansen, Cook Fms
Reservoir Thickness	173 [m]
Slope	2 °N-S
Porosity	7.3-31.4 [%]
Horizontal Permeability	0.1 to 500 [mD]
Vertical to Horizontal Permeability Ratio	0.1
Well name	WGI-1
Well Depth	2983 [m]
Well Location (I,J)	(43,49)
Perforation	Fully Perforated
Injection Rate	1.5 [Mt/year]
Grid type	Cornerpoint
Grid Dimension	$78 \times 130 \times 120$
No. of active grids	747,890
No. of faults	13
Initial pressure	260 [bar] at 2600 [m]
Temperature	98 °C
Water Density at Standard Condition	1050.48 [kg/m^3]
CO_2 Density at Standard Condition	1.87 [kg/m^3]
Salinity	7.6 [%]
Residual Gas Saturation	0.2 [%]
Irreducible water saturation	0.07 [%]

3.4 MRST and ECLIPSE model comparison

In order to make a comparison between ECLIPSE and MRST, the comparison scenario should be designed since this item plays a very significant role in the comparison. Finally, It is decided to compare CO_2 plume migration pattern shape in MRST and ECLIPSE. As a result, since MRST produces 2D grid model simulation results, ECLIPSE gas saturation distribution should be converted to 2D from 3D in order to be able to compare both simulation results. Therefore, based on the pore volume of each cell and column, the corresponding gas saturation for each column in ECLIPSE is averaged by Zeynolabedini (2022) in order to make the 3D ECLIPSE model comparable with the 2D MRST model.

Zeynolabedini (2022) imported ECLIPSE data file into MRST by using `deckformat` module, which is described earlier. The module's most crucial function is "readEclipseDeck(fn)", which takes the input file and creates a structure deck with one field for each section in the input file—aside from EDIT and SUMMARY—as well as a list of all the sections. Along with the functionality for reading and processing ECLIPSE output files, this module contains a number of functions to generate objects for grids, rock characteristics, and wells. As a result, the results of ECLIPSE simulations may be visualized. Moreover, initializing simulation cases in MRST using current ECLIPSE runs is also conceivable.

3.4.1 MRST Grid Model Discrepancy

After visualizing the 2D grid model in MRST that was imported from ECLIPSE, one difference was discovered by Zeynolabedini (2022). Pore volumes in some areas of the model vary extremely abruptly, as shown in Figure 3.11-Left. The main reason of this behavior is explored by assessing the theory and mechanism of Vertical Equilibrium Averaging in the MRST. First, MRST detects the active columns in the VE simulation. In a grid model, active columns are any columns that have at least one active grid in the top levels. The problem is that even if there are some active cells under the inactive cell, all cells placed under the last active cell in the column are eliminated.

After looking at the model's active columns, it was discovered that the blue zones (Figure 3.11), which have the lowest pore volumes, contain some middle-layer inactive cells, which led MRST to decide to delete the active cells below them. As a result, the average pore volume is much lower than that of the nearby grids. Therefore, the logical average pore volumes produced by the default method of VE averaging in MRST have been modified and is displayed in Figure 3.11-Right.

3.4.2 MRST and ECLIPSE Fluid Model Comparison

After importing and correcting the grid model from ELIPSE to MRST by Zeynolabedini (2022), it is time to compare the fluid model between ECLIPSE and MRST in order to make sure that the

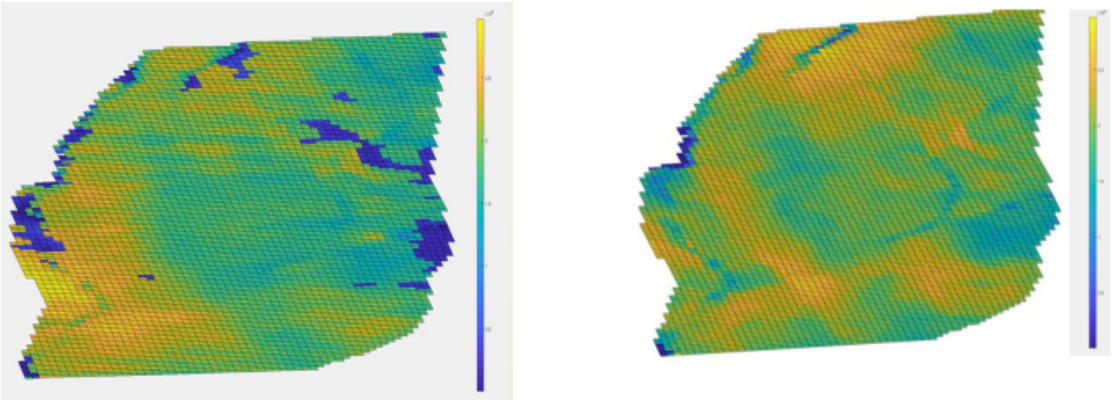

Figure 3.11: Initial Average Pore Volume distribution in MRST (Left); Modified Pore Volume Distribution (Right)

complete model is imported correctly. Therefore, densities and viscosities of water and gas (CO_2) in ECLIPSE are compared with the related function and values in MRST.

MRST PVT model import

Generally, for fluid density and viscosity definition below equations are used in MRST:

$$\rho = \rho_{ref}(1 + c(p - p_{ref})) \tag{3.1}$$

$$\mu = \mu_{ref}(1 + c(p - p_{ref})) \tag{3.2}$$

in which ρ [kg/m^3] and μ [Pa.s] are density and viscosity at reservoir pressure and temperature respectively, ρ_{ref} [kg/m^3] and μ_{ref} [Pa.s] are density and viscosity at reference condition, which should be defined in MRST, c [bar^{-1}] is compressibility, and p [bar] and p_{ref} [bar] are reservoir and reference pressure respectively. Since the fluid model in ECLIPSE is a black-oil model, the reservoir temperature is assumed constant, 98 °C, as mentioned in Table 3.2.

There are three options in order to import fluid models, including Density and Viscosity, from ECLIPSE into MRST.

1. **Zero Compressibility:** Compressibility in mentioned equations is considered zero, as a result, density and viscosity in any pressure are equal to reference values.
2. **Constant Compressibility:** Compressibility is a non-zero value, therefore fluid properties are changed linearly versus pressure.
3. **Table interpolation:** In this option, a sample table should be provided in MRST beforehand in order to interpolate fluid properties based on reservoir pressure.

Although sample table interpolation (Option number 3) is the most precise way to define the fluid model in MRST, the constant compressibility method (option number 2) is used in this study. In order to apply option number 3, CoolProps software is necessary to generate PVT data for CO_2, but unfortunately, this software is not included in the current version of MRST, therefore we decided to use option number 2, which is constant compressibility. Updating MRST in order to Generate real data by using CoolProps software for future work is highly recommended.

MRST Relative Permeability model import

As MRST uses the Vertical Equilibrium method in order to convert the 3D model into a 2D model, the relative permeability model should be upscaled. In order to define the upscaled relative permeability model in MRST, below options are available:

1. **simple:** sharp-interface model with linear relative permeabilities, no residual saturation, and vertically homogeneous rock.
2. **integrated:** sharp-interface model with linear relative permeabilities. This option allows vertically heterogeneous rock and the impact of caprock rugosity.
3. **sharp interface:** sharp-interface model with linear relative permeabilities and vertically homogeneous rock. It includes the impact of caprock rugosity.
4. **linear cap:** Linear capillary fringe model with Brooks-Corey type relative permeability and endpoint scaling.
5. **S table:** capillary fringe model based on sampled tables in the upscaled saturation parameter.
6. **P-scaled table:** capillary fringe model based on sampled tables in the upscaled capillary pressure parameter.
7. **P-K-scaled table:** capillary fringe model based on sampled tables in the upscaled capillary pressure parameter and taking variations in permeability into account through a Leverett J-function relationship.

Nilsen et al. (2016) described these different relative permeability models completely. In this study, since the default relative permeability model in MRST is the "P-scaled table" and ECLIPSE also uses the table for relative permeabilities, the "P-scaled table" is applied for the relative permeability definition. It is highly recommended to investigate more deeply into other options to find a more fit relative permeability model in future studies.

3.5 Sensitivity Analysis

As reservoir models are reliant on field observations, geological research, and interpretations, these models used for numerical simulation can be quite imprecise in a variety of ways, especially in the beginning phases of a field's development. The industry began to gain experience in this new field of CO_2 storage in saline aquifers after the Sleipner CO_2 storage project in 1996, which was followed by the In Salah and Snøhvit projects. This indicates that there are far fewer data points accessible and industry experiences than for other subsurface initiatives like hydrocarbon production or even CO2 EOR. Thus, in order to prevent failure from substantial expenditures, it is vital to assess and examine the hazards related to CO_2 storage in saline aquifers.

After several years of injection, gathering enough information regarding pressure, temperature values, and tracking the CO2 footprint using repeated seismic surveys and/or other useful monitoring methods, the uncertainty and risk related to CO2 storage will greatly reduce. In order to improve the estimation of the CO2 storage process in the reservoir, reservoir models could be adjusted.

To assess the uncertain parameters in reservoir modeling, such as porosity, permeability, and relative permeability curve, several simulation runs are required in order to analyze the risk in CO_2 storage projects.

In this study, five uncertain parameters are analyzed in the sensitivity study, and their related effects on injection pressure, CO_2 plume distribution, and levels of stored CO_2 in different mechanisms are investigated. The five parameters are as follows:

1. Porosity
2. Permeability
3. Residual Gas Saturation
4. Rock Compressibility
5. Relative Permeability Curve

4 Results and Discussion

This chapter presents the results of the fluid model import, including the relative permeability and PVT model, from ECLIPSE into MRST, which is followed by the sensitivity study of some parameters of CO_2 injection into MRST reservoir model.

4.1 Relative Permeability Models comparison

Figure 4.1 shows gas relative permeability which is used in ECLIPSE and MRST. While ECLIPSE uses the table of relative permeability versus saturation, a polynomial function is defined in MRST in order to fit the model in ECLIPSE. As it is obvious, it is a very good match between these two relative permeability models.

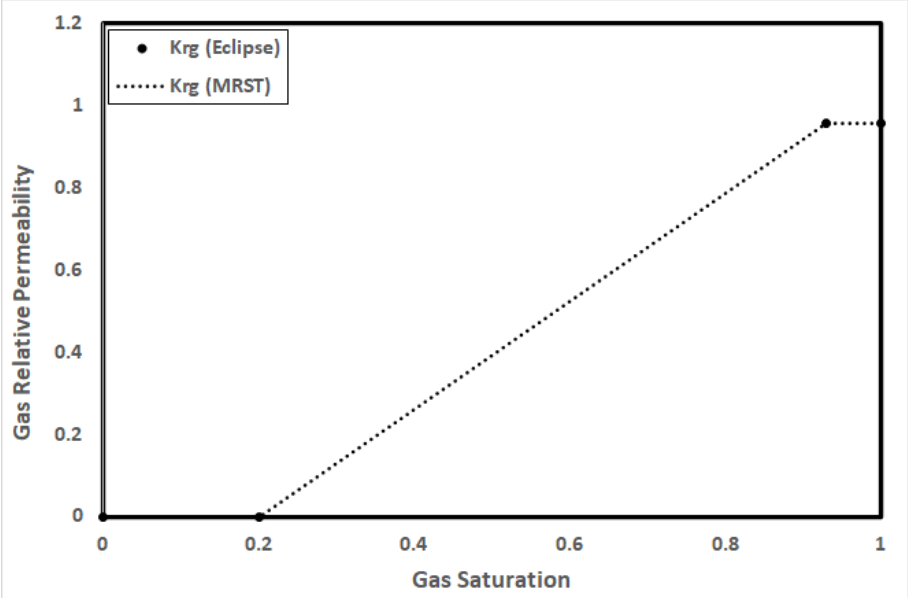

Figure 4.1: Gas Relative Permeability model in ECLIPSE and MRST.

Figure 4.2 illustrates the water relative permeability model in MRST and ECLIPSE. As it is clear, while the default MRST relative permeability of water, which has zero value for both irreducible water and residual gas saturations, is a linear function with a slope of unity, the irreducible water saturation and residual gas saturation in the ECLIPSE water relative permeability are 0.07 and 0.2 respectively.

At first glance, it seems that MRST water relative permeability is not matched with the ECLIPSE model, since there are zero values for both irreducible water and residual gas saturations, but the residuals are defined in the main script code in MRST in order to be applied in the relative permeability model. Therefore, the default MRST relative model is matched with the ECLIPSE model, since it takes the residuals into consideration.

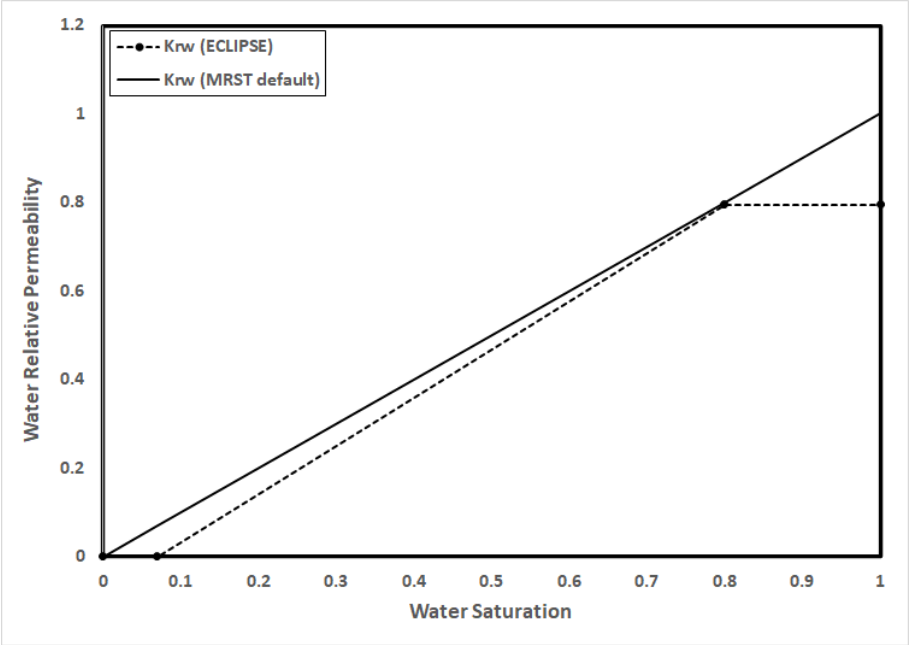

Figure 4.2: Water Relative Permeability model in ECLIPSE and MRST.

4.2 MRST Pressure Initialization

Zeynolabedini (2022) showed an issue regarding pressure initialization in the MRST reservoir model compared with the ECLIPSE reservoir model. As shown in Figure 4.3, at the start of CO_2 injection, the initial well bottom-hole pressure in MRST is not the same as ECLIPSE well bottom-hole pressure.

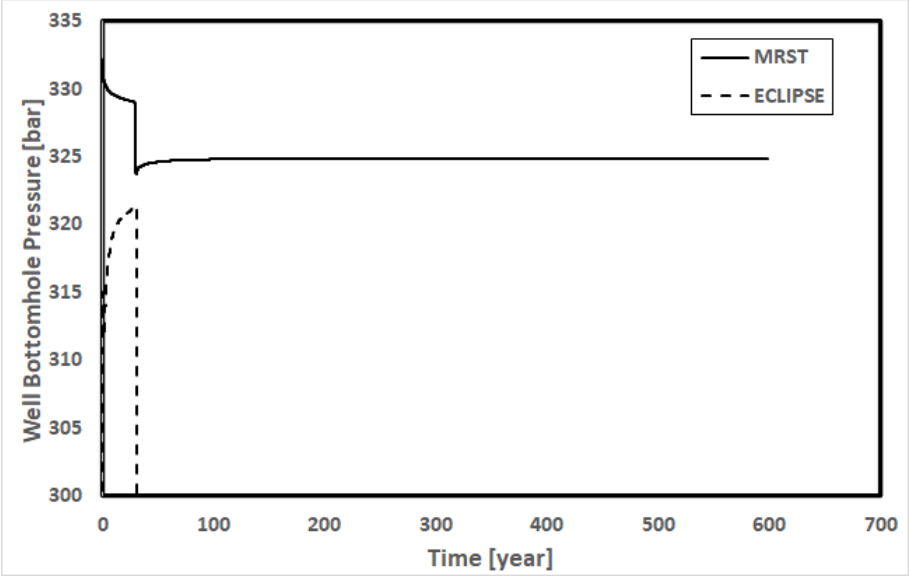

Figure 4.3: Previous case of ECLIPSE and MRST Pressure initialization comparison (Zeynolabedini, 2022)

This conflict is investigated and resolved in this study. Firstly, it should be clarified how pressure

is initiated in MRST. MRST calculates the pressure based on the below equation for each grid block at the reservoir condition:

$$p = \rho_w g h \tag{4.1}$$

in which p is the pressure of each grid block in the reservoir model in [Pa], ρ_w is water density in [kg/m^3] at reservoir condition, g is gravity factor which is [m/s^2], and h is the depth of each grid block in the reservoir model in [m].

After analyzing and investigating, it turned out that the problem was related to water density, which is used in MRST. Since the MRST initial pressure should be the same as ECLIPSE, the water density, which should be used in MRST, is calculated based on the ECLIPSE initial pressure. Finally, the MRST water density is changed to 1020.19 [kg/m^3], and consequently, the pressure initialization problem is resolved, which is shown in Figure 4.4.

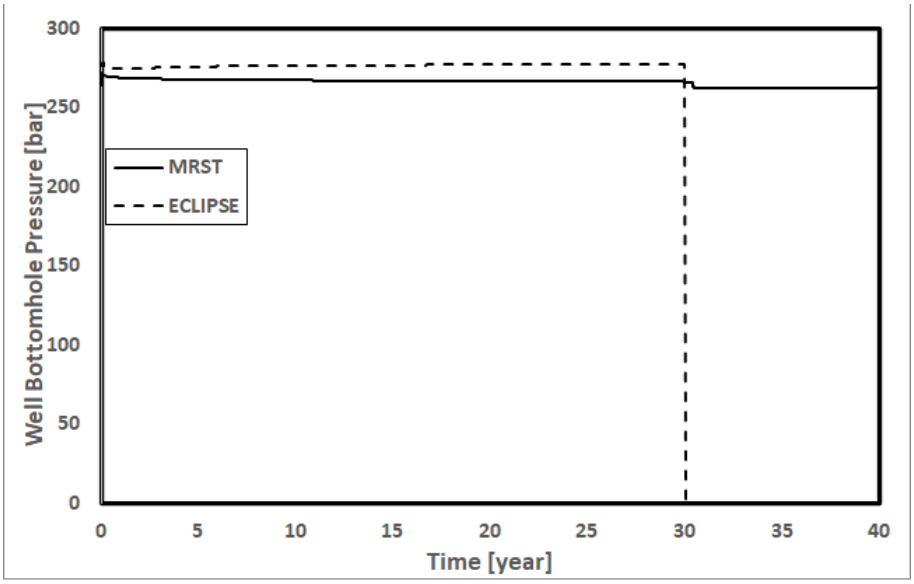

Figure 4.4: Updated case of ECLIPSE and MRST Pressure initialization comparison

In order to make sure that the injection rates are the same in MRST and ECLIPSE, this parameter is compared in Figure 4.5. As it is obvious, the injection rates in both ECLIPSE and MRST are equal in the injection period.

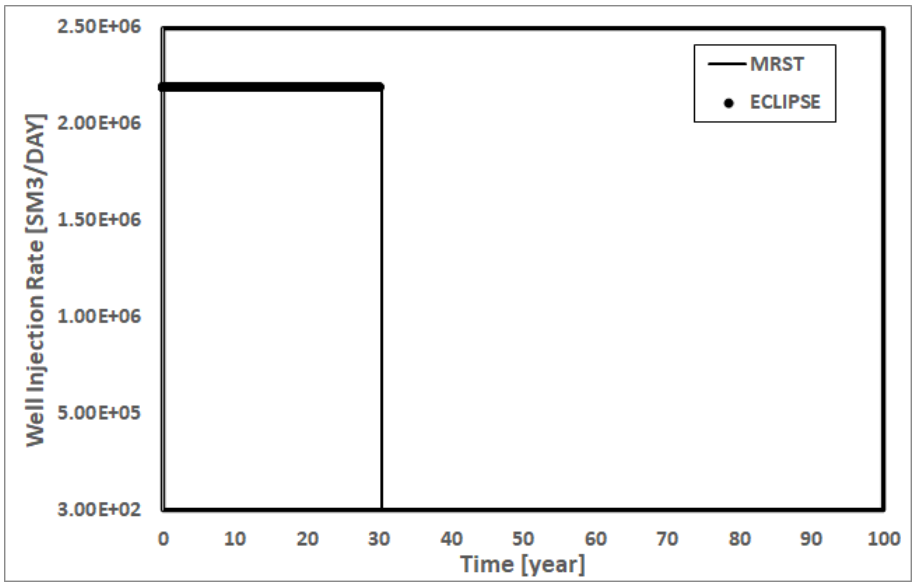

Figure 4.5: ECLIPSE and MRST Gas Injection rate comparison

4.3 MRST and ECLIPSE PVT model comparison

This section describes the MRST PVT model, which is used in this study, and compares it with the ECLIPSE PVT model. Firstly, it should be clarified what is the pressure variation range during and after injection. Figure 4.6 shows that the pressure variation range in the injection period and post-injection period is between 220-320 [bar]. Therefore, both PVT models in ECLIPSE and MRST should be matched in this pressure range.

Based on the ECLIPSE PVT model, the CO_2 compressibility should be defined in MRST in order to use Equation 3.1 and Equation 3.2 for Density and viscosity calculation. Therefore, as CO_2 compressibility is not defined explicitly in the ECLIPSE data file, the compressibility is calculated as per Equation 4.2 at each pressure, and shown in Figure 4.7.

$$c_g = \ln\left(B_g / B_{gref}\right) / \left(p_{ref} - p\right) \tag{4.2}$$

in which c_g [bar^{-1}] is CO_2 compressibility, B_g and B_{gref} [Rm^3/Sm^3] are gas formation volume factor at the reservoir and reference conditions respectively, and p_{ref} and p [bar] are the reference and reservoir pressure respectively.

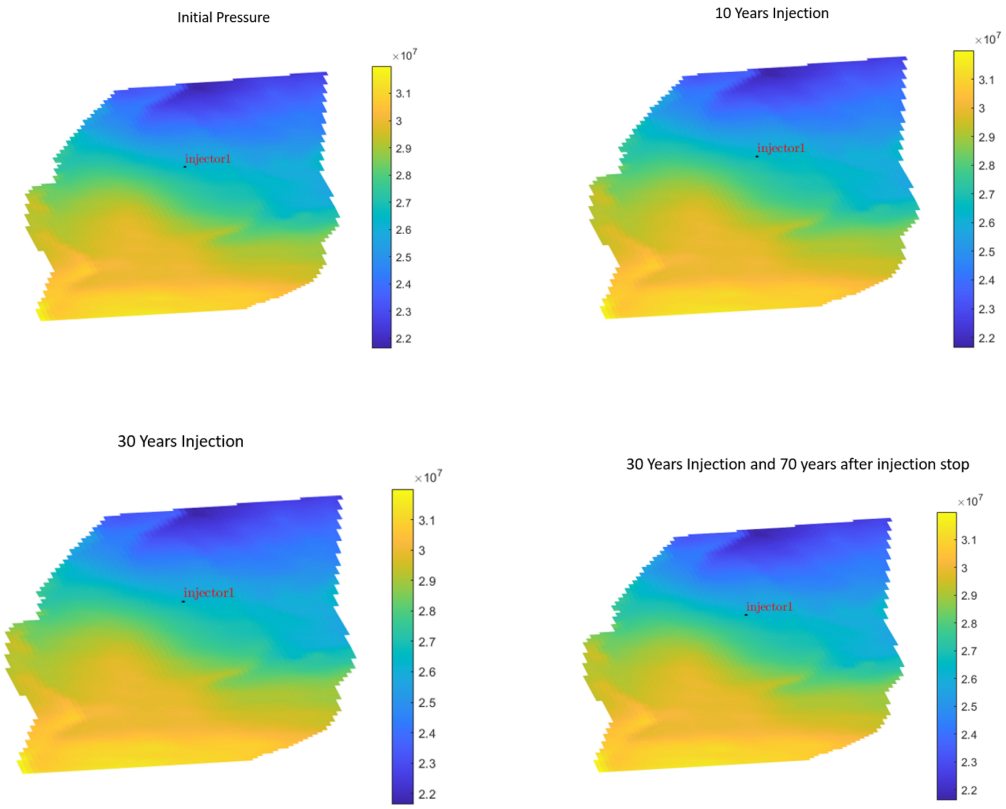

Figure 4.6: Field Pressure [Pa] development during and after injection

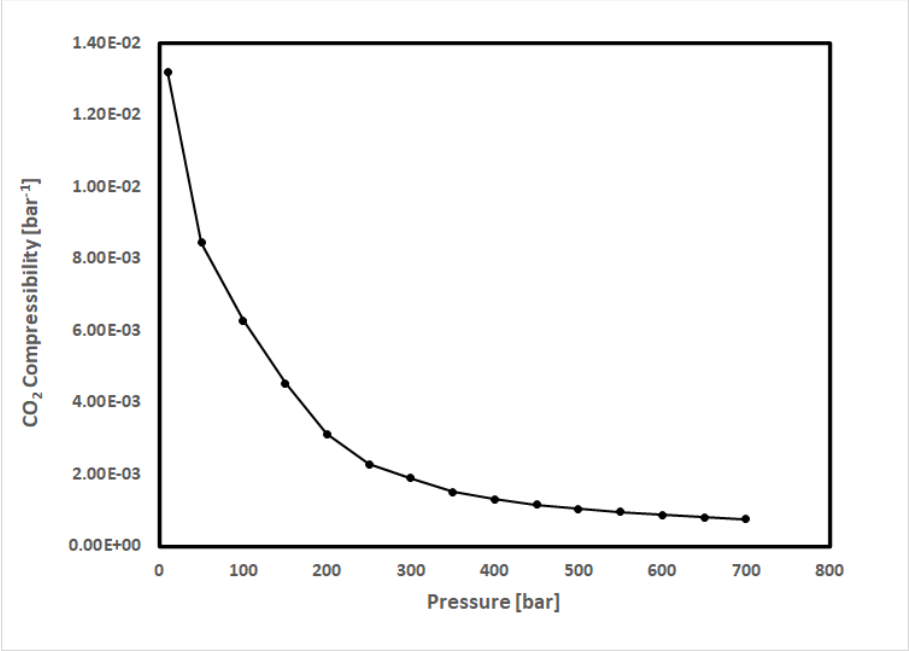

Figure 4.7: ECLIPSE CO_2 Compressibility

The reference pressure which is used to calculate density and viscosity in MRST is 300 [bar]. Therefore, the water and gas compressibility should be selected in this reference pressure for

Equation 3.1 and Equation 3.2 in order to calculate density and viscosity. As per Figure 4.7, the CO_2 compressibility, which is used in the ECLIPSE model, is approximately 1.8E-03 [bar^{-1}] at 300 [bar].

Figure 4.8 compares CO_2 density model in MRST and ECLIPSE. As it is obvious, while the ECLIPSE density model is non-linear, the MRST density model is a fully linear function, since it is decided to apply Equation 3.1 in order to calculate densities in each pressure. It is worth mentioning that since there is no explicit density information in the ECLIPSE data file, CO_2 density is calculated based on Equation 4.3.

$$\rho_g = \bar{\rho_g}/B_g \tag{4.3}$$

in which ρ_g [kg/Rm^3] is CO_2 density at reservoir condition, $\bar{\rho_g}$ [kg/Sm^3] is CO_2 density at surface condition, and B_g [Rm^3/Sm^3] is CO_2 formation volume factor.

As per Figure 4.8, it is obviously shown that CO_2 density in both ECLIPSE and MRST are approximately the same in the injection pressure range (220-320 [bar]).

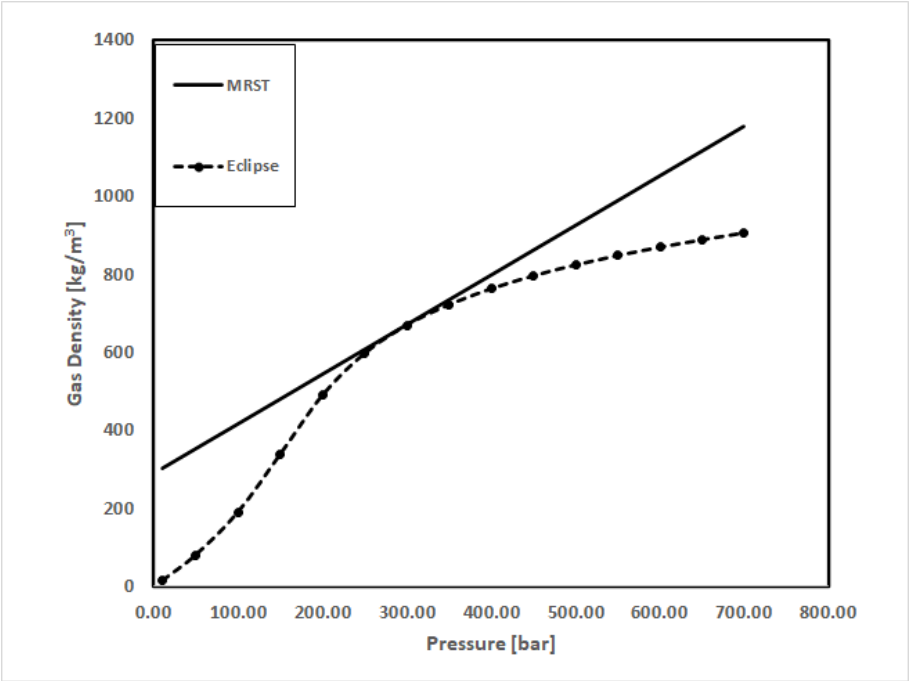

Figure 4.8: ECLIPSE and MRST CO_2 Density comparison

The same scenario as the gas density model definition has been applied to water density model definition in MRST. Firstly, the water compressibility, which should be used in Equation 3.1, is calculated in different solution gas-water ratios (R_s) based on Equation 4.4 from the ECLIPSE PVT model, and shown in Figure 4.9:

$$c_w = \ln\left(B_w/B_{wref}\right)/(p_{ref} - p) \tag{4.4}$$

in which c_w [bar^{-1}] is water compressibility, B_w and B_{wref} [Rm^3/Sm^3] are water formation volume factor at the reservoir and reference conditions respectively, and p_{ref} and p [bar] are the reference and reservoir pressure respectively.

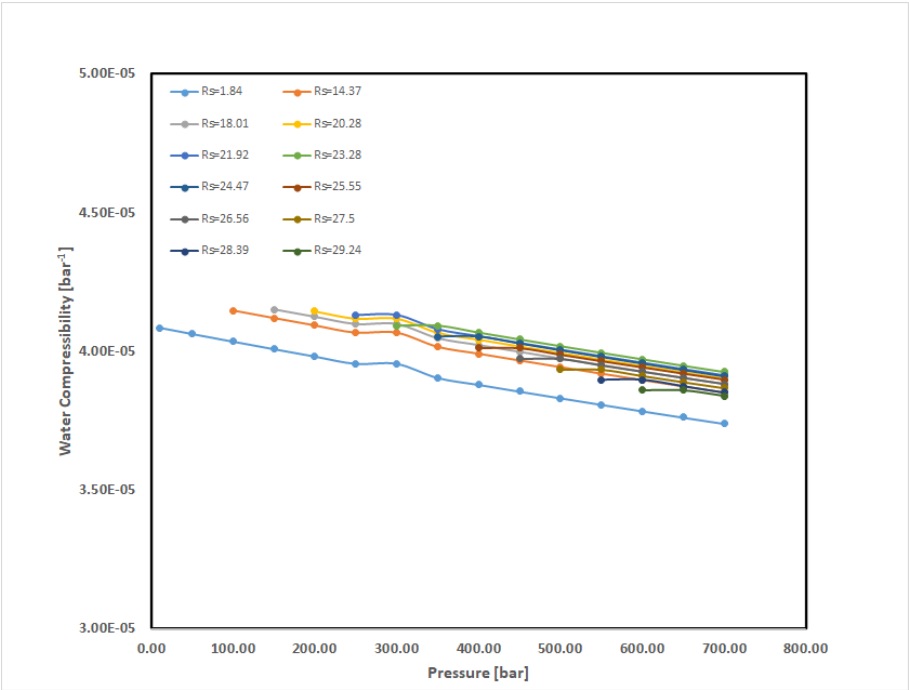

Figure 4.9: ECLIPSE Water Compressibility

Based on Figure 4.9, water compressibility at reference pressure (300 [bar]) is approximately 3.97E-05 [bar^{-1}]. Therefore, by knowing water compressibility, Equation 3.1 can be applied to calculate water density in MRST. Figure 4.10 illustrates the comparison between ECLIPSE and MRST water density model. Although the MRST water density at reference pressure and water compressibility are selected appropriately based on the pressure initialization and the ECLIPSE PVT model, there is some minor gap between the MRST water density including the water compressibility factor and average ECLIPSE water density. Therefore, the final water density model in MRST is tuned by some small factor to produce more similar results with ECLIPSE data.

It is worth mentioning that since there is no explicit density information in the ECLIPSE data file, water density is calculated based on Equation 4.5.

$$\rho_w = (\bar{\rho_w} + R_s\bar{\rho_g})/B_w \tag{4.5}$$

in which ρ_w [kg/Rm^3] is water density at reservoir condition, $\bar{\rho_w}$ [kg/Sm^3] is water density at surface condition, R_s [Sm^3/Sm^3] is solution gas-water ratio, $\bar{\rho_g}$ [kg/Sm^3] is CO_2 density at surface condition, and B_w [Rm^3/Sm^3] is water formation volume factor.

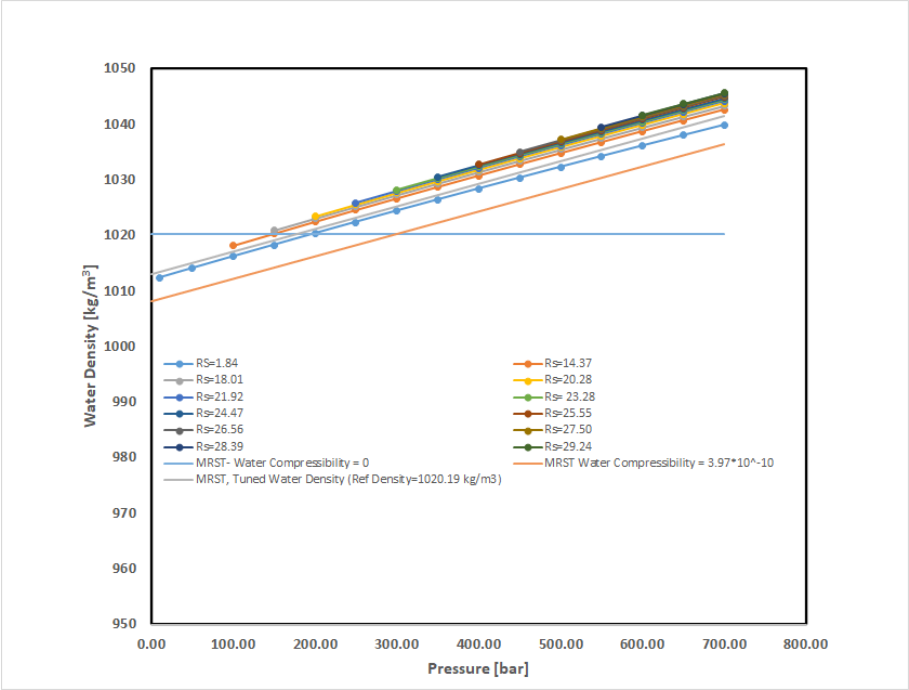

Figure 4.10: MRST and ECLIPSE Water Density comparison

Figure 4.11 compares the MRST and ECLIPSE CO_2 viscosity models in different pressure. While by knowing CO_2 compressibility value, MRST CO_2 viscosity is calculated based on Equation 3.2, ECLIPSE CO_2 viscosity is extracted from the data file, which is explicitly defined. Both viscosity models are approximately the same, especially in the injection pressure range (220-320 [bar]).

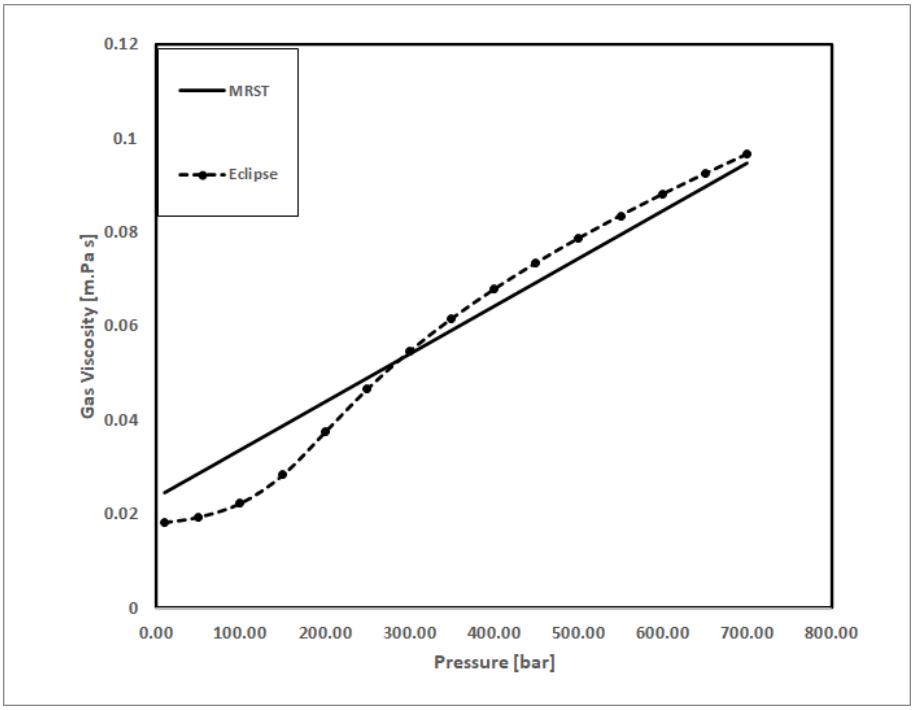

Figure 4.11: MRST and ECLIPSE CO_2 Viscosity Comparison

Moreover, as per Figure 4.12, MRST water viscosity including water compressibility is roughly the same as the ECLIPSE water viscosity model. It should also be noted that by knowing the water compressibility value, the MRST water viscosity is calculated based on Equation 3.2, and the ECLIPSE viscosity model is extracted from the data file.

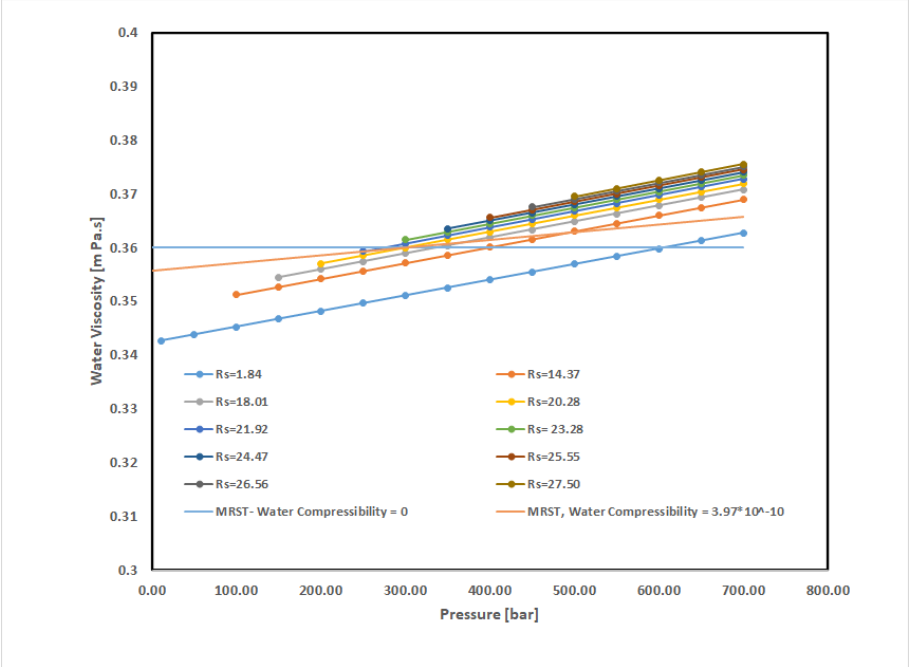

Figure 4.12: MRST and ECLIPSE Water Viscosity

4.4 CO_2 plume comparison

Figure 4.13 and Figure 4.14 show the CO_2 plume development and migration in ECLIPSE and MRST respectively. While upper figures (a and b) illustrate the plume migration after 10 and 30 years of injection, lower figures (c and d) show the plume migration of 70 and 500 years after injection stops. After 10 years, ECLIPSE shows a more rounded plume shape compared with MRST in 10 years. Moreover, not only ECLIPSE CO_2 saturation near the injection well (~ 0.45) is higher than near well-bore CO_2 saturation in MRST (~ 0.25), but also MRST shows wider plume shape compared with ECLIPSE. After 30 years, while MRST also results in a more spread plume shape compared with ECLIPSE, the near well-bore CO_2 saturation is not changed significantly in ECLIPSE and MRST compared with 10-year CO_2 migration.

After 30 years, the injection operation is seized, and plume migration is monitored for 500 years. After 100 years (70 years after injection stops), the difference between plumes is much more significant. While the near well-bore CO_2 saturation is decreased in both ECLIPSE and MRST, the MRST plume shape is much wider than the ECLIPSE plume. Although ECLIPSE CO_2 plume is not reached the boundary yet, the MRST plume touches the boundary and shows accumulated CO_2 saturation in this region.

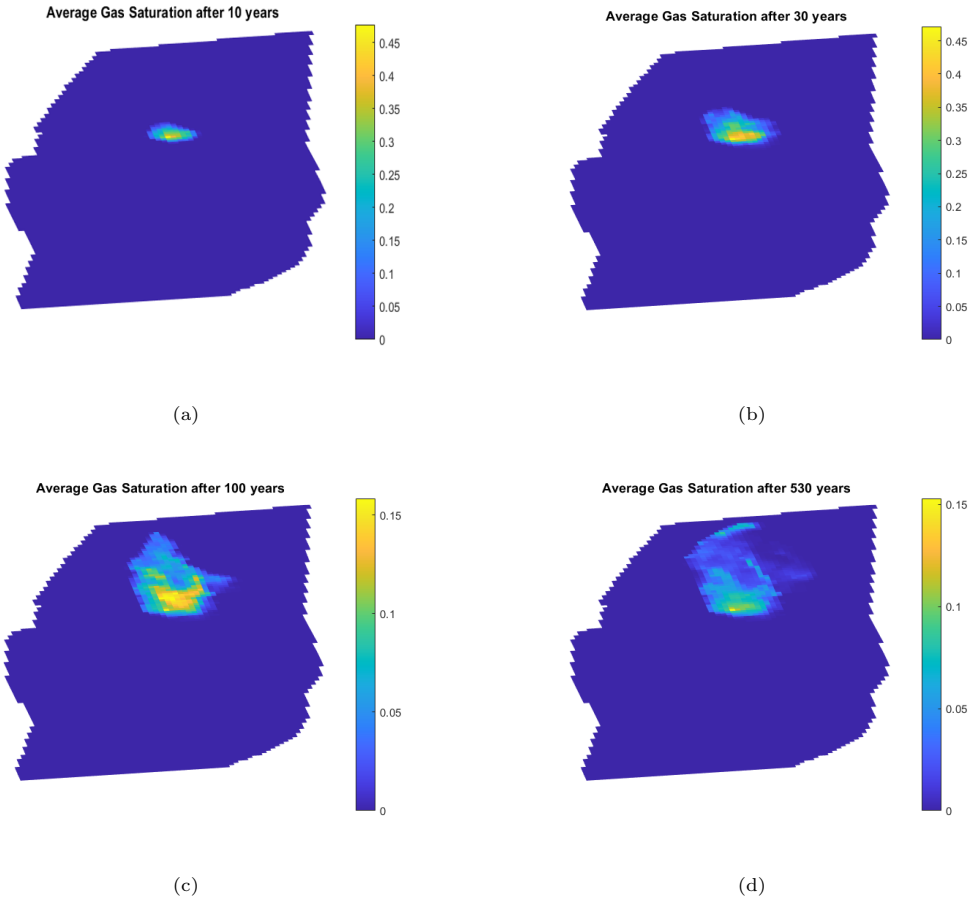

Figure 4.13: ECLIPSE Gas Saturation during and after injection

Finally, after 530 years (500 years after injection stops), while the ECLIPSE plume is not reached the boundary yet, MRST CO_2 plume started to exit from the boundary, and CO_2 saturation decreased generally in the CO_2 plume.

It is worth mentioning that at first, while the dissolution mechanism was deactivated in the MRST, the simulation was running smoothly and very fast. However, when the dissolution mechanism is activated by introducing the solution gas-oil ratio (Rs) in MRST, the running time increased significantly. In order to resolve this issue, the MRST version is updated to the latest one (2023) which resulted in a smooth and fast running time. This observation confirms that in the latest version of MRST, the methods of equation solving have been upgraded.

Generally, the MRST plume shape is much wider than ECLIPSE plume in each time frame. The main reason behind that is **"Reservoir Heterogeneity"**. As mentioned, vertical equilibrium used in MRST `co2 module` takes the vertical average of reservoir model properties including porosity and permeability. Since the porosity in the upper layers of the Aurora reservoir model is much lower than the lower layers, the one-layer averaged MRST model has more porosity than the upper layers in the ECLIPSE reservoir model, which has the highest contribution in CO_2 flow. Therefore, the MRST plume shape is much wider than the ECLIPSE plume. Although there can be other

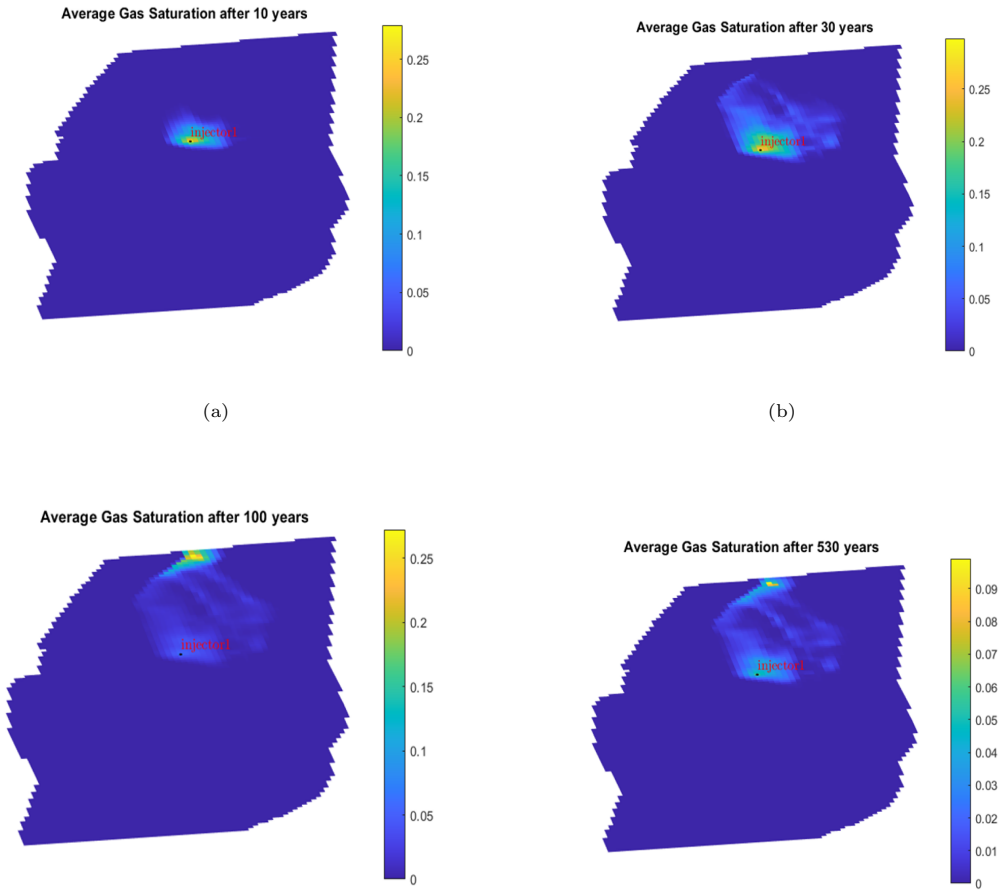

Figure 4.14: MRST Gas Saturation during and after injection

several factors that contribute to making the difference between these plume shapes, including relative permeability curves and end-point upscaling, explained reservoir heterogeneity has a much more significant effect.

As per Figure 4.15, in the first 50 years, the most significant storage mechanism is free plume with approximately 17 [MT] of CO_2, followed by residual and dissolution mechanisms. Then, gradually CO_2 started to exit from the reservoir, and consequently free plume disappeared after around 200 years. After that, residual and exited amounts remained constant, and dissolved CO_2 amount is increased linearly. Finally, while approximately 17 [MT] (1 [MT] = 1E+09 [kg]) CO_2 can be stored in the reservoir after 530 years by Residual and Dissolution mechanisms, 28 [MT] CO_2 exited from the reservoir boundary.

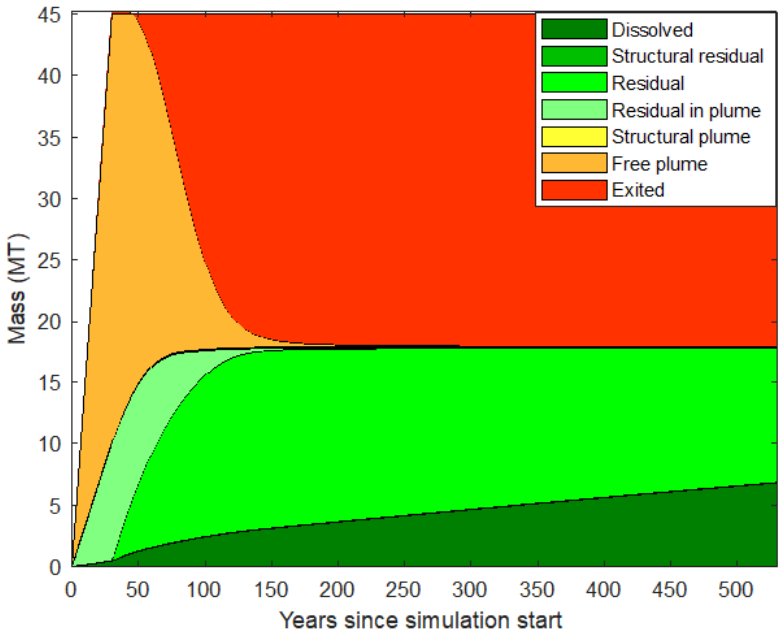

Figure 4.15: CO_2 mass stored breakdown in different storage mechanisms

One of the features of MRST Vertical Equilibrium is converting the 2D model into the 3D model by using analytical capillary pressure equations. Figure 4.16 illustrates 3D CO_2 saturation converted from the 2D model, which is created by the MRST Vertical Equilibrium feature.

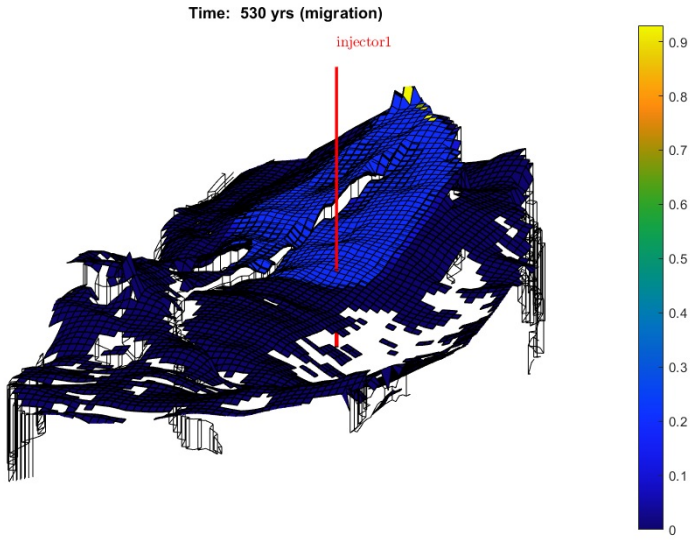

Figure 4.16: 3D CO_2 saturation in MRST

4.5 Sensitivity Analysis

In this section, five uncertain parameters including permeability, porosity, Residual gas saturation, rock compressibility, and relative permeability curve are investigated in the sensitivity analysis and the results of well bottom hole injection pressure, CO_2 plume shape, and storage mechanisms breakdown have been illustrated.

4.5.1 Permeability Sensitivity Analysis

As VE model just considers horizontal permeability in 2D model, the permeability sensitivity is carried out on the Horizontal permeability. Three permeability arrays including $K = 0.5K_{base}$, $K = 1.5K_{base}$, and $K = 3K_{base}$ have been chosen to perform permeability sensitivity analysis.

Figure 4.17 illustrates the effect of permeability alteration on the well bottom hole injection pressure. As it is obvious, increasing the permeability values decreases the well bottom-hole injection pressure, since the pressure dissipation is faster.

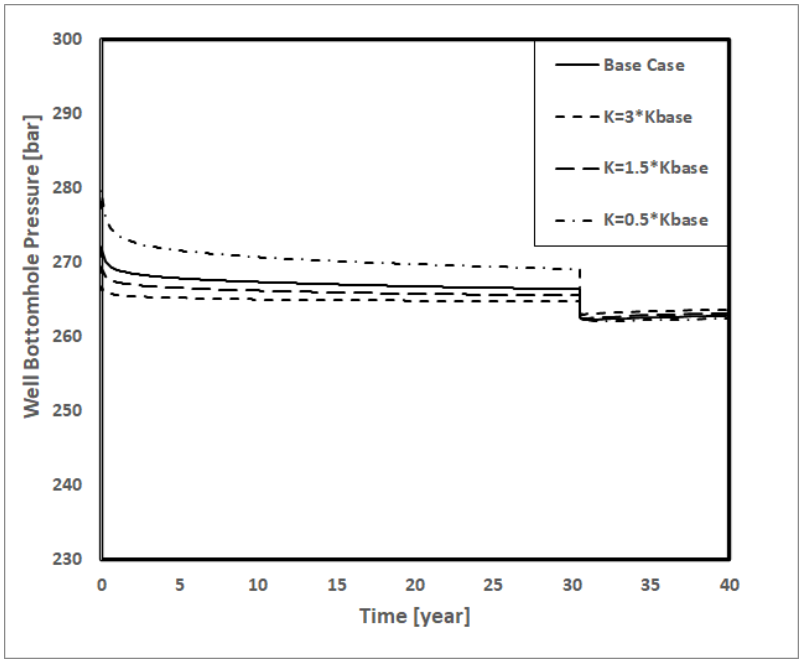

Figure 4.17: Well Bottomhole Pressure in Permeability Sensitivity Analysis

The effect of permeability change on the CO_2 plume shape after 50 years can be seen in Figure 4.18. It can be understood that increasing the permeability results in faster plume migration toward the upper boundary (d) and decreasing this parameter can prevent the plume from expanding (b). While the near well-bore gas saturation is around 0.2 in the case of $K = 0.5K_{base}$, the gas saturation in the same region is less than 0.1 in other cases.

The effect of permeability variations on the breakdown of different storage mechanisms including

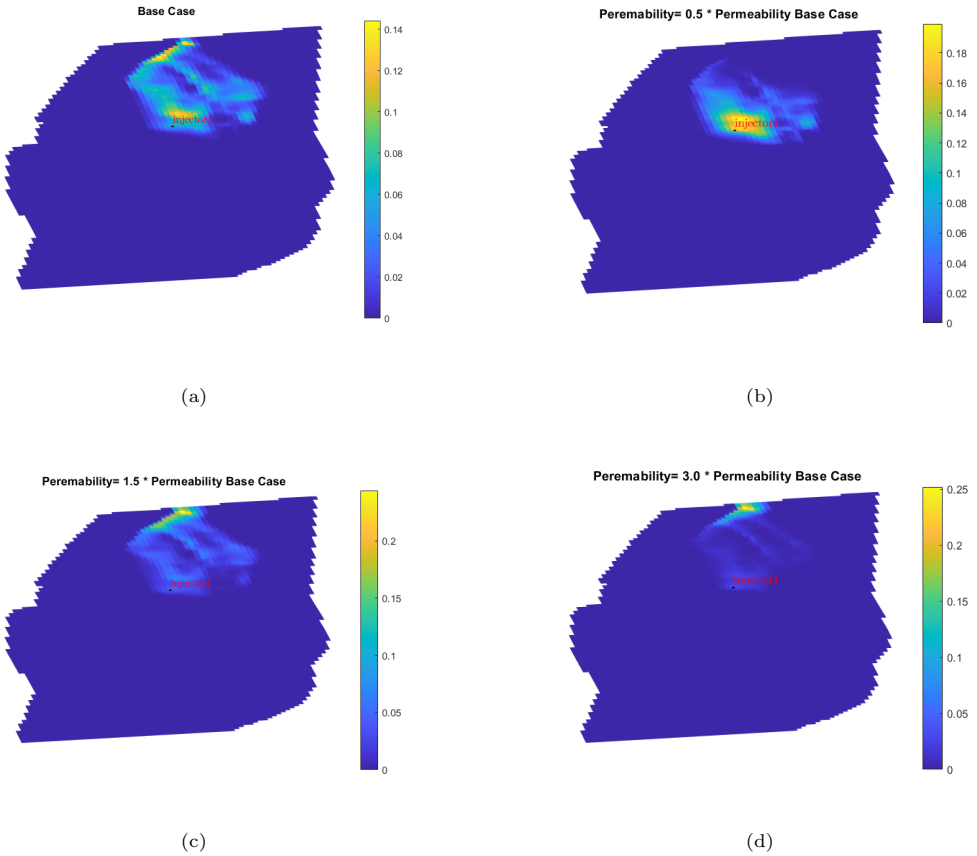

Figure 4.18: Plume shape in Permeability Sensitivity Analysis after 50 years (20 years after injection stops)

Residual, free plume, and dissolved are shown in Figure 4.19 after 530 years. While the main storage mechanisms in all permeability cases are Residuals and Dissolved, no free plume exists in the reservoir model, since it exited from the upper boundary. As it is expected, increasing permeability contributes to decreasing the Residual storage mechanisms, since by roughly the same injection pressure, CO_2 plume can move much easier in the high permeability case, which results in decreasing residual storage amount. It is worth mentioning that the level of dissolved storage amount is approximately the same in all permeability cases.

4.5.2 Porosity Sensitivity Analysis

In order to perform porosity sensitivity analysis, three porosity arrays including $\phi = 0.5\phi_{base}$, $\phi = 1.5\phi_{base}$, and $\phi = 2\phi_{base}$ are selected.

As per Figure 4.20, the MRST reservoir model is slightly sensitive to porosity variation, because the well bottom-hole pressure is not changed significantly. Based on the author's knowledge, generally for the constant injection rate, decreasing porosity can result in increasing injection pressure, but in this porosity sensitivity analysis, the injection pressure for the case of $\phi = 0.5\phi_{base}$ is less than the base case. This issue needs further study and investigation.

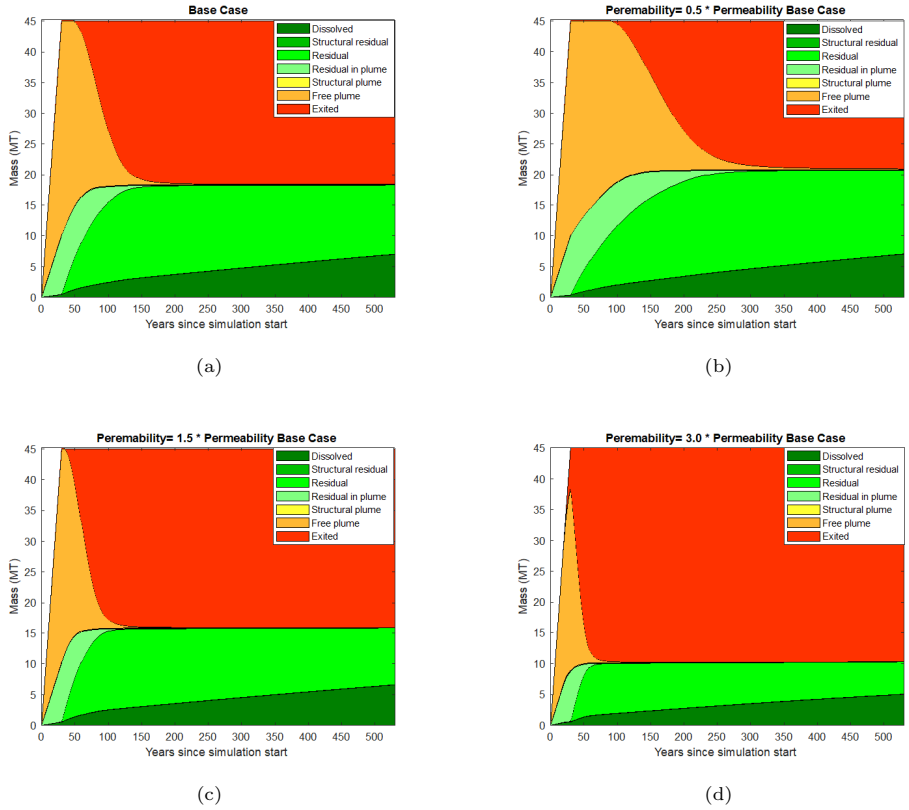

Figure 4.19: Storage Mechanisms in Permeability Sensitivity Analysis after 50 years (20 years after injection stops)

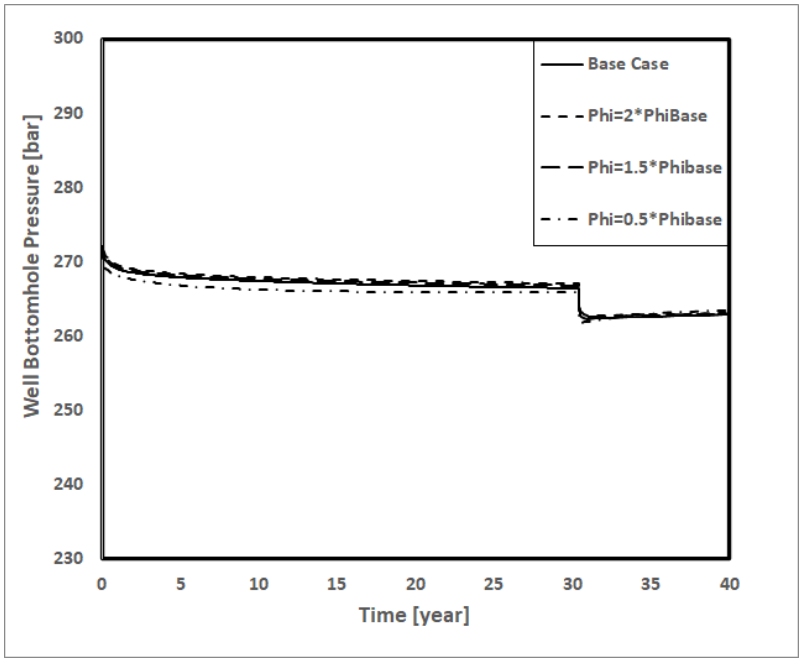

Figure 4.20: Well Bottomhole Pressure in Porosity Sensitivity Analysis

As per Figure 4.21, it is obviously shown that increasing porosity results in less plume expansion. This behavior causes by the fact that considering a constant injection rate, there is less volume in each grid to store CO_2 for the lower porosity case, therefore a more expanded plume is expected.

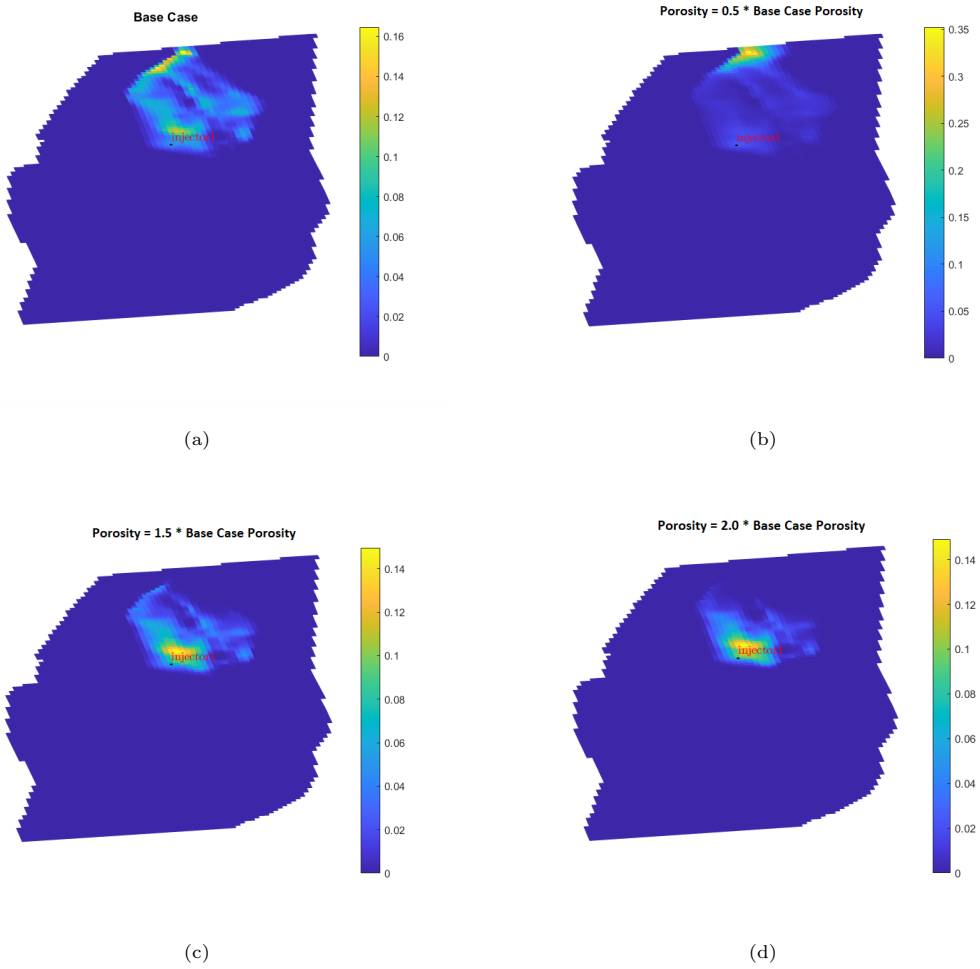

Figure 4.21: Plume shape in Porosity Sensitivity Analysis after 50 years (20 years after injection stops)

Moreover, compared with the base case, there is more saturation near the well-bore in the higher porosity cases (c and d).

Figure 4.22 indicates that higher porosity case studies can store more CO_2 by residual and dissolved mechanisms (c and d) compared with the lower porosity cases (a and b). More storage in higher porosity cases results from the fact that there is much more volume to store CO_2 compared with the less porosity case, in which the significant portion of free plume exited from the upper boundary.

4.5.3 Residual Gas Saturation Sensitivity Analysis

Residual gas saturation of 0.1, 0.3, and 0.6 have been selected besides the base case residual gas saturation of 0.2 in order to study the residual gas saturation sensitivity of the MRST reservoir model.

Figure 4.23 confirms that the well bottom hole injection pressure of the reservoir model is not sensitive with respect to residual gas saturation, since the injection pressure for the different saturation cases is roughly the same.

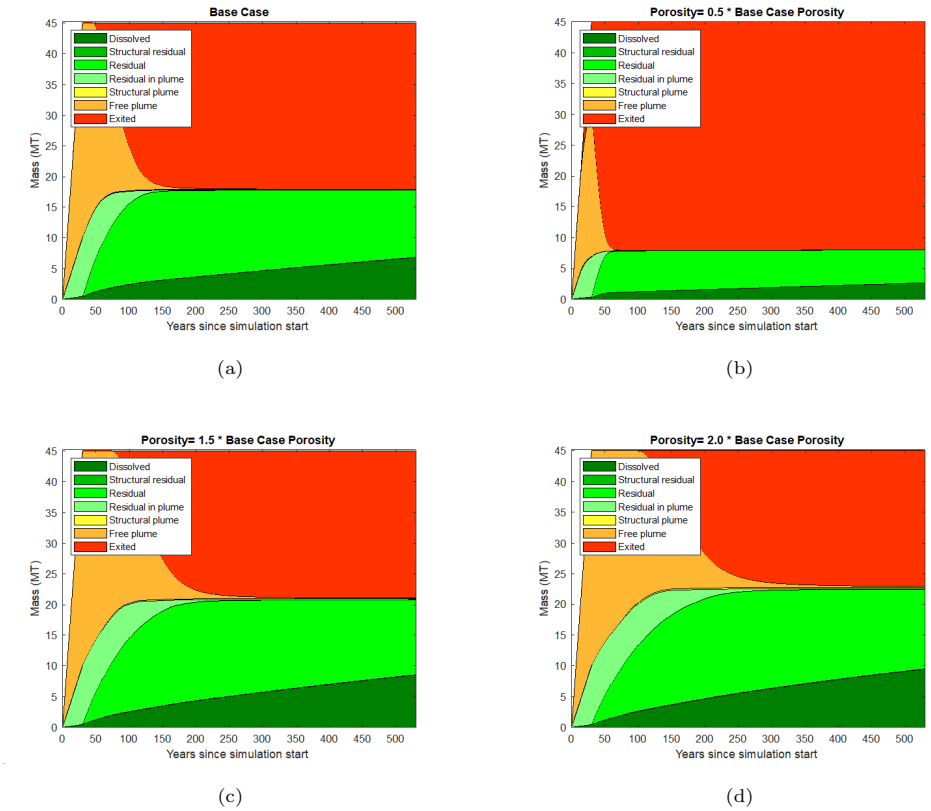

Figure 4.22: Storage Mechanisms in Porosity Sensitivity Analysis after 50 years (20 years after injection stops)

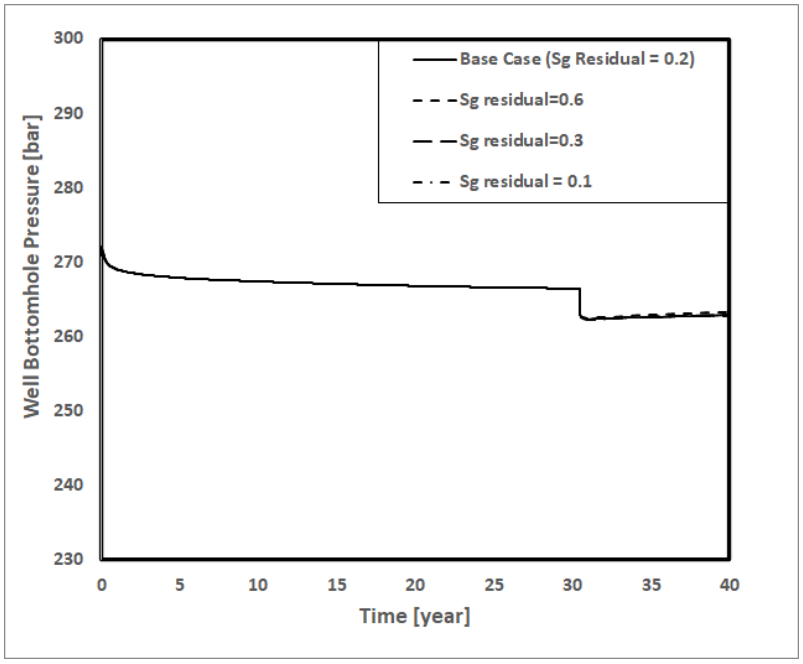

Figure 4.23: Well Bottomhole Pressure in Residual Gas Saturation Sensitivity Analysis

While injection pressure is not affected by residual gas saturation, the CO_2 footprint in the plume shape is roughly responsive in terms of change in residual gas saturation. As per Figure 4.24, increasing residual gas saturation prevents the gas plume from expanding, since simulation grids

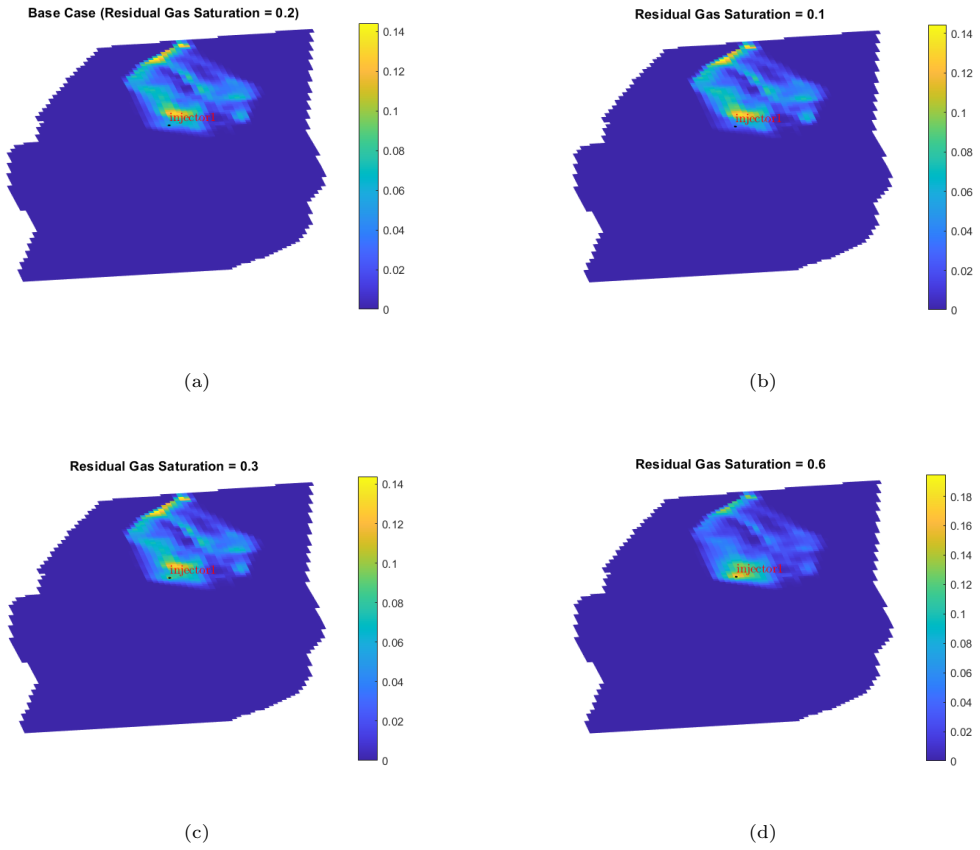

Figure 4.24: Plume shape in Residual Gas Saturation Sensitivity Analysis after 50 years (20 years after injection stops)

prefer to hold more CO_2 compared with the less residual gas saturation.

Although Residual gas saturation does not affect the injection pressure and plume shape significantly, CO_2 storage mechanism breakdown is changed considerably with this parameter, which is depicted in Figure 4.25. As per this figure, while the dissolved mechanism contributes similarly in CO_2 storage for different residual gas saturation cases, increasing residual gas saturation raises the level of stored CO_2 since the CO_2 as a non-wetting phase has a tendency to stay in the grid block in higher residual saturations. Moreover, as it is clearly shown, Residual and Dissolved mechanisms are the strongest storage mechanisms in Residual gas saturation sensitivity analysis.

4.5.4 Rock Compressibility Sensitivity Analysis

Rock compressibility as an uncertain parameter is also investigated in the sensitivity analysis by considering three values including C_{Rock}=2.5E-5 $[bar^{-1}]$, C_{Rock}=7.5E-5 $[bar^{-1}]$, and C_{Rock}=15E-5 $[bar^{-1}]$ besides C_{Rock}=5E-5 $[bar^{-1}]$, which is Rock compressibility for the Base Case.

Based on Figure 4.26, increasing rock compressibility can result in a slight drop in well bottom hole injection pressure. The reason behind such behavior is pressure dissipation along the reservoir rock structure, as rock compressibility is high, the pressure transmits much easier compared with

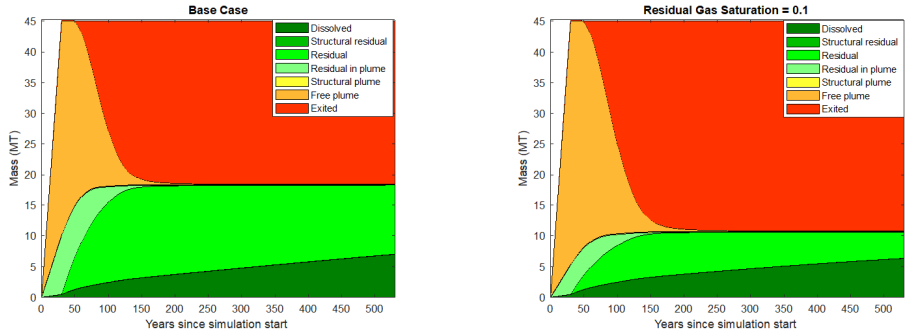

(a)

(b)

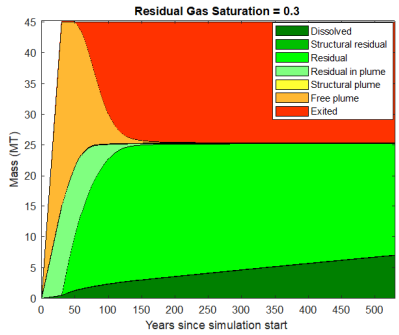

(c)

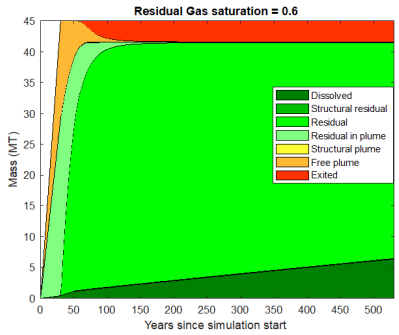

(d)

Figure 4.25: Storage Mechanisms in Residual Gas Saturation Sensitivity Analysis after 50 years (20 years after injection stops)

low compressibility, which results in a pressure injection decrease.

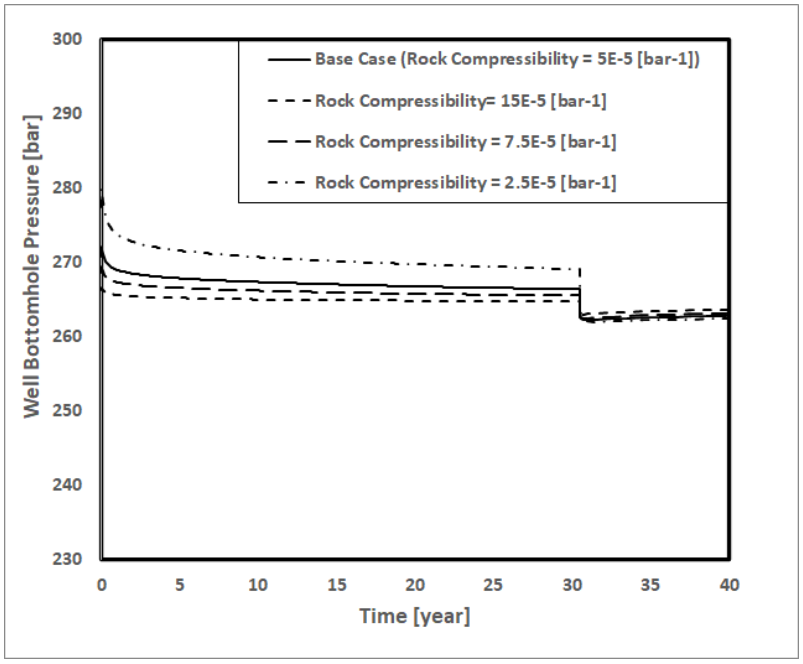

Figure 4.26: Well Bottomhole Pressure in Rock Compressibility Sensitivity Analysis

Figure 4.27 illustrates the effect of rock compressibility on the CO_2 footprint in plume shape. As

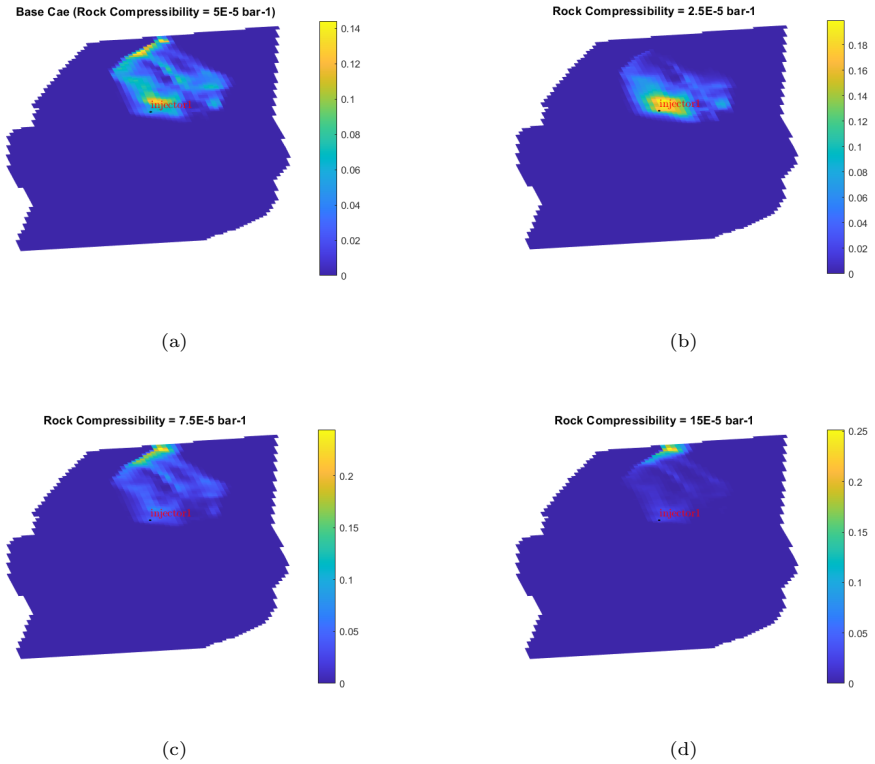

(a) (b)

(c) (d)

Figure 4.27: Plume shape in Rock Compressibility Sensitivity Analysis after 50 years (20 years after injection stops)

expected, high values of rock compressibility can push CO_2 plume further, which results from rock elasticity, therefore plume is dissipated in high rock compressibility (d) compared to other compressibility cases. As a result, the amount of exited injected CO_2 is more in the case of higher rock compressibility, which is shown in Figure 4.28. This figure also depicts that the main storage mechanism in the rock compressibility sensitivity analysis is Residual and Dissolved mechanisms, which is similar to other sensitivity parameters. It is worth mentioning that the rate of free plume exit from the upper boundary is the highest in the compressibility of $C_{Rock} = 15E - 5$ since high rock compressibility can contribute to push the plume towards the boundary similar to spring. Therefore, the lowest amount of CO_2 (around 10 [MT]) can be stored in the highest compressibility case.

4.5.5 Relative permeability curve sensitivity analysis

Besides the base case, two relative permeability curves, including Johansen and Tubåen reservoir, were chosen for sensitivity analysis (Marashi, 2021). The base case relative permeability is extracted from the Utsira formation. The saturation endpoint information is described in Table 4.1.

As per Figure 4.29, the well bottom-hole pressure has not shown significant sensitivity regarding relative permeability cure, since the pressure profiles of different Relative permeability cases are fairly matched together.

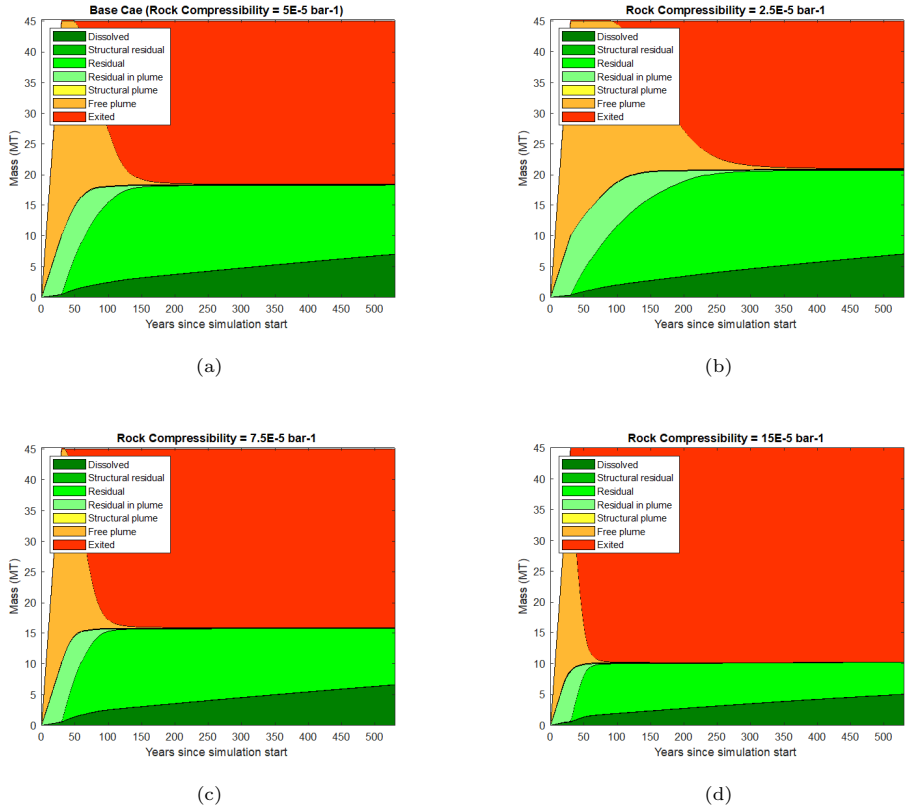

Figure 4.28: Storage Mechanisms in Rock Compressibility Sensitivity Analysis after 50 years (20 years after injection stops)

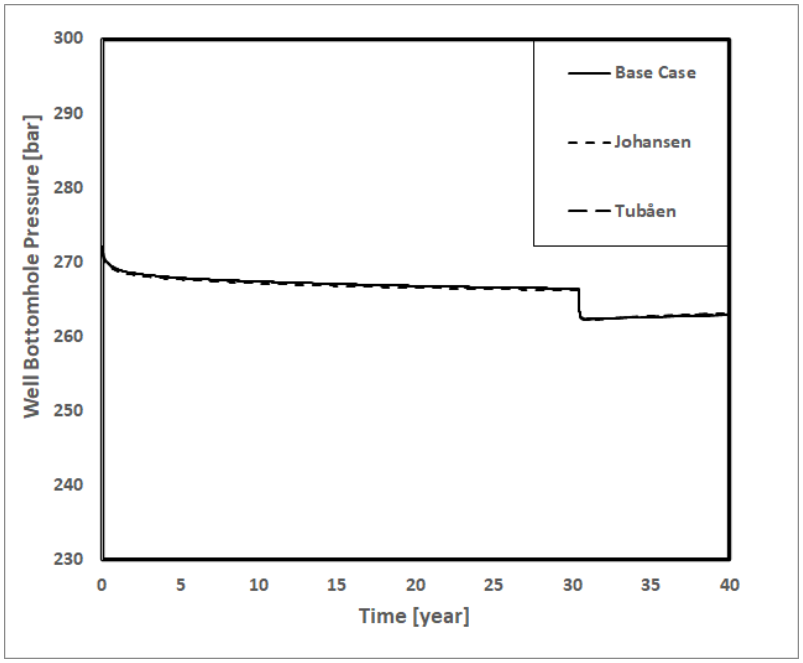

Figure 4.29: Well Bottomhole Pressure in Relative Permeability Curve Sensitivity Analysis

As it is clearly shown in Figure 4.30, while the general plume shapes are roughly the same in three different scenarios, there is less gas saturation near the well-bore in the Johansen case after 50

Table 4.1: Saturation End-point values used in Relative permeability curve sensitivity analysis (Marashi, 2021).

Formation	$\mathbf{S_{gr}}$	$\mathbf{S_{wirr}}$
Utsira (Base Case)	0.2	0.07
Johansen	0.298	0.337
Tubåen	0.330	0.1

years, since the irreducible water saturation, which is the maximum compared with the other two cases, results in less gas volume in drainage mechanism (injection), and faster migration of gas in imbibition process (after injection).

As per Figure 4.31, although residual trapped CO_2 in Tubåen and Johansen case are roughly similar, there is less residual amount in the Base case, since the residual gas saturation in the Base case is the minimum (0.2) compared to other two cases. It is worth mentioning that while the dissolved amount in all cases is fairly similar to each other, the free CO_2 plume migration in the Johansen case is faster compared with the other two cases since the irreducible water saturation is the highest among these three cases, which results in less space for injected CO_2 and faster migration towards the northern boundary.

There is an issue regarding the precise assessment of residual trapped CO_2 in the Johansen and Tubåen cases. Although the residual gas saturation in Johansen (0.298) is less than in Tubåen (0.33), more CO_2 is trapped in the Johansen case by residual mechanism, which is not compatible with the end-point saturation information. This issue should be investigated more in future studies.

Finally, while injection well bottom-hole pressure is strongly sensitive with permeability and rock compressibility variation, no sensitivity is shown in porosity, residual gas saturation, and relative permeability curve for this parameter. Although plume migration is highly sensitive to permeability, porosity, and rock compressibility variation, it shows a slight change with residual gas saturation and relative permeability curve. Regarding storage mechanisms' contribution, while all five parameters have an impact on the level of storage for each mechanism, Residual gas saturation and Rock compressibility show a more strong effect on the storage mechanisms' breakdown.

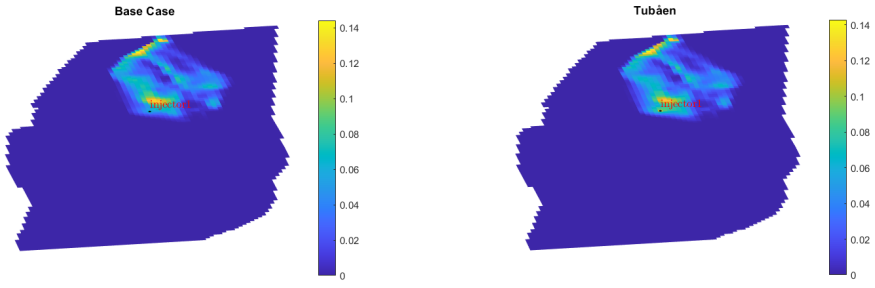

(a)

(b)

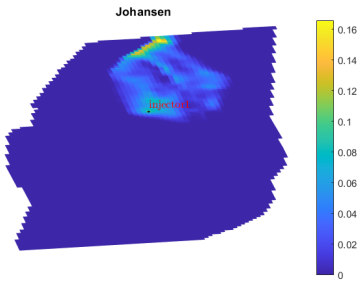

(c)

Figure 4.30: Plume shape in Relative Permeability Curve Sensitivity Analysis after 50 years (20 years after injection stops)

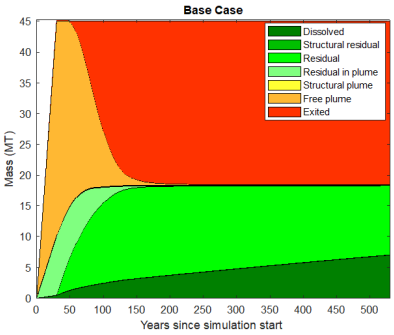

(a)

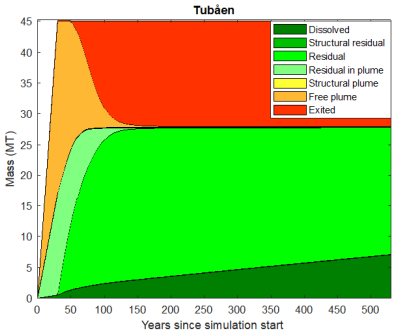

(b)

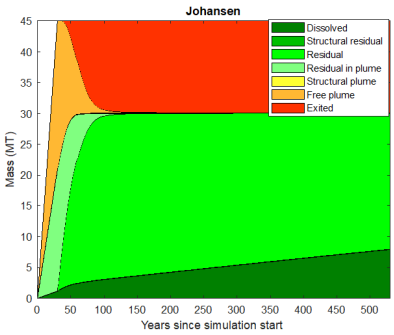

(c)

Figure 4.31: Storage Mechanisms in Relative Permeability Curve Sensitivity Analysis after 50 years (20 years after injection stops)

5 Conclusion and Recommendation

Below items can be concluded from this study:

1. As mentioned, the VE method cannot detect the active cells under the non-active cells in a column, which results in discrepancies in the pore volume of the 2D model. Therefore, The MRST pore volume distribution has been corrected based on the Vertical Equilibrium concept and active grid column (Figure 3.11).

   The options and equations related to PVT and the relative permeability model used in MRST have been investigated, which has resulted in below point:

2. It is decided to use the constant compressibility option to import the PVT model from ECLIPSE into MRST, and the P-scaled table to define relative permeability in MRST.

3. While a polynomial function is defined in MRST to import CO_2 relative permeability model from ECLIPSE into MRST, a linear function from P-scaled option in MRST is applied in order to define water relative permeability in MRST.

4. MRST pressure initialization has been corrected by updating the water density in the MRST model, which is done by comparing the pressure in ECLIPSE and MRST. The final result is shown in Figure 4.4.

5. In order to make sure that the injection rate is similar between MRST and ECLIPSE, this parameter is compared in Figure 4.5, which is obviously shown that the injection rates are the same.

6. Gas and water compressibility equations have been investigated, and the results are shown in Figure 4.7 and Figure 4.9. Based on these figures, The CO_2 and water compressibility, which are used in the ECLIPSE model, are approximately 1.8E-03 [bar^{-1}] and 3.97E-05 [bar^{-1}] at 300 [bar] respectively.

7. Field pressure development has been investigated during and after injection operation in Figure 4.6. The pressure range is between 220-320 [bar]. Therefore, the PVT model comparison between MRST and ECLIPSE has been done in this pressure range. Gas and water density equations are investigated, and the related results are compared between ECLIPSE and MRST in Figure 4.8 and Figure 4.10 respectively in this pressure range. These figures confirm that the water and gas densities used in the MRST and ECLIPSE are fairly similar to each other.

8. While CO_2 density shows a very similar trend between ECLIPSE and MRST in the injection pressure range, MRST water density is tuned by a small factor to produce more similar results compared to ECLIPSE.

9. As per Figure 4.11, and Figure 4.12 gas and water viscosities illustrate very similar behavior in ECLIPSE and MRST.

10. Although MRST PVT and Grid Model are verified in comparison with the ECLIPSE model, there are differences between plume shapes in MRST and ECLIPSE. The main reason for this difference is **"Reservoir Heterogeneity"**. Since the porosity in the upper layers of the Aurora reservoir model is much lower than the lower layers, the one-layer averaged MRST model has more porosity than the upper layers in the ECLIPSE reservoir model, which has the highest contribution in CO_2 flow. Therefore, the MRST plume shape is much wider than the ECLIPSE plume.

11. Generally, the MRST plume shape is much wider than ECLIPSE.

12. As per Figure 4.15, in the first 50 years, the most significant storage mechanism is the free plume with approximately 17 [MT] of CO_2. While approximately 17 [MT] (1 [MT] = 1E+09 [kg]) CO_2 can be stored in the reservoir after 530 years by Residual and Dissolution mechanisms, 28 [MT] CO_2 exited from the reservoir boundary.

13. While injection well bottom-hole pressure is strongly sensitive with permeability and rock compressibility variation, no sensitivity is shown in porosity, residual gas saturation, and relative permeability curve for this parameter.

14. Although plume migration is highly sensitive to permeability, porosity, and rock compressibility variation, it shows a slight change with residual gas saturation and relative permeability curve.

15. Regarding storage mechanisms' contribution, while all five parameters have an impact on the level of storage for each mechanism, Residual gas saturation and Rock compressibility show a more strong effect on the storage mechanisms' breakdown.

The below items are also recommended for future studies and investigations:

1. The methods applied in MRST in order to differentiate between different Rs values in the PVT fluid model are recommended to be studied.

2. Investigation about the reasons why the injection pressure decreases in MRST while injecting.

3. The reason behind the decrease in injection pressure by increasing porosity in the porosity sensitivity analysis should be analyzesd.

4. Methods of Capillary pressure definition in MRST should be investigated.

5. Although the residual gas saturation in Johansen (0.298) is less than in Tubåen (0.33), more CO_2 is trapped in the Johansen case by residual mechanism, which is not compatible with the end-point saturation information. This issue should be investigated more in future studies.

6. Although internal faults cannot be detected in VE model used in the current version of MRST, the probable possibilities of fault transmissibility sensitivity analysis can be investigated in future studies.

Bibliography

Ajayi, T., Gomes, J. S., & Bera, A. (2019). A review of co2 storage in geological formations emphasizing modeling, monitoring and capacity estimation approaches. *Petroleum Science*, *16*(5), 1028–1063. https://doi.org/10.1007/s12182-019-0340-8

Alnes, H., Eiken, O., Nooner, S., Sasagawa, G., Stenvold, T., & Zumberge, M. (2011). Results from sleipner gravity monitoring: Updated density and temperature distribution of the co2 plume. *Energy Procedia*, *4*, 5504–5511. https://doi.org/10.1016/j.egypro.2011.02.536

Amarasinghe, W., Fjelde, I., Rydland, J.-A., & Guo, Y. (2020). Effects of permeability on co2 dissolution and convection at reservoir temperature and pressure conditions: A visualization study. *International Journal of Greenhouse Gas Control*, *99*, 103082. https://doi.org/10.1016/j.ijggc.2020.103082

Anderson, J., Bachu, S., Nimir, H. B., Basu, B., Bradshaw, J., Deguchi, G., Gale, J., von Goerne, G., Heidug, W., Holloway, S., et al. (2005). Underground geological storage. Cambridge University Press.

Bachu, S. (2002). Sequestration of co2 in geological media in response to climate change: Road map for site selection using the transform of the geological space into the co2 phase space. *Energy Conversion and Management*, *43*(1), 87–102. https://doi.org/https://doi.org/10.1016/S0196-8904(01)00009-7

Bachu, S. (2008). Co2 storage in geological media: Role, means, status and barriers to deployment. *Progress in Energy and Combustion Science*, *34*(2), 254–273. https://doi.org/https://doi.org/10.1016/j.pecs.2007.10.001

Bachu, S., Bonijoly, D., Bradshaw, J., Burruss, R., Holloway, S., Christensen, N. P., & Mathiassen, O. M. (2007). Co2 storage capacity estimation: Methodology and gaps. *International Journal of Greenhouse Gas Control*, *1*(4), 430–443. https://doi.org/https://doi.org/10.1016/S1750-5836(07)00086-2

Beck, S., & Mahony, M. (2018). The ipcc and the new map of science and politics. *WIREs Climate Change*, *9*(6), e547. https://doi.org/https://doi.org/10.1002/wcc.547

Bennion, D. B., & Bachu, S. (n.d.). Dependence on temperature, pressure, and salinity of the ift and relative permeability displacement characteristics of co2 injected in deep saline aquifers. *SPE Annual Technical Conference and Exhibition, All Days*. https://doi.org/10.2118/102138-ms

Bensabat, J. (2017). *Geological storage of co2 in deep saline formations* (Vol. 29). https://doi.org/10.1007/978-94-024-0996-3

Benson, S., Cook, P., Anderson, J., Bachu, S., Nimir, H., Basu, B., Bradshaw, J., Deguchi, G., Gale, J., Goerne, G., He, D., Heidug, W., Holloway, S., Keith, D., Lloyd, P., Rocha, P., Senior, B., Thomson, J., Torp, T., & Whittaker, S. (2005). Capter 5 - underground geological storage. ipcc special report on co2 capture and sequestration.

Berg, R. R. (1975). Capillary pressures in stratigraphic traps1. *AAPG Bulletin*, *59*(6), 939–956. https://doi.org/10.1306/83d91ef7-16c7-11d7-8645000102c1865d

Bergmo, P., Lindeberg, E., Riis, F., & Johansen, W. T. (2009). Exploring geological storage sites for co2 from norwegian gas power plants: Johansen formation [Greenhouse Gas Control Technologies 9]. *Energy Procedia*, *1*(1), 2945–2952. https://doi.org/https://doi.org/10.1016/j.egypro.2009.02.070

Black, J., Carroll, S., & Haese, R. (2015). Rates of mineral dissolution under co2 storage conditions. *Chemical Geology*, *399*, 134–144. https://doi.org/10.1016/j.chemgeo.2014.09.020

Bradshaw, J., Bachu, S., Bonijoly, D., Burruss, R., Holloway, S., Christensen, N. P., & Mathiassen, O. M. (2007). Co2 storage capacity estimation: Issues and development of standards [8th International Conference on Greenhouse Gas Control Technologies]. *International Journal of Greenhouse Gas Control*, *1*(1), 62–68. https://doi.org/https://doi.org/10.1016/S1750-5836(07)00027-8

Busch, A., Alles, S., Gensterblum, Y., Prinz, D., Dewhurst, D. N., Raven, M. D., Stanjek, H., & Krooss, B. M. (2008). Carbon dioxide storage potential of shales [EGU General Assembly 2007: Advances in CO2 Storage in Geological Systems]. *International Journal of Greenhouse Gas Control*, *2*(3), 297–308. https://doi.org/https://doi.org/10.1016/j.ijggc.2008.03.003

Carroll, S. A., McNab, W. W., & Torres, S. C. (2011). Experimental study of cement - sandstone/shale - brine - co2 interactions [1467-4866 Carroll, Susan A McNab, Walt W Torres, Sharon C Journal Article England 2011/11/15 Geochem Trans. 2011 Nov 11;12(1):9. doi: 10.1186/1467-4866-12-9.]. *Geochem Trans*, *12*(1), 9. https://doi.org/10.1186/1467-4866-12-9

Cavanagh, A., Haszeldine, R. S., & Nazarian, B. (2015). The sleipner co2 storage site: Using a basin model to understand reservoir simulations of plume dynamics. *First Break*, *33*, 61–68. https://doi.org/10.3997/1365-2397.33.6.81551

Chamock, M., Kristiansen, I., Ryseth, A., & Fenton, J. (2001). Sequence stratigraphy of the lower jurassic dunlin group, northern north sea. In O. J. Martinsen & T. Dreyer (Eds.), *Sedimentary environments offshore norway — palaeozoic to recent* (pp. 145–174). Elsevier. https://doi.org/https://doi.org/10.1016/S0928-8937(01)80012-6

CO2CRC. (2021). https://co2crc.com.au/about-ccus/storage/

Cooper, C., et al. (2009). *A technical basis for carbon dioxide storage: London and new york.* (tech. rep.). Cambridge. http://www.CO2captureproject.org/

Eigestad, G. T., Dahle, H. K., Hellevang, B., Riis, F., Johansen, W. T., & Øian, E. (2009). Geological modeling and simulation of co2 injection in the johansen formation. *Computational Geosciences*, *13*(4), 435. https://doi.org/10.1007/s10596-009-9153-y

Equinor. (2021). *Sharing data from Northern Lights well - equinor.com*. Retrieved 29th March 2023, from https://www.equinor.com/news/archive/20201019-sharing-data-northern-lights

Flett, M., Gurton, R., & Weir, G. (2007). Heterogeneous saline formations for carbon dioxide disposal: Impact of varying heterogeneity on containment and trapping [Petroleum Exploration and Production Research in Australia]. *Journal of Petroleum Science and Engineering*, *57*(1), 106–118. https://doi.org/https://doi.org/10.1016/j.petrol.2006.08.016

Flude, S., & Alcade, J. (2020). Carbon capture and storage has stalled needlessly – three rasons why fears of co leakage are overblown. https://theconversation.com/carbon-capture-and-storage-has-stalled-needlessly-three-reasons-why-fears-of-co-leakage-are-overblown-130747

Furre, A.-K., Meneguolo, R., Ringrose, P., & Kassold, S. (2019). Building confidence in ccs: From sleipner to the northern lights project. *First Break*, *37*(7), 81–87. https://doi.org/https://doi.org/10.3997/1365-2397.n0038

Furre, A. K., Meneguolo, R., Pinturier, L. M., & Bakke, K. (2020). Planning deep subsurface co2 storage monitoring for the norwegian full-scale ccs project. *First Break*, *38*, 55–60.

Gassnova. (2007). *Beslutningsgrunnlag knyttet til transport og deponering av co2 fra kårstø og mongstad*. Gassnova.

Gassnova. (2012). *Geological storage of co2 from mongstad. interim report johansen formation.* (Report).

Gibson-Poole, C., Svendsen, L., Underschultz, J., Watson, M., Ennis-King, J., Ruth, P., Nelson, E., Daniel, R., & Cinar, Y. (2008). Site characterisation of a basin-scale co2 geological storage system: Gippsland basin, southeast australia. *Environmental Geology*, *54*, 1583–1606. https://doi.org/10.1007/s00254-007-0941-1

Gibson-Poole, C., Svendsen, L., Watson, R., M.N.and Daniel, Ennis-King, J., Rigg, A., Grobe, M., Pashin, J., & Dodge, R. (2010). Understanding stratigraphic heterogeneity: A methodology to maximize the efficiency of the geological storage of CO2, In *Carbon Dioxide Sequestration in Geological Media* (pp. 347–364). AAPG.

Gough, C., Shackley, S., Holloway, S., Cockerill, T., Bentham, M., Bulatov, I., McLachlan, C., Kirk, K., Angel, M., & Gg, N. (2005). Carbon dioxide capture and storage in the uk: An integrated.

Holden, N., Osmond, J. L., Mulrooney, M. J., Braathen, A., Skurtveit, E., & Sundal, A. (2022). Structural characterization and across-fault seal assessment of the aurora co2 storage site, northern north sea. *Petroleum Geoscience*, *28*(4). https://doi.org/10.1144/petgeo2022-036

Husmo, T., Hamar, G., Høiland, O., Johannessen, E., Rømuld, A., Spencer, A., Titterton, R., Evans, D., Graham, C., Armour, A., et al. (2003). Lower and middle jurassic. *The Millennium Atlas: Petroleum Geology of the Central and Northern North Sea. Geological Society, London*, *129*, 156.

Jackson, W. A., Hampson, G. J., Jacquemyn, C., Jackson, M. D., Petrovskyy, D., Geiger, S., Machado Silva, J. D., Judice, S., Rahman, F., & Costa Sousa, M. (2022). A screening assessment of the impact of sedimentological heterogeneity on co2 migration and stratigraphic-baffling potential: Johansen and cook formations, northern lights project, offshore norway.

International Journal of Greenhouse Gas Control, *120*, 103762. https://doi.org/https://doi.org/10.1016/j.ijggc.2022.103762

Kaszuba, J., Janecky, D., & Snow, M. (2003). Carbon dioxide reaction processes in a model brine aquifer at 200°c and 200 bars: Implications for geologic sequestration of carbon. *Applied Geochemistry*, *18*, 1065–1080. https://doi.org/10.1016/S0883-2927(02)00239-1

Krevor, S., Blunt, M. J., Benson, S. M., Pentland, C. H., Reynolds, C., Al-Menhali, A., & Niu, B. (2015). Capillary trapping for geologic carbon dioxide storage – from pore scale physics to field scale implications [Special Issue commemorating the 10th year anniversary of the publication of the Intergovernmental Panel on Climate Change Special Report on CO2 Capture and Storage]. *International Journal of Greenhouse Gas Control*, *40*, 221–237. https://doi.org/https://doi.org/10.1016/j.ijggc.2015.04.006

Lauritsen, H., Kassold, S., Meneguolo, R., & Furre, A. (2018). Assessing potential influence of nearby hydrocarbon production on co2 storage at smeaheia. *2018*(1), 1–5. https://doi.org/https://doi.org/10.3997/2214-4609.201802970

Lie, K.-A. (2019). *An introduction to reservoir simulation using matlab/gnu octave: User guide for the matlab reservoir simulation toolbox (mrst)*. Cambridge University Press. https://doi.org/DOI:10.1017/9781108591416

Lindeberg, E., & Bergmo, P. (2003). - the long-term fate of co2 injected into an aquifer. In J. Gale & Y. Kaya (Eds.), *Greenhouse gas control technologies - 6th international conference* (pp. 489–494). Pergamon. https://doi.org/https://doi.org/10.1016/B978-008044276-1/50078-7

Liu, Y., Wang, L., Liu, X., & Ding, T. (2014). Effects of capillary pressure – fluid saturation – relative permeability relationships on predicting carbon dioxide migration during injection into saline aquifers. *Energy Procedia*, *63*, 3616–3631. https://doi.org/https://doi.org/10.1016/j.egypro.2014.11.392

Longship-Report. (2020). *Tlongship – carbon capture and storage*. Norwegian Ministry of Petroleum and Energy.

Lothe, A., Bergmo, P., & Grimstad, A.-A. (2019). Storage resources for future european ccs deployment; a roadmap for a horda co2 storage hub, offshore norway.

Lothe, A. E., et al. (2019a). Heterogeneities in the reservoir models; effect on co2storage capacity and plume modelling in areas with pressure depletion.

Lothe, A. E., Bergmo, P. E. S., Emmel, B., & Eliasson, P. (2019b). Effects of uncertainties in fault interpretations on pressure depletion and co2 storage injection at horda platform, offshore norway. *SSRN Electronic Journal*.

Marashi, V. (2021). *Northern lights project: Aurora model investigation with sensitivity studies and using different simulation methods* (Thesis). https://ntnuopen.ntnu.no/ntnu-xmlui/handle/11250/2992379

Marchetti, C. (1977). On geoengineering and the co2 problem. *Climatic Change*, *1*(1), 59–68. https://doi.org/10.1007/BF00162777

Marcussen, Ø., Faleide, J. I., Jahren, J., & Bjørlykke, K. (2009). Mudstone compaction curves in basin modelling: A study of mesozoic and cenozoic sediments in the northern north sea. *Basin Research*, *22*, 324–340. https://doi.org/10.1111/j.1365-2117.2009.00430.x

Marjanac, T. (1995). Architecture and sequence stratigraphic perspectives of the dunlin group formations and proposal for new type- and reference-wells. In R. Steel, V. Felt, E. Johannessen & C. Mathieu (Eds.), *Sequence stratigraphy on the northwest european margin* (pp. 143–165). Elsevier. https://doi.org/https://doi.org/10.1016/S0928-8937(06)80067-6

Marjanac, T., & Steel, R. J. (1997). Dunlin group sequence stratigraphy in the northern north sea: A model for cook sandstone deposition. *AAPG Bulletin*, *81*, 276–292.

Meneguolo, R., Sundal, A., Martinius, A. W., Veselovsky, Z., Cullum, A., & Milovanova, E. (2022). Impact of the lower jurassic dunlin group depositional elements on the aurora co2 storage site, el001, northern north sea, norway. *International Journal of Greenhouse Gas Control*, *119*, 103723. https://doi.org/https://doi.org/10.1016/j.ijggc.2022.103723

Metz, B., Davidson, O., Coninck, H. d., Loos, M., & Meyer, L. (2005). *Ipcc special report on carbon dioxide capture and storage*. Cambridge University Press, New York, NY (United States). https://www.osti.gov/biblio/20740954

Metz, B., Davidson, O., De Coninck, H., Loos, M., & Meyer, L. (2005). *Ipcc special report on carbon dioxide capture and storage* (Report). Cambridge.

Miri, R., & Hellevang, H. (2016). Salt precipitation during co2 storage—a review. *International Journal of Greenhouse Gas Control*, *51*, 136–147. https://doi.org/10.1016/j.ijggc.2016.05.015

Nazarian, B., Thorsen, R., & Ringrose, P. (2019). Storing co2 in a reservoir under continuous pressure depletion; a simulation study. *SSRN Electronic Journal*. https://doi.org/10.2139/ssrn.3365822

Nilsen, H. M., Lie, K.-A., & Andersen, O. (2016). Fully-implicit simulation of vertical-equilibrium models with hysteresis and capillary fringe. *Computational Geosciences*, *20*(1), 49–67. https://doi.org/10.1007/s10596-015-9547-y

Nordbotten, J. M., Celia, M. A., Bachu, S., & Dahle, H. K. (2005). Semianalytical solution for co2 leakage through an abandoned well [Nordbotten, Jan Martin Celia, Michael A Bachu, Stefan Dahle, Helge K Journal Article Research Support, Non-U.S. Gov't United States 2005/02/15 Environ Sci Technol. 2005 Jan 15;39(2):602-11. doi: 10.1021/es035338i.]. *Environ Sci Technol*, *39*(2), 602–11. https://doi.org/10.1021/es035338i

Nordbotten, J. M., & Celia, M. A. (2006a). Similarity solutions for fluid injection into confined aquifers. *Journal of Fluid Mechanics*, *561*, 307–327. https://doi.org/10.1017/S0022112006000802

Nordbotten, J. M., & Celia, M. A. (2006b). An improved analytical solution for interface upconing around a well. *Water Resources Research*, *42*(8). https://doi.org/https://doi.org/10.1029/2005WR004738

Nordbotten, J. M., Celia, M. A., & Bachu, S. (2004). Analytical solutions for leakage rates through abandoned wells. *Water Resources Research*, *40*(4), Article W04204, W04204. https://doi.org/10.1029/2003WR002997

Nordbotten, J. M., Celia, M. A., & Bachu, S. (2005). Injection and storage of co2 in deep saline aquifers: Analytical solution for co2 plume evolution during injection. *Transport in Porous Media*, *58*(3), 339–360. https://doi.org/10.1007/s11242-004-0670-9

Northern-Lights. (2022). *Northern lights*. Retrieved 27th March 2023, from http://https://northernlightsccs.com/what-we-do/

Partington, M., COPESTAKE, P., MITCHENER, B., Underhill, J., & Parker, J. (1993). Biostratigraphic calibration of genetic stratigraphic sequences in the jurassic lowermost cretaceous (hettangian to ryazanian) of the north-sea and adjacent areas. *Petroleum geology of north-west europe: proceedings of the 4th conference*, 371–386.

Patruno, S., Hampson, G. J., Jackson, C. A.-L., & Dreyer, T. (2015). Clinoform geometry, geomorphology, facies character and stratigraphic architecture of a sand-rich subaqueous delta: Jurassic sognefjord formation, offshore norway. *Sedimentology*, *62*(1), 350–388. https://doi.org/https://doi.org/10.1111/sed.12153

Pau, G. S. H., Bell, J., Pruess, K., Almgren, A., Lijewski, M., & Zhang, K. (2010). High-resolution simulation and characterization of density-driven flow in co2 storage in saline aquifers. *Advances in Water Resources*, *33*, 443–455. https://doi.org/10.1016/j.advwatres.2010.01.009

Peters, G., & Sognnæs, I. (2019). *The role of carbon capture and storage in the mitigation of climate change*. CICERO.

Pruess, K., Xu, T., Apps, J., & Garcia, J. (2003). Numerical Modeling of Aquifer Disposal of CO2. *SPE Journal*, *8*(01), 49–60. https://doi.org/10.2118/83695-PA

Reynolds, C. A., & Krevor, S. (2015). Characterizing flow behavior for gas injection: Relative permeability of co2-brine and n2-water in heterogeneous rocks. *Water Resources Research*, *51*(12), 9464–9489. https://doi.org/https://doi.org/10.1002/2015WR018046

Riaz, A., & Hesse, M. (2006). Onset of convection in a gravitationally unstable diffusive boundary layer in porous media. *Journal of Fluid Mechanics*, *548*, 87–111. https://doi.org/10.1017/S0022112005007494

Riis, F. (2018). Norway ccs demonstration project: Evaluation of jurassic reservoirs for safe co2 injection and storage. *2018*(1), 1–5. https://doi.org/https://doi.org/10.3997/2214-4609.201802954

Ringrose, P. S., & Meckel, T. A. (2019). Maturing global co2 storage resources on offshore continental margins to achieve 2ds emissions reductions. *Scientific Reports*, *9*(1), 17944. https://doi.org/10.1038/s41598-019-54363-z

Ringrose, P. (2020). *How to store co2 underground: Insights from early-mover ccs projects* (1st 2020.) [(role)]. http://lib.ugent.be/catalog/ebk01:4940000000159086

Ringrose, P. S. (2018). The ccs hub in norway: Some insights from 22 years of saline aquifer storage [Carbon in natural and engineered processes: Selected contributions from the 2018 International Carbon Conference]. *Energy Procedia*, *146*, 166–172. https://doi.org/https://doi.org/10.1016/j.egypro.2018.07.021

Ringrose, P. S., Furre, A.-K., Gilfillan, S. M., Krevor, S., Landrø, M., Leslie, R., Meckel, T., Nazarian, B., & Zahid, A. (2021). Storage of carbon dioxide in saline aquifers: Physicochemical processes, key constraints, and scale-up potential [PMID: 33872518]. *Annual Review of Chemical and Biomolecular Engineering*, *12*(1), 471–494. https://doi.org/10.1146/annurev-chembioeng-093020-091447

Ringrose, P., Yardley, G., Vik, E., Shea, W., & Carruthers, D. (2000). Evaluation and benchmarking of petroleum trap fill and spill models. *Journal of Geochemical Exploration*, *69-70*, 689–693. https://doi.org/https://doi.org/10.1016/S0375-6742(00)00072-8

Rogelj, J., Shindell, D., Jiang, K., Fifita, S., Forster, P., Ginzburg, V., Handa, C., Kheshgi, H., Kobayashi, S., Kriegler, E., Mundaca, L., Seferian, R., Vilarino, M. V., Calvin, K., Edelenbosch, O., Emmerling, J., Fuss, S., Gasser, T., Gillet, N., ... Zhou, W. (2018). Chapter 2: Mitigation pathways compatible with 1.5oc in the context of sustainable development. In *Global warming of 1.5 oc an ipcc special report on the impacts of global warming of 1.5 oc above pre-industrial levels and related global greenhouse gas emission pathways, in the context of strengthening the global response to the threat of climate change*. Intergovernmental Panel on Climate Change. https://www.ipcc.ch/report/sr15/

Sclater, J., & Christie, P. (1980). Continental stretching: An explanation of the post-mid-cretaceous subsidence of the central north sea basin. *Journal of Geophysical Research*, *85*, 3711–3739. https://doi.org/10.1029/JB085iB07p03711

SINTEF. (2014). *Mrst*. Retrieved 30th April 2023, from https://www.sintef.no/projectweb/mrst/modules/co2lab/ve-models/

SINTEF. (2023). *Mrst*. Retrieved 9th April 2023, from https://www.sintef.no/projectweb/mrst/

Steel, R. J. (1993). Triassic–jurassic megasequence stratigraphy in the northern north sea: Rift to post-rift evolution. *Geological Society, London, Petroleum Geology Conference Series*, *4*(1), 299–315. https://doi.org/10.1144/0040299

Sundal, A., Miri, R., Ravn, T., & Aagaard, P. (2015). Modelling co2 migration in aquifers; considering 3d seismic property data and the effect of site-typical depositional heterogeneities. *International Journal of Greenhouse Gas Control*, *39*, 349–365. https://doi.org/10.1016/j.ijggc.2015.05.021

Sundal, A., Nystuen, J. P., Dypvik, H., Miri, R., & Aagaard, P. (2013). Effects of geological heterogeneity on co2 distribution and migration - a case study from the johansen formation, norway [GHGT-11 Proceedings of the 11th International Conference on Greenhouse Gas Control Technologies, 18-22 November 2012, Kyoto, Japan]. *Energy Procedia*, *37*, 5046–5054. https://doi.org/https://doi.org/10.1016/j.egypro.2013.06.418

Sundal, A., Nystuen, J. P., Rørvik, K.-L., Dypvik, H., & Aagaard, P. (2016). The lower jurassic johansen formation, northern north sea – depositional model and reservoir characterization for co2 storage. *Marine and Petroleum Geology*, *77*, 1376–1401. https://doi.org/https://doi.org/10.1016/j.marpetgeo.2016.01.021

Thompson, N., Andrews, J. S., & Bjørnarå, T. I. (2021). Assessing potential thermo-mechanical impacts on caprock due to co2 injection—a case study from northern lights ccs. https://doi.org/10.3390/en14165054

Torp, T. A., & Gale, J. (2004). Demonstrating storage of CO2 in geological reservoirs: The Sleipner and SACS projects. *Energy*, *29*(9), 1361–1369. https://doi.org/10.1016/j.energy.2004.03.

Walderhaug, O. (1996). Kinetic modeling of quartz cementation and porosity loss in deeply buried sandstone reservoirs. *AAPG Bulletin*, *80*(5). https://www.osti.gov/biblio/249780

Wilkinson, M., Haszeldine, R. S., Fallick, A., Odling, N., Stoker, S., & Gatliff, R. (2009). Co2mineral reaction in a natural analogue for co2 storage–implications for modeling. *Journal of Sedimentary Research - J SEDIMENT RES*, *79*. https://doi.org/10.2110/jsr.2009.052

Williams, G. A., & Chadwick, R. A. (2021). Influence of reservoir-scale heterogeneities on the growth, evolution and migration of a co2 plume at the sleipner field, norwegian north sea. *International Journal of Greenhouse Gas Control*, *106*, 103260. https://doi.org/https://doi.org/10.1016/j.ijggc.2021.103260

Zeynolabedini, M. (2022). *Proxy modelling for co2 storage (specialization project)*. NTNU.

Appendix

A ECLIPSE DATA File

```
RUNSPEC
TITLE
3DCO2 Injection Johansen Formation, Grid from Anja Sundal (
    Regional_NEW_JOINED)

-- Grid 400x400m faults sealing

DIMENS
-- Grid Dimensions
-- NX    NY        NZ
-- ------  ---------  ------
     78        130         120   /


-- Active Phases Present
OIL
GAS
DISGAS

METRIC
-- Unit Convention

--BIGMODEL
-- DIFFUSE
-- Enables Molecular Diffusion

--PARALLEL
-- 2 DISTRIBUTED /


--MEMORY
-- 1000 /


TABDIMS
```

```
-- Table Of Dimensions
-- NTSFUN  NTPVT  NSSFUN
-- ------  -----  ------
     1       1      40   1* 2 /

-- NTSFUN: No. of saturation tables entered.
-- NTPVT : No. of PVT tables entered (in the PROPS section).
-- NSSFUN: Max. no. of saturation node in each saturation table, ie.,
--         Max. no. of data points in each table.

WELLDIMS
-- Well Dimension Data
-- NWMAXZ NCWMAX NGMAXZ NWGMAX
-- ------ ------ ------ ------
     20      120    5     10    /

-- NWMAXZ: Max. no. of wells in the models.
-- NCWMAX: Max. no. of conncections per well (i.e., no. of perforations
   ).
-- NGMAXZ: Max. no. of groups in the model.
-- NWGMAX: Max. no. of wells in any group.

REGDIMS
-- NTFIP   NMFIPR----
 9 1 /

--EQLDIMS
-- 6 /

FAULTDIM
2000 /


START
-- Spesifies a Start Date
-- DAY    MONTH   YEAR
-- -----  -----   -----
    1      JAN    2023 /
```

```
--NSTACK
------ Stack Size For Linear Solver
-- 250 /

UNIFOUT
-- Restart And Summary Files Are To Be Unified

UNIFIN
-- Restart From A Unified Restart File




--
    ==========================================================================

GRID
--
    ==========================================================================

INIT

INCLUDE
 '../INCLUDE/Regional_NEW_JOINED.GRDECL' /

INCLUDE
 '../INCLUDE/Regional_NEW_FAULTS_AAG.grdecl' /


--INCLUDE
--  '../INCLUDE/Smh_north_Ext_400x400.inc' /

RPTGRID
ALLNNC/


COPY
 'PERMX'  'PERMY' /
/
```

```
--MINPV
-- 3000 /

--DX
--1216800*10/
--
--DY
--1216800*10/
--
--DZ
--1216800*10/
--
--PERMX
--1216800*100.0
--/
--
--PERMY
--1216800*100.0
--/
--
--PERMZ
--1216800*100.0
--/
--
--PORO
--1216800*0.2/
--
-----BOX
----- 1 , 10 , 1 , 10 , 1 , 1/
--
--TOPS
-- 10140*835/
--
-----ENDBOX




--
```

```
================================================================================

EDIT



MULTFLT
'F*' 1.0 /
/

--==============================================================================

PROPS
--
================================================================================

INCLUDE
'../INCLUDE/PVT_SH_TUBAAEN98C_1.TXT' /



INCLUDE
'../INCLUDE/UTSIRA_RELP_LINEAR_W07_G20.INC' /
-- '../INCLUDE/SATFN_gassum_1.inc' /

--PVTW
--        4014.7      1.029         3.13D-6             0.31                0 /
--
------ ROCK COMPRESSIBILITY
------
------     REF. PRES    COMPRESSIBILITY
--ROCK
--          14.7             3.0D-6            /
--
------ SURFACE DENSITIES OF RESERVOIR FLUIDS
------
------           OIL    WATER    GAS
--DENSITY
--          49.1    64.79   0.06054   /
--
```

—PVDO

——— P Bo Vo

— 2000 1.340 0.60

— 3000 1.330 0.65

— 4000 1.300 0.70

— 5000 1.280 0.75

— 6000 1.260 0.80

— 7000 1.240 0.82

— 8000 1.220 0.83

—/

—

—SWOF

——— Sw Krw Krow Pcow

——0.20 0.0000 1.0000 4.000

——0.25 0.0010 0.6800 2.700

——0.30 0.0200 0.4200 2.000

——0.40 0.0400 0.1500 1.200

——0.55 0.1200 0.0200 0.600

——0.70 0.2400 0.0000 0.100

—/

—==========ls

==========

REGIONS

———

==========

—

INCLUDE

'../INCLUDE/Regional_NEW_PROP_FIPNUM.GRDECL' /

—

==========

SOLUTION

—

==========

```
EQUIL
-- Equilibration Data Spesification
-- Datum   Pi@Datum   WOC    Pc@WOC    GOC    Pc@GOC   Rs   Rv   Accuracy
-- ------  ---------  ----   -------  ------  -------  --   --   --------
       2600     260.0    5050.0      0.0     100.0      0.0     1    0          /

/


RPTRST
BASIC=2 DENO /

RPTSOL
DENO /


RSVD
-- Variation Of Solution GOR With Depth
-- Depth       Rs
-- ------   --------
    800    0.00000
    4150    0.00000 /
/

--EQUIL
--         8400    4800    8500     0       8200     0        1        0        0  /




--
    ==========================================================================================


SUMMARY
--
    ==========================================================================================
```

```
--FIELD AVERAGES
FPR
FRS
FGIR
FGIT
FOPR
FOPT
FGIPL
FGIP
FGVIS
FGDEN
FOIP
--FOIPR
FRPV
FOPV
FGPV

--WELL
WBHP
  'WG*'
  'WO*' /

WGIR
  'WG*' /

WGIT
  'WG*' /

WGOR
  'WO*' /

WOPR
  'WO*' /

WOPT
  'WO*' /
```

```
BGSAT
1* 1* 1*/
/
--Block
--BPR
-- 92 170 1 /
-- 137 170 1 /
-- 121 48 1 /
-- /

EXCEL

--
    ==========================================================================

SCHEDULE
--
    ==========================================================================



MESSAGES
-- Resets Message Print and Stop Limits
-- Messages    Comments  Warnings  Problems  Error     Bug
-- ---------   --------  --------  --------  -----     ---
     10000   10000 10000 10000   100 100 100000 100000 100000 10000 /

RPTSCHED
'RESTART' 'FIP=2' 'CPU=2' /
/

WELSPECS
 WGI-1   'G1'     43       49       1*       'GAS'    0.2      /
-- WGI-2         'G1'     37       92       1*       'GAS'    0.2      /
-- WOP-1         'G2'     33       6        1*       'OIL'    0.2      /
-- WOP-2         'G2'     55       4        1*       'OIL'    0.2      /
-- WOP-3         'G2'     41       75       1*       'OIL'    0.2      /
-- WOP-4         'G2'     11       175      1*       'OIL'    0.2      /
-- WOP-5         'G2'     58       177      1*       'OIL'    0.2      /
```

```
/


COMPDAT
WGI-1     43      49      6       120     'OPEN'  0       1*      0.2
          3*      Z       /
--WGI-2   37      92      6       120     'OPEN'  0       1*      0.2
          3*      Z       /
--WOP-1   33      6       1       22      'OPEN'  0       1*      0.2
          3*      Z       /
--WOP-2   55      4       1       22      'OPEN'  0       1*      0.2
          3*      Z       /
--WOP-3   41      75      1       22      'OPEN'  0       1*      0.2
          3*      Z       /
--WOP-4   11      175     1       22      'OPEN'  0       1*      0.2
          3*      Z       /
--WOP-5   58      177     1       22      'OPEN'  0       1*      0.2
          3*      Z       /
/


--INCLUDE
---- '../INCLUDE/SCH_Faults_Friis_all_Troll_extended.inc' /
-- /

-- 0.8 Mt/y for 2 years (1 jan 25)

WCONINJE
          'WGI-1' 'GAS'   'OPEN'  'RATE'  2289000   1*    450     /

--        'WGI-2' 'GAS'   'OPEN'  'RATE'  2289000   1*    450     /
/

------ Time steps until 2025 years. No leap years
TSTEP
  90 91 92 92
  90 91 92 92
  90 91 92 92
  90 91 92 92
```

```
  90  91  92  92
  90  91  92  92
  90  91  92  92
  90  91  92  92
  90  91  92  92
  90  91  92  92
  90  91  92  92
  90  91  92  92
  90  91  92  92
  90  91  92  92
  90  91  92  92
  90  91  92  92
  90  91  92  92
  90  91  92  92
  90  91  92  92
  90  91  92  92
  90  91  92  92
  90  91  92  92
  90  91  92  92
  90  91  92  92
  90  91  92  92
  90  91  92  92
  90  91  92  92
  90  91  92  92
  90  91  92  92
/

WELOPEN
 WGI-1 SHUT /
/

DATES
 1 JAN 2055 /
 1 JAN 2060 /
 1 JAN 2065 /
 1 JAN 2070 /
 1 JAN 2075 /
 1 JAN 2080 /
```

```
 1 JAN 2085 /
 1 JAN 2090 /
 1 JAN 2095 /
 1 JAN 2100 /
 1 JAN 2105 /
 1 JAN 2110 /
 1 JAN 2115 /
 1 JAN 2120 /
 1 JAN 2125 /
 1 JAN 2130 /
 1 JAN 2140 /
 1 JAN 2150 /
 1 JAN 2160 /
 1 JAN 2180 /
 1 JAN 2200 /
 1 JAN 2220 /
 1 JAN 2240 /
 1 JAN 2260 /
 1 JAN 2280 /
 1 JAN 2300 /
 1 JAN 2350 /
 1 JAN 2400 /
 1 JAN 2450 /
 1 JAN 2553 /
/
END
```

B MRST code

```
mrstModule add deckformat ad-core ad-props co2lab coarsegrid

current_dir = fileparts(mfilename('fullpath'));
fn     = fullfile(current_dir, 'AURORA.data');
deck = readEclipseDeck(fn);
deck = convertDeckUnits(deck);
zero_Poro=find(~deck.GRID.PORO);
deck.GRID.ACTNUM(zero_Poro)=0;
```

```
%%% EDIT PORO & ACTNUM
load 'Removing.mat'
deck.GRID.ACTNUM(Removing)=0;
G = initEclipseGrid(deck);
G = computeGeometry(G);
[Gt,G2,transMult] = topSurfaceGrid(G);
load 'Final Gt.mat'
load transMult.mat
rock  = initEclipseRock(deck);
rock  = compressRock(rock, G.cells.indexMap);

%% Fluid parameters
gravity reset on;
g       = gravity;
rhow    = 1020.19;
co2     = CO2props();               % CO2 property functions
p_ref   = 30 *mega*Pascal;          % reference pressure
t_ref   = 98+273.15;                % reference temperature
co2_rho = 669.36;% CO2 density
co2_c   = co2.rhoDP(p_ref, t_ref) / co2_rho; % CO2 compressibility
wat_c   = 3.97*10^-10; %[Pa-1]
c_rock  = 5e-5 / barsa;
srw     = 0.07;                             % residual water
src     = 0.20;                             % residual CO2
pe      = 5 * kilo * Pascal; % capillary entry pressure
muw     = 3.6e-4 * Pascal * second;         % brine viscosity
muco2=5.4e-5 * Pascal * second; % co2 viscosity
%% Boundary Condition
ix1 = searchForBoundaryFaces(Gt, 'BACK');
ix2 = searchForBoundaryFaces(Gt, 'LEFT');
ix3 = searchForBoundaryFaces (Gt, 'RIGHT');
ix4 = searchForBoundaryFaces(Gt, 'FRONT');

bcIxVE = [ix1; ix2; ix3; ix4];
plotGrid(Gt, 'faceColor', 'none', 'EdgeAlpha', 0.1)
plotGrid(Gt, sum(Gt.faces.neighbors(ix1,:),2), 'faceColor', 'r')
plotGrid(Gt, sum(Gt.faces.neighbors(ix2,:),2), 'faceColor', 'g')
plotGrid(Gt, sum(Gt.faces.neighbors(ix3,:),2), 'faceColor', 'y')
plotGrid(Gt, sum(Gt.faces.neighbors(ix4,:),2), 'faceColor', 'm')
```

```
axis tight off
title('2D grid of top surface');

%% Setup the well
wc_global1 = false(G.cartDims); wc_global1(43, 49, 6:120) = true;
wc1        = find(wc_global1(G.cells.indexMap));
inj_rate   = 1.5 * mega * 1e3 / year / co2_rho; % m3/s

W1         = addWell([], G, rock, wc1, 'name','injector1',...
                'type', 'rate', ...  % inject at constant rate
                'val', inj_rate, ... % volumetric injection rate
                'comp_i', [0 1]);    % inject CO2, not water
%% Top surface grid, petrophysical data, well, and initial state
rock2D             = averageRock(rock, Gt);
W2D                = convertwellsVE(W1, G, Gt, rock2D);
initState.pressure = rhow * g(3) * Gt.cells.z;
initState.s        = repmat([1, 0], Gt.cells.num, 1);
initState.sGmax    = initState.s(:,2);
initState.rs       = zeros(Gt.cells.num, 1);

%% Fluid model
invPc3D = @(pc) (1-srw) .* (pe./max(pc, pe)).^2 + srw;
p=[-3.04014564000589, 4.84121226800706, -0.846636628001177,
   6.81086017326756e-16];
kr3D    = @(s) max(p(1)*s.^3+p(2)*s.^2+p(3)*s+p(4),0);

fluid   = makeVEFluid(Gt, rock, 'P-scaled table', ...
                'fixedT'       , t_ref, ...
                'co2_mu_ref'   , muco2, ...%6e-5 * Pascal * second , ...
                'wat_mu_ref'   , muw, ...%8e-4 * Pascal * second , ...
                'co2_rho_ref'  , co2_rho                , ...
                'wat_rho_ref'  , rhow                   , ...
                'co2_mu_pvt'   , [co2_c, p_ref]         , ...
                'wat_mu_pvt'   , [wat_c, p_ref]         , ...
                'co2_rho_pvt'  , [co2_c, p_ref]         , ...
                'wat_rho_pvt'  , [wat_c, p_ref]         , ...
                'residual'     , [srw, src]             , ...
                'pvMult_p_ref', p_ref                   , ...
                'pvMult_fac'   , c_rock                 , ...
```

```
                'invPc3D'       , invPc3D                   , ...
                'kr3D'          , kr3D                      , ...
                'transMult'     , transMult);

%% Set up simulation schedule

% hydrostatic pressure conditions for open boundary faces
p_bc      = Gt.faces.z(bcIxVE) * rhow * g(3);
bc2D      = addBC([], bcIxVE, 'pressure', p_bc);
bc2D.sat = repmat([1  0], numel(bcIxVE), 1);

% Setting up two copies of the well and boundary specifications.
% Modifying the well in the second copy to have a zero flow rate.
schedule.control    = struct('W', W2D, 'bc', bc2D);
schedule.control(2) = struct('W', W2D, 'bc', bc2D);
%val=num2cell([0 ,0]);
%val=val';
%[schedule.control(2).W.val] = val{:};
schedule.control(2).W.val = 0;

% Specifying length of simulation timesteps
%schedule.step.val = [repmat(hour,     2400, 1); ...
%                     repmat(hour, 50, 1)];

T1= 30*year;
T2= 500*year;
dt1 = rampupTimesteps(T1,30*day);
dt2 = rampupTimesteps(T2,365*day);

schedule.step.val = [dt1;dt2];

schedule.step.control = [ones(374, 1);
                         ones(509, 1) * 2 ];


%% Create and simulate model
model = CO2VEBlackOilTypeModel(Gt, rock2D, fluid);
[wellSol, states] = simulateScheduleAD(initState, model, schedule);
states = [{initState} states(:)'];
```

```
%% Animate the plume migration over the whole simulation period
clf
oG = generateCoarseGrid(Gt.parent, ones(Gt.parent.cells.num,1));
plotFaces(oG, 1:oG.faces.num,'FaceColor','none');
plotWell(Gt.parent, W1,'FontSize',10);
view(-63, 50); axis tight; colorbar, caxis([0 1-srw]); colormap(parula
    .^2);
hs     = [];
time   = cumsum([0; schedule.step.val])/year;
period = [1; schedule.step.control];
ptxt   = {'injection','migration'};

for i=1:numel(states)
    delete(hs)
    [h, h_max] = upscaledSat2height(states{i}.s(:,2), states{i}.sGmax,
        Gt, ...
                                    'pcWG', fluid.pcWG, ...
                                    'rhoW', fluid.rhoW, ...
                                    'rhoG', fluid.rhoG, ...
                                    'p', states{100}.pressure);
    sat = height2Sat(struct('h', h, 'h_max', h_max), Gt, fluid);
    title(sprintf('Time: %4d yrs (%s)', time(i),ptxt{period(i)}));
    ix = sat>0; if ~any(ix), continue; end
    hs = plotCellData(Gt.parent, sat, ix); drawnow
end


%% Trapping inventory
%# Structural residual - CO2 residually trapped inside a structural
    trap
%# Residual - CO2 residually trapped outside any structural traps
%# Residual in plume - fraction of the CO2 plume outside any
    structural
%   traps that will be left behind as residually trapped droplets when
    the
%   plume migrates away from its current position
%# Structural plume - mobile CO2 volume that is currently contained
    within
```

```
%   a residual trap;  if the containing structure is breached, this
    volume
%   is free to migrate upward
% # Free plume - the fraction of the CO2 plume outside of structural
    traps
%   that is free to migrate upward and/or be displaced by imbibing
    brine.
% # Exited - volume of CO2 that has migrated out of the domain through
    its
%   lateral boundaries
%
% This model only has very small structural traps and residual trapping
     is
% therefore the main mechanism.
ta = trapAnalysis(Gt, false);
reports = makeReports(Gt, states, model.rock, model.fluid, ...
                      schedule, [srw, src], ta, []);

h1 = figure; plot(1); ax = get(h1, 'currentaxes');
plotTrappingDistribution(ax, reports, 'legend_location', 'northwest');
```

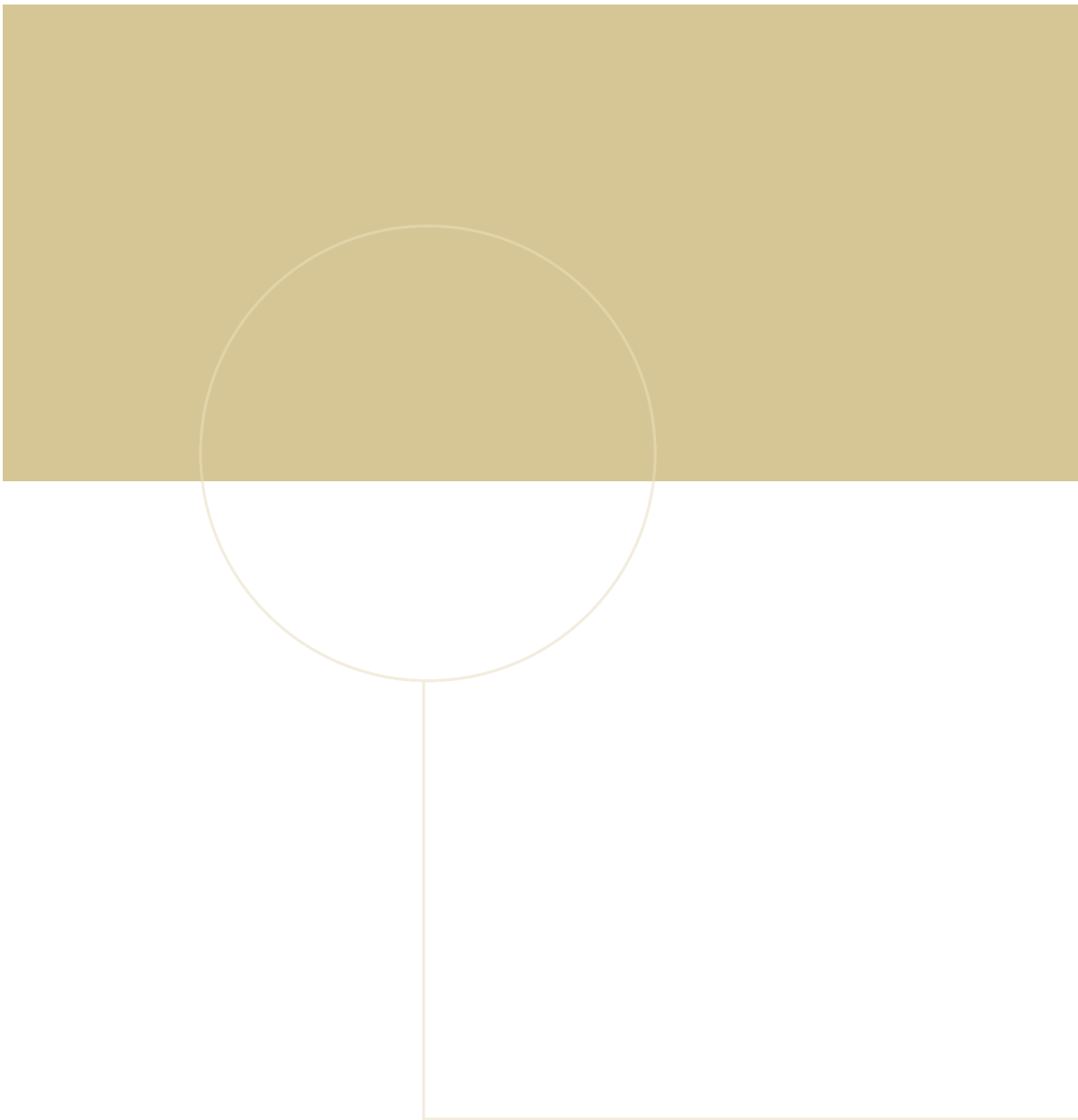

NTNU

Norwegian University of
Science and Technology